No. 323
November 1992

NONLINEAR RADIATION PROBLEMS FOR A SURFACE-PIERCING BODY

Tzung-Hang Lee

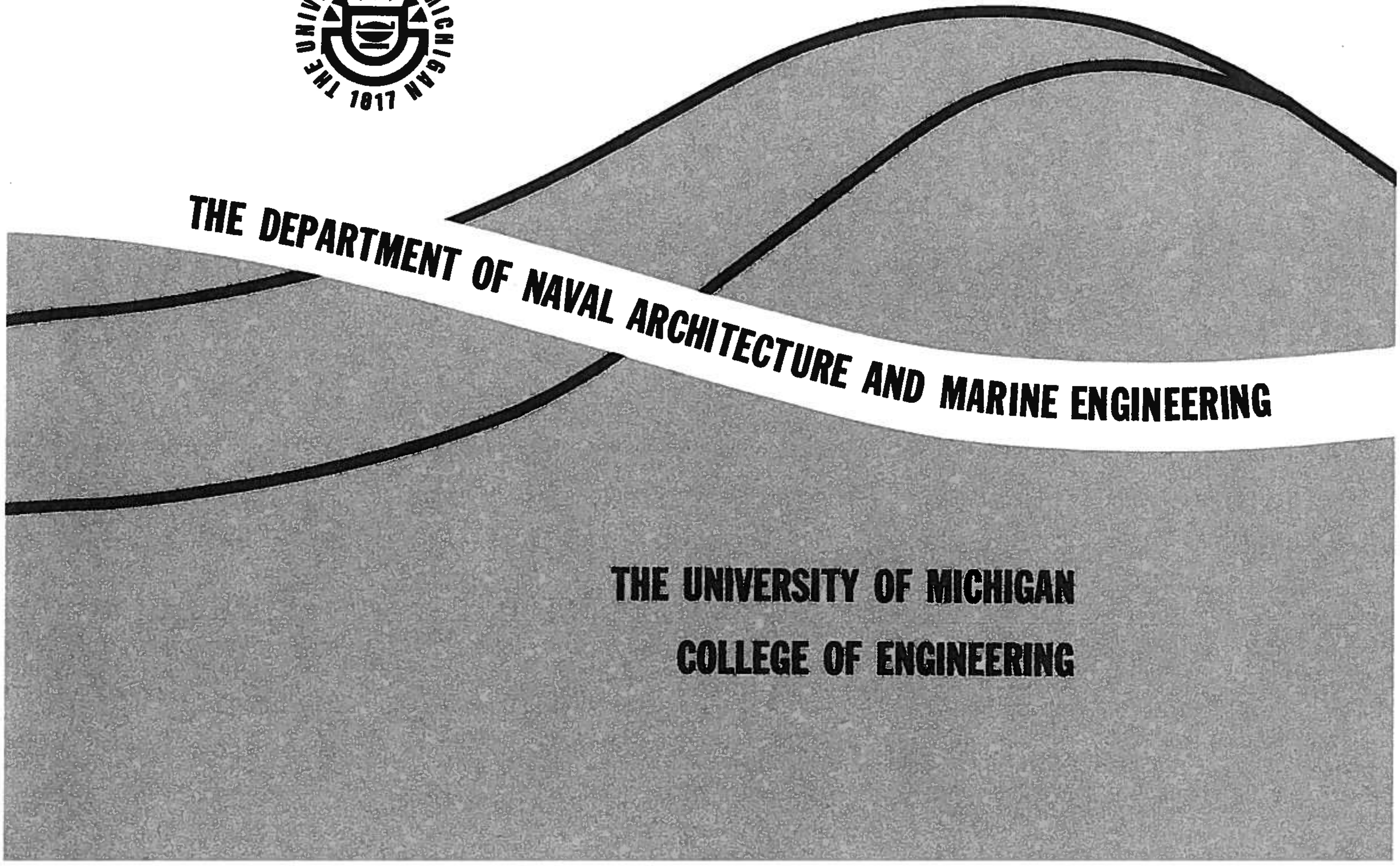

THE DEPARTMENT OF NAVAL ARCHITECTURE AND MARINE ENGINEERING

THE UNIVERSITY OF MICHIGAN
COLLEGE OF ENGINEERING

NONLINEAR RADIATION PROBLEMS FOR A SURFACE-PIERCING BODY

by

Tzung-Hang Lee

A dissertation submitted in partial fulfillment
of the requirements for the degree of
Doctor of Philosophy
(Naval Architecture and Marine Engineering)
in The University of Michigan
1992

Doctoral Committee:

Professor Robert F. Beck, Chairperson
Research Fellow Yusong Cao
Assistant Professor Marc Perlin
Professor Bram van Leer
Associate Professor Armin W. Troesch

ABSTRACT

NONLINEAR RADIATION PROBLEMS FOR A SURFACE-PIERCING BODY

by

Tzung-Hang Lee

Chairperson: Robert F. Beck

A Desingularized Eulerian-Lagrangian Time-domain Approach (DELTA method) is used to investigate fully nonlinear radiation problems of surface-piercing bodies. At each time step, a boundary-value problem is solved by placing fundamental singularities outside the computational domain and satisfying the boundary conditions at prescribed collocation points. This desingularization allows the use of simple isolated sources while retaining the necessary accuracy.

A large outer region is investigated to postpone the free surface mean shift and wave reflection from the truncation boundary. The outer region is divided into exponential increasing panel sizes. The length, the first panel size and the panel number are found to be the crucial factors determining the effectiveness of the outer region. The effectiveness is relatively unaffected by forcing frequency and motion amplitude.

Both two- and three-dimensional problems are studied. A floating body is oscillated vertically or laterally. For two-dimensional problems, results from the desingularized method agree well with experiments and other algorithms. For three-dimensional heaving motions, the results of the symmetry-plane method show good agreement with the quarter-plane and Rankine-ring source approaches. Primary convergence and stability analyses are also conducted. The convergence rate is slightly lower for swaying motions than heaving motion because the singularity at the body-free surface intersection line (points) is more crucial for swaying motions. The desingularized scheme is more stable than the conventional boundary integral method. Large-amplitude computations are also performed for an upright cylinder with a larger bottom. The results of computations demonstrate the power of the DELTA method for use in offshore applications.

To my parents

ACKNOWLEDGEMENTS

Professor R.F. Beck's sharp thinking and insight into the floating body radiation problem have always saved me from making many mistakes. I would like to express my deepest appreciation to him for his excellent guidance, continuous encouragement and infinite patience. I would like to thank Dr. Yusong Cao, not only as a committee member but also as a dear friend, for his continuous discussion and encouragement during the course of this work. I am also grateful to Professor A. W. Troesch , Professor M. Perlin and Professor B. van Leer for their comments, discussions and suggestions, and for their accepting to serve on my dissertation committee.

Special thanks are also directed to Dr. W.C. Lin in DTNSRDC for his optimistic upbeat spiritual support; to Professor R.W. Yeung in U.C. Berkeley for initiating my research interest; to Dr. W.M. Lin in SAIC and Dr. C.W Lin in DTNSRDC for their valuable discussions; and to Mr. Y. Chen for his graphic program to make the animation of the computed waves presented at the thesis defense possible.

Professor J.L. Hwang, Professor Y.J. Lee, and Professor Y.N. Chen are also acknowledged for teaching me while at National Taiwan University. I also appreciate faculty, staff members and colleagues of the Department of Naval Architecture and Marine Engineering, especially Mrs. Virgina Konz, Dr. Allen Magee, Dr. Jeffrey Falzarano, Ms. Yi-Ling Chen, Ms. Mary Wise and Mr. Krish Thiagarajan for their help and friendship which have made my stay in Ann Arbor a very pleasant memory.

This work is supported by the Office of Naval Research Accelerated Research Initiations in Nonlinear Ship Motions under Contract Number N00014-90-J-1818. Computations were made in part using a CRAY Grant at the University Research and Development Program of the San Diego Supercomputer Center.

Finally, my hearty thanks go to my parents and my sisters who have always tried to understand and support me. This dissertation is dedicated to my parents with great indebtedness for their loving encouragements and patience in the completion of my study.

TABLE OF CONTENTS

CHAPTER

LIST OF FIGURES

Figure

LIST OF TABLES

Table

CHAPTER I

INTRODUCTION

1.1 Historical Review

The interest in time marching procedures to solve water wave problems has been greatly expanded recently. One of the important advantages of the time-domain analysis over the conventional frequency-domain analysis is that the time-domain approach can handle arbitrary body motions. When body motion becomes large, nonlinear waves are generated and higher-order hydrodynamic forces appear. These phenomena can not be explained by linear theory since nonlinear effects are essentially excluded. Therefore, time-domain calculations are necessary for fully nonlinear problems since frequency-domain computations are only good for linear problems or a few very specific body-exact problems.

For linear calculations, the frequency-domain methods are extensively used. In the linear Neumann-Kelvin approach, the body boundary condition is applied on the mean position of the exact body surface and a linearized free surface boundary condition is used. These assumptions allow solutions to be developed using a Green's function technique. At steady forward speed, the frequency-domain linear Neumann-Kelvin method encounters difficulties because the Green's function is complicated and difficult to compute. Nevertheless, results have been obtained by several researchers including Chang (1977), Inglis & Price (1981), Guevel & Bougis (1982), Wu and Eatock Taylor (1987), and Iwashita & Ohkusu (1992). However, if the body boundary condition is not applied on the mean position, the result is a time variant linear system. In the so called body-exact problem, the body boundary condition is satisfied on the instantaneous wetted surface of the body while the linearized free surface boundary condition is retained. In order to describe the fluid field and obtain the hydrodynamic forces for large body motions, a time-domain approach is desired.

Finkelstein (1957) obtained the time-domain solution for the fundamental $\frac{1}{r}$ singularity. Discussions of direct time-domain solutions are presented by various authors such as : Stoker (1957), Cummins (1962), Ogilive (1964) and Wehausen (1967). A three-dimensional time domain model for arbitrary-shaped slender bodies with forward speed was developed by Beck & Liapis (1986) and Beck & King (1987). The extension of the model to include the exact body boundary condition for a submerged body performing arbitrary motions has been developed by Beck & Magee (1990) and Magee & Beck (1988). In this model, the linearized free surface boundary condition and the radiation condition are satisfied by a free surface Green's function. Then, the body boundary condition remains the only boundary condition to be satisfied. The integral equation is a Fredholm integral equation of the second kind which can be solved by numerical techniques. Other researchers such as Krosmeyer (1988), Krosmeyer *et al.* (1988), King *et al.* (1988), Ferrant (1989,1990) and Lin & Yue (1990) also have successfully obtained results of free surface flow problems using time-domain methods.

Longuet-Higgins & Cokelet (1976) first introduced the mixed Eulerian-Lagrangian time-stepping scheme for solving two-dimensional fully nonlinear water wave problems. Faltinsen (1977) used a similar scheme to study the nonlinear transient problem of a body oscillating on a free surface. In his work, he found the velocity potential at each time step due to a distribution of dipoles and sources over the wetted body surface as well as the free surface: tracing the fluid particles on the free surface to advance the solution forward in time.

Vinje & Brevig (1981) continued the approach of Longuet-Higgins & Cokelet to include finite depth and floating bodies but retained the assumption of spatial periodicity. Baker, Meiron & Orszag (1982) used a dipole distribution on the free surface where Dirichlet conditions were posed. Dommermuth & Yue (1987) used the mixed Eulerian-Lagrangian method and postulated a far-field boundary matching algorithm by matching the nonlinear computational solution to a general linear solution of transient outgoing waves.

An initial boundary value problem is set up to study the free surface waves generated by body motions or to compute the hydrodynamic forces acting on a body. A Desingularized Eulerian-Lagrangian Time-domain Approach method (DELTA method) is one of many methods used to solve the boundary value problem at each time step. Similar to conventional boundary integral method, the desingularized method reformulates the problem into a boundary integral equation. The difference is that the desingularized method separates the integration and control surfaces, resulting in nonsingular integrals. The solution is constructed by integrating a distribution of fundamental singularities over an auxiliary surface (the integration surface) outside the fluid domain. The integral equation for the unknown distribution is obtained by satisfying the boundary conditions on the problem boundary (the control surface).

The desingularization method was first developed by von Karman (1930) in which an axial source distribution was used to determine the flow about an axisymmetric body. The strength of the source distribution was determined by the kinematic body boundary condition. A non-singular formulation of the boundary integral equation method was proposed by Kupradze (1967). The exterior Dirichlet problem was solved by using an auxiliary surface located outside the computational domain. Webster (1975) investigated the numerical properties of the desingularization technique for the external potential flow around an arbitrary, three-dimensional smooth body. A singularity sheet was discretized into triangular source patches and the patches were placed outside the problem domain with a proper distance. He concluded that the use of this desingularization technique greatly improved the accuracy of the solution.

Heise (1978) examined the numerical properties of an integral equation system for plane elastostatic problems, in which singular points were distributed on an auxiliary boundary outside the solution domain. Martin (1981) obtained the non-singular integral equation for water wave radiation problems by placing singular points inside the body and applying Green's theorem to the solution. Schlutz & Hong (1989) obtained a non-singular formulation to solve two-dimensional potential problems. The singularity of the fundamental solution was moved away from the body contour thus desingularizing the kernels. Consequently, simple numerical quadratures can be used to evaluate the integrals since special care is not required for these integrals. Jensen, Soding & Mi (1986), Jesen, Bertram & Soding (1989) and Raven (1992) applied the desingularized method to the steady wave resistance problem. A similar approach is used by Bertram (1990) to simulate ship motions.

Cao, Schultz & Beck (1990, 1991a, 1991b, 1992) solved nonlinear problems for waves generated by a free surface pressure disturbance or a submerged body by combining the time-stepping scheme and the desingularized boundary integral equation method. The so called 'direct' and 'indirect' methods were tested, and the results of the comparisons in computational complexity and time consumed suggested that the 'indirect' method was preferable. Cao, Lee & Beck (1992) extended the indirect method to study nonlinear water wave problems with floating bodies.

When panel methods are used in conjunction with Rankine sources to solve nonlinear boundary value problems, the computational domain on the free surface must be discretized into a large number of panels in order to properly describe the flow field. This results in a large matrix of influence functions; consequently, a fast iterative solver for large matrices is required. The General Minimal Residual Method (GMRES) developed by Saad & Schultz (1986) and Olson (1989) can be used to iteratively solve the system of linear equations.

A preconditioning matrix used with the iterative solver GMRES was explored by Cao (1991). An appropriate preconditioning matrix was chosen to be the matrix of influence functions at time equal to zero. A sufficiently small value of the convergence tolerance was chosen so that the computational error was negligible compared with the truncation error. It was found that the preconditioning saved over 80% of the total CPU time in solving the system compared with the non-preconditioned matrix.

A 'sawtooth' instability on the free surface was observed by Longuet-Higgins & Cokelet (1976) for a steady progressive wave in deep water. They concluded that the instability was not caused by the time stepping procedure only; suggesting that the growth of the instability may be partially physical, being similar to the amplification of short gravity waves by horizontal compression at the crest of long waves. Therefore, a smoothing technique should be applied to remove the instability when necessary.

A similar smoothing technique is required when the local steepness of the waves is large. Baker *et al.* (1982) and Lin, Newman & Yue (1984) both needed a smoothing operator to reduce the instabilities when the waves were steep. Roberts (1983) analyzed this problem using Fourier spectral representations for the position and potential of a free shear layer and was able to remove the numerical instability by modifying the highest Fourier mode.

A confluence of the body and free surface boundary conditions exists at the intersection line. As a result, the solution exhibits a singularity at the intersection line. Kravtchenko (1954) showed that the velocity potential for a two-dimensional vertical wall moving horizontally is logarithmically singular at the contact point in linear theory. Miloh (1980) studied the singularity for general three-dimensional flows and found that this singularity persists even when full nonlinearity was introduced. Peregrine (1972) derived a perturbation result for wavemaker problems in which the free surface elevation displayed a $t \; log \; (tanh(\frac{\pi x}{4h}))$ behavior for small time t, where x is the distance from the wavemaker. The two-dimensional result has been confirmed and investigated numerically and experimentally by Greenhow & Lin (1983) and Lin (1984). Nevertheless, Joo, Schultz & Messiter (1990) developed a Fourier-integral method to avoid the artificial singularity at the intersection point by introducing a small time expansion.

Vinje & Brevig (1981) treated the body-free surface intersection points as part of the body boundary, and the position and potential at that point were obtained by extrapolation. Their results were not completely satisfactory. Greenhow *et al.* (1982) found it necessary to use experimental measurements to fix the locations of the intersection points. For the two-dimensional wavemaker problem, Lin (1984) used a Cauchy integral method and specified both the values of the stream function and the potential at the intersection point. The stream function value was determined from the body boundary condition and the potential value from the free surface boundary conditions. For axisymmetric problems, Dommermuth & Yue (1987) applied both body and free surface boundary conditions at the intersection points to solve boundary value problems.

When numerically solving boundary value problems, a finite computational domain should be used. For constant forward speed problems, Cao, Schultz & Beck (1990a) used a computational window moving with the disturbance. They adopted a window shifting technique to investigate waves generated by a moving underwater disturbance using the desingularized Eulerian-Lagrangian time-domain approach. When the window was shifted, one row of node points were dropped at the downstream side of the window and a row of new node points entered the window from upstream. The upstream was assumed to be undisturbed, so that the velocity potential and free surface elevation were both set equal to zero. In other words, a calm water far field boundary condition was enforced on the upstream boundary. The treatment also prevented wave reflection at the downstream boundary. This approach has been shown to work successfully in numerical computations for cases in which the disturbance moved with forward speed (Cao, Schultz & Beck, 1990, 1991a, 1991b, 1992 and Cao, 1991).

For zero forward speed problems, the technique of a shifting computational window is not applicable. There exists neither an ‘upstream’ where the calm water condition can be imposed nor a ‘downstream’ where the node points possibly contaminated by wave reflection can be dropped off the window from time to time. Consequently, the radiated wave reflects from the truncation boundaries and there is a free surface mean shift if the far field boundary condition is neglected. In order to avoid the free surface mean shift and wave reflection, a proper far field boundary condition must be used or a special treatment on the truncation boundaries should be applied.

Lindman (1975) used nonreflecting boundary conditions for simulations in which the linear, time-dependent wave equation was solved. The method was used successfully only for nondispersive waves. For general nonlinear, dispersive waves governed by equations which are more complicated than the wave equation, Chan (1975) proposed a technique using artificial damping to absorb radiating waves. A damping region was set up near the upstream and downstream boundaries of the computational domain to absorb waves incident upon it. Chan found that the efficiency of this artifice depends heavily on how the damping term was added to the momentum equations, on the magnitude and spatial variation of the viscosity in the damping zone, and on the length of the damping zone relative to the wavelength of the various components in the wave system. This approach can be modified and used for a nonlinear potential flow problem by adding an artificial pressure term to the dynamic free surface boundary condition outside the domain of interest. However, the artificial pressure might causes waves to travel into the domain of interest.

Longuet-Higgins & Cokelet (1976) avoided the reflection problem by using periodic boundary conditions. When the physical problem possessed spatial periodicity, the computational domain was simply folded onto itself and the exterior boundaries were eliminated. Vinge & Brevig (1981), Greenhow *et al.* (1982) were able to use this assumption to study the dynamics of a floating body by keeping a relatively large domain. However, the assumption of spatial periodicity or of fixed boundaries at some distance is not quite realistic when an isolated body is present in an unbounded region. In addition, more field points are necessary to discretize a larger domain, and thus, more computational effort is required.

Faltinsen (1977) matched the nonlinear inner solution to that of a Rankine dipole in the far field in his study of the heaving motion of a two dimensional floating body. Since wave effects are not present in the latter, Faltinsen found that unless the interior computational domain was increased as a function of simulation time, the computations would soon break down because the single dipole method, when used in an initial boundary value problem, is valid only until the traveling wave reaches the truncation boundary. Assuming a boundary integral formulation for the nonlinear interior domain with N_f free surface points, N_f must increase approximately linear with time. The storage and computational effort per time step would increase as $O(N_f^2, N_f^3)$ in two-dimensional problems. The situation is even more critical for three-dimensional problems. For this reason, the cost may become prohibitive, and Faltinsen's results, for example, were typically restricted to less than one oscillating period. Thus, in Isaacson's (1982) Eulerian calculation of the nonlinear diffration by a vertical cylinder, where the fluid velocities were assumed to be zero on a finite truncation boundary, the motion for only a fraction of a wave period could be simulated.

Kang(1988) derived the three-dimensional form of Faltinsen's boundary matching scheme for axisymmetric bodies. Park & Troesch (1992) applied Kang's three-dimensional far field closure to study the stability properties of free surface flows caused by an inverted cone undergoing forced heaving motion. They found that the potential on the free surface drops exponentially when the waves generated by the motions of a cone reached the truncation boundary; therefore, the computation must be stopped.

For two-dimensional problems, a hybrid integral equation method was described in Liu & Abbaspour (1982). They studied the diffraction of waves by an infinite cylinder and solved the potential problem in the inner domain with a boundary integral equation method. An analytical solution for the outer domain satisfying the linearized free surface conditions and Sommerfeld's radiation condition at infinity were also used.

Dommermuth and Yue (1986) posed a far field closure by matching the nonlinear computational solution to a general linear solution of transient radiated waves. Through a matching of the two solutions on a fictitious boundary some distance away, the outer linear wavefield can be determined and the boundary condition for the nonlinear interior problem can be specified. Fundamentally, such a scheme is not suitable for two-dimensional flow since the nonlinearity of the radiated waves persists into the far field, and a simple matching of the two solutions on the boundary is not acceptable. In three-dimensions, the energy density of the radiating waves must decrease with radial distance. Therefore, a matching to a general linear solution is plausible on the truncation boundary. However, the matching should be made at a great enough distance so that the nonlinearity of the waves is weak. Furthermore, the technique will eventually spoil the results in the domain of interest if the phases of the nonlinear and linear radiating waves at the matching boundaries are not coincident.

Grosenbaugh and Yeung (1988) considered the far field boundary to be a material surface whose position changes with time in their study of nonlinear bow flows. Thus, the positions of fluid particles on this boundary moved according to the same equation that described the motion of free surface particles. The far field potential was represented by a linear time-dependent wave source which was proposed by Finkelstein (1957). The approximation of the far field boundary condition was obtained by taking the material derivative of pressure and neglecting quadratic terms. The linearized far field boundary requires that the boundary be far enough away to apply the linearization and no radiating wave was allowed to reach the truncation boundary. Therefore, the method was only good for the cases of a two-dimensional semi-infinite body with a forward speed.

Numerical stability problems occur in any numerical iteration scheme. Yeung (1982) investigated the stability criteria using a simplified von Neumann analysis. He assumed the velocity potential had a form of $\phi^n e^{ikx+ky}$ where k is a wave number. The criteria derived was independent of the panel size and the type of the boundary conditions, and of the form $f = kg\frac{(\Delta t)^2}{2}$. Dommermuth & Yue (1986) used a linearized von Neumann stability analysis to examine the stability of a mixed Eulerian-Lagrangian technique applied to axi-symmetric flows. The same assumption on velocity potential made by Yeung and a Taylor-series expansion were applied to find the stability criteria for the explicit fourth-order Runge-Kutta scheme and the fourth-order multi-step Adams-Bashforth-Moulton predictor-corrector scheme. They defined a stability parameter, a Courant condition, as $(\Delta t)^2 \leq \frac{8}{g}\frac{\Delta x}{\pi}$.

Park & Troesch (1992) investigated the numerical stability of different time marching schemes for a variety of two- and three-dimensional problems. Both Von

Neumann and matrix analyses were applied to examine the stability of the conventional boundary integral method. They found that the stability depends on the geometry of the specific problem, the far field closure and the time integration method. Three-dimensional problems tend to be more stable than two-dimensional problems. Moderate nonlinearities do not produce significantly different stability regions than equivalent linear problems, therefore, they suggest that a preliminary stability analysis can be completed on a linearized problem before the solution to the fully nonlinear problem is attempted. They found that the stability can be determined in terms of a local free surface stability index defined as $FSS = \pi g \frac{(\Delta t)^2}{\Delta x}$. The upper limits of the FSS number depend on the geometry and time marching scheme. Explicit Euler schemes are unconditionally unstable while implicit-like and implicit Euler schemes and fourth-order Runge-Kutta schemes are conditionally stable. A 'Green's function constant c' was used to improve the numerical stability, and the constant was found to be extremely helpful in stabilizing the numerical scheme in two-dimensions but not three-dimensions.

The convergency of a numerical scheme is also of critical concerned. Cao, Schultz & Beck (1990) investigated the convergence properties of the desingularized Eulerian-Lagrangian time-domain approach. In the study of the truncation effect of a infinitive plane, the computational domain was extended by adding uniformly sized panels and a quadratical convergence was found. When keeping the computational domain unchanged but reducing the panel size (therefore, increasing the panel number), they found that the numerical scheme converged linearly.

Newman & Lee (1992) tested the rate of convergence by increasing the number of panels on the body and free surface. Two different discretization schemes, equal spacing and cosine spacing, were examined, and three corresponding algorithms are utilized to evaluate the exciting force. The convergence rates are obtained and compared. When the unequal spacing technique is used, a smooth change in their dimensions should be used. They found that the cosine spacing near the cylinder corner and free surface led to more accurate results with fewer panels although the maximum difference between the predictions of the two schemes was only $\frac{1}{2}\%$.

1.2 Overview

The present work is an extension of the work of Cao, Schultz & Beck (1990, 1991a, 1991b) and Cao (1991), who succeeded in solving three-dimensional fully nonlinear wave problems for submerged bodies and for two-dimensional solitons in shallow water. The present study examines surface-piercing bodies in two and three-dimensions using the Eulerian-Lagrangian method in conjunction with the desingularized boundary integral equation technique.

In this work, consideration is only given to the zero forward speed radiation problem in which floating bodies are forced to oscillate in a prescribed manner. As usual, the fluid is assumed ideal and incompressible. No surface tension is considered. The free surface boundary conditions are fully nonlinear, and the body boundary condition is exact. The fluid in the far field is also assumed to be undisturbed and the far field boundary condition $\nabla\phi \rightarrow 0$ is satisfied.

A fast iterative solver GMRES (Saad & Schultz, 1986 and Olson, 1989) is used to solve the descretized three-dimensional boundary integral equations. A preconditioning technique developed by Cao (1991) is adopted to work with the GMRES method so that the speed of GMRES in solving the system is improved. A fourth-order Runge-Kutta method with cubic-spline redistribution as necessary is used for the time stepping. For the problems we have investigated, this technique appears to be numerically stable if a proper time step size is chosen.

The mathematical formulation of the problem is presented in Chapter II. The flow created by the body motion is represented by a singularity distribution above the free surface and inside the body surface. After the singularity strength at each point is solved, the velocity of the free surface can be obtained and the position of the free surface updated. Hydrodynamic forces can also be obtained using Bernoulli equation.

In Chapter III, wave reflection and free surface mean shift are investigated. A large outer region is designed to delay the wave reflection from the truncation boundary and the free surface mean shift. The mean shift results because the far field boundary conditions are ignored. Several outer regions in two and three-dimensions are tested. The distribution factor γ is determined so that a small number of uneven panel spacings can be smoothly distributed in a large outer region. The ever increasing spacing arrangement extends the virtual range of the domain of interest, and wave reflection is delayed.

The stability and convergency properties of the method for two- and three-dimensional floating bodies are investigated in Chapter IV and V, respectively. The convergence rates for heaving and swaying motions are obtained. The Free Surface Stability (FSS) numbers of the desingularized method are found, and the numbers are compared with those of Park & Troesch (1992) and the Courant condition of Dommermuth & Yue (1986). For two-dimensional cases, the numerical results for the added mass and wave damping are compared with those of Vugts (1968). In three-dimensions, the wave elevations and hydrodynamic force of an axisymmetric vertical cylinder are compared with those of Dommermuth & Yue (1987).

Finally, Chapter VI concludes the dissertation and offers suggestions for further research.

CHAPTER II

MATHEMATICAL FORMULATION AND NUMERICAL APPROACH

2.1 Initial-Boundary Value Problem

As shown in Figure (2.1), cartesian coordinates that refer to an absolute inertial frame are used. The z-axis points upward and the $x - y$ plane is coincident with the still water level. The fluid domain, D, is bounded by the free surface, S_f, the body surface, S_b, the bottom surface, S_h and the enclosing surface at infinity, S_∞. Nonlinear waves are generated by a floating body undergoing forced oscillations. The problem will be formulated as an initial boundary value problem in the time-domain.

The fluid is assumed to be inviscid, incompressible and surface tension is neglected. The problem is started from rest so that the flow remains irrotational. This implies the existence of a velocity potential such that the fluid velocity $\vec{\mathbf{u}}$ is given by

$$\vec{\mathbf{u}}(\vec{\mathbf{X}}, t) = \nabla \phi \tag{2.1}$$

where $\vec{\mathbf{X}} = (x, y, z)$ is the field point and t is time.

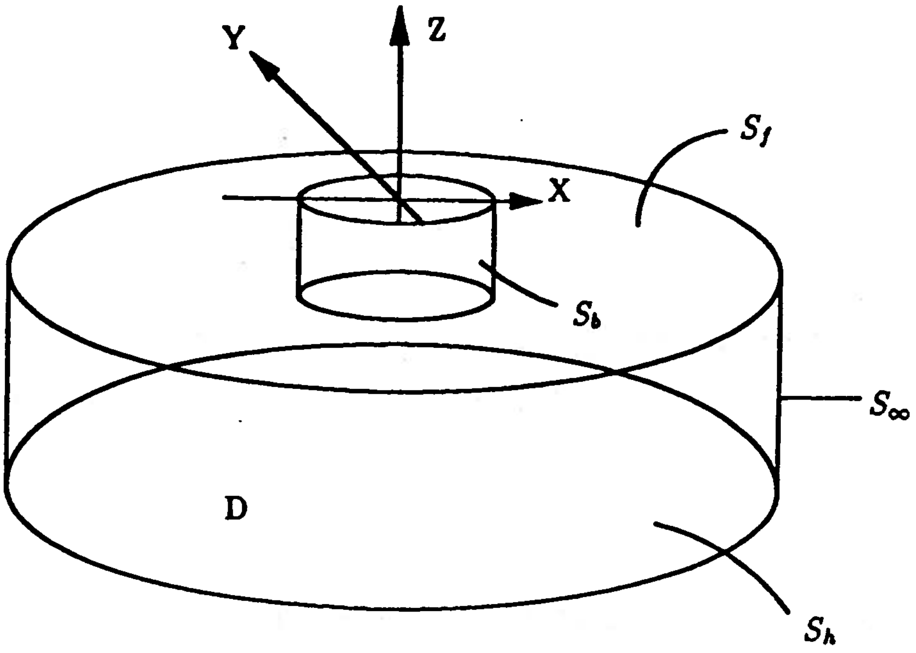

Figure 2.1: Problem definition and coordinate system

2.1.1 Governing Equation and Boundary Conditions

By satisfying the continuity equation, the covering equation in the fluid domain for the boundary value problem is the Laplace equation

$$\Delta\phi = 0 \qquad \text{(in } D\text{)} \qquad (2.2)$$

Proper boundary conditions must be applied on all the boundary surfaces. The kinematic boundary conditions on the body surface and the bottom are given by

$$\frac{\partial\phi}{\partial n_b} = \vec{V}_b \cdot \vec{n}_b \qquad \text{(on S}_b\text{)} \qquad (2.3)$$

$$\frac{\partial\phi}{\partial n_h} = \vec{V}_h \cdot \vec{n}_h \qquad \text{(on S}_h\text{)} \qquad (2.4)$$

where $\vec{V}_b$ and $\vec{V}_h$ are the velocities of the body surface and the bottom surface, and $\vec{n}_b$ and $\vec{n}_h$ are the unit normal vectors to the two surfaces respectively. Positive $\vec{n}$ is defined as out of the fluid into the body.

For an infinitely deep water case, equation (2.4) reduces to

$$\nabla\phi \rightarrow 0 \qquad \text{(as z} \rightarrow -\infty)$$

The boundary condition applied on the far field boundary requires that the disturbance vanish at infinity such that

$$\nabla\phi \rightarrow 0 \qquad (\text{on } S_\infty)$$

The kinematic free surface boundary condition requires that the normal velocity of the fluid and of the free surface are equal

$$\frac{D}{Dt}(\eta - z) = 0 \qquad (\text{on } S_f)$$

or

$$\frac{\partial\eta}{\partial t} + \frac{\partial\phi}{\partial x}\frac{\partial\eta}{\partial x} + \frac{\partial\phi}{\partial y}\frac{\partial\phi}{\partial y} - \frac{\partial\phi}{\partial z} = 0 \qquad (\text{on } S_f). \qquad (2.5)$$

where $\eta = \eta(x, y, t)$ is the free surface elevation. The dynamic boundary condition requires that the pressure on the free surface equals the air pressure, p_{air}

$$\frac{p_{air}}{\rho} = -\frac{\partial\phi}{\partial t} - \frac{1}{2}|\nabla\phi|^2 - g\eta \qquad (\text{on } S_f). \qquad (2.6)$$

2.1.2 Initial Conditions

For a three-dimensional initial boundary value problem, the initial conditions correspond to starting the body from rest. The position of the free surface and the velocity potential on free surface should also be given. When time is equal to zero,

$$\begin{aligned} \phi_o &= 0 \qquad && (\text{in D, at t} = 0) \\ \eta_o &= 0 \qquad && (\text{on } S_f, \text{ at t} = 0) \end{aligned} \qquad (2.7)$$

where p_a is the ambient pressure on free surface and is also set to zero. Equation (2.6) and the above initial conditions implies that $\frac{\partial\phi}{\partial t}$ is zero when time is zero.

The initial position and velocity of the body are prescribed as

$$\begin{aligned} X &= X_o && (\text{on } \mathrm{S_b},\ \text{at } \mathrm{t}=0) \\ v &= v_o(x,y,z) && (\text{on } \mathrm{S_b},\ \text{at } \mathrm{t}^+=0) \end{aligned} \tag{2.8}$$

where

X_o is a known initial body position in the absolute coordinate system

v_o is a known initial body velocity

2.1.3 Pressure, Forces and Moments

Once the velocity potential ϕ is determined, the pressure at any point on the body surface can be evaluated using the Bernoulli equation

$$\begin{aligned} \frac{p}{\rho} &= -\frac{\partial\phi}{\partial t} - \frac{1}{2}|\nabla\phi|^2 - gz \\ &= -\frac{\delta\phi}{\delta t} - (\frac{1}{2}\nabla\phi - \vec{V}_b)\cdot\nabla\phi - gz && (\text{on } \mathrm{S_b}) \end{aligned} \tag{2.9}$$

where

$$\frac{\delta\phi}{\delta t} = (\frac{\partial\phi}{\partial t} + \vec{V}_b\cdot\nabla)\phi$$

is the time derivative of the potential following the point on S_b moving with velocity $\vec{V}_b$. The second form of Eq.(2.9) is more useful when computing pressure on the moving body. The forces and the moments can be calculated by integrating the pressure over the body surface,

$$\vec{F} = \int\int_{S_b} p\vec{n}_b ds \tag{2.10}$$

and

$$\vec{M} = \int\int_{S_b} p(\vec{r} \times \vec{n_b})ds \tag{2.11}$$

where $\vec{r}$ is the position vector of a body surface point to the origin.

2.2 Numerical Approach : the Desingularized Eulerian-Lagrangian Time-domain Approach (the DELTA method)

A boundary integral equation method (BEIM) is generally used to solve water wave problems if the fluid is ideal fluid and the flow is irrotational so that the Laplace equation is the governing equation. The method has been successfully applied to a large variety of two- and three-dimensional nonlinear free surface flow problems. Longuet-Higgins & Cokelet (1976) used a mixed Eulerian-Lagrangian time-stepping scheme for solving two-dimensional fully nonlinear surface wave problems.

Their time stepping procedure requires two major steps:

1. solving a boundary value problem in an Eulerian frame to obtain the velocity on the free surface; and
2. updating the positions and velocity potential of Lagrangian points by integrating the nonlinear kinematic and dynamic free surface boundary conditions with respect to time.

These in turn serve as the boundary conditions of the field equation at the next time step.

In this thesis, the mixed Eulerian-Lagrangian scheme is used. The free surface boundary conditions, equations (2.5) and (2.7), can be rewritten in terms of the material derivative at a point moving with a velocity $\nabla\phi$. By adding $\nabla\phi \cdot \nabla\eta$ to both sides of (2.5) and $\nabla\phi \cdot \nabla\phi$ to both sides of (2.7), the kinematic and dynamic conditions can be put in the form

$$\begin{aligned} \frac{D\vec{X}_f}{Dt} &= \nabla\phi && \text{(on S}_\text{f}\text{)} \\ \frac{D\phi}{Dt} &= -\frac{p_{air}}{\rho} + \frac{1}{2}\left|\nabla\phi\right|^2 - gz_f && \text{(on S}_\text{f}\text{)} \end{aligned} \tag{2.12}$$

where the material derivative is given by

$$\frac{D}{Dt} = \frac{\partial}{\partial t} + \nabla\phi \cdot \nabla$$

and the position vector of a free surface particle is $\vec{X}_f = (x_f, y_f, z_f)$.

For the present time-dependent form of the nonlinear initial boundary value problem, the technique of the desingularized Eulerian-Lagrangian time-domain approach developed by Cao, Schultz and Beck (1990) is extended to solve boundary value problems with a floating body oscillating in deep or shallow water. In contrast to the conventional boundary integral equation method, the singularities in the DELTA method are placed away from the boundary and outside the domain of the problem.

After studying both the direct and indirect versions of the DELTA method, Cao, Schultz & Beck (1991a) suggested that the indirect version of the method was more favorable because it was more efficient and easier to code. When initial boundary value problems with infinite boundaries were considered in time-domain calculations, the indirect method used less computational time and gave more accurate solutions. In addition, the indirect version of the method showed no difficulty in handling irregular meshes.Considering these advantages, the indirect version of the desingularized Eulerian-Lagrangian time-domain approach will be used throughout this thesis.

When the desingularized method is used to solve the initial boundary value problem, the nondimensional desingularization distance is set to be

$$L_d = l_d(D_m)^\alpha, \tag{2.13}$$

where l_d reflects how far the integral equation is desingularized, D_m is the nondimensional local mesh size (usually the square root of the local mesh area in a three-dimensional problem and the local mesh size in a two-dimensional problem) and α is a parameter associated with the convergence of the solution as the mesh is refined.

Cao, Schultz & Beck (1991a) conducted numerical tests in which an integral of a constant source distribution over a square flat surface is evaluated at a point above the center of the square with a distance given by equation (2.13). They found that $\alpha = 0.5$ and $l_d = 1.0$ are about the optimum values for the performance of the desingularized method. These two values are used for all calculations presented in this thesis.

At each time step, the boundary value problem is

$$\Delta\phi = 0 \qquad \text{(in } D\text{).} \tag{2.14}$$

$$\phi = \phi_o \qquad \text{(on } S_{f_o}\text{).} \tag{2.15}$$

$$\frac{\partial\phi}{\partial n_b} = \vec{V}_b \cdot \vec{n}_b \qquad \text{(on S}_\text{b}\text{)} \tag{2.16}$$

$$\frac{\partial\phi}{\partial n_h} = \vec{V}_h \cdot \vec{n}_h \qquad \text{(on S}_\text{h}\text{)} \tag{2.17}$$

$$\nabla\phi \to 0 \qquad \text{(on S}_\infty\text{).} \tag{2.18}$$

where ϕ_o and S_{f_o} are known from the previous time step.

With the given potential on the free surface and the known normal velocity on the body surface and the bottom, the potential at any point in the fluid domain is obtained by

$$\phi(\vec{X}) = \int\int_{\Omega} \sigma(\vec{X}_s) \frac{1}{|\vec{X} - \vec{X}_s|} d\Omega, \tag{2.19}$$

where Ω is the integration domain outside the problem domain.

Applying the boundary conditions, the desingularized boundary integral equations for the unknown strength of the singularities $\sigma(\vec{X}_s)$ are :

$$\int\int_{\Omega} \sigma(\vec{X}_s) \frac{1}{|\vec{X}_f - \vec{X}_s|} d\Omega = \phi_o(\vec{X}_f) \qquad (\vec{X}_f \in \Gamma_d) \tag{2.20}$$

and

$$\int\int_{\Omega} \sigma(\vec{X}_s) \frac{\partial}{\partial n} \left(\frac{1}{|\vec{X}_f - \vec{X}_s|} \right) d\Omega = \chi(\vec{X}_f) \qquad (\vec{X}_f \in \Gamma_n) \tag{2.21}$$

where

$\vec{X}_s$	is the point on the integration surface, Ω
$\vec{X}_f$	is the field point on the real boundaries
ϕ_o	is the given potential value at $\vec{X}_f$
χ	is the given normal velocity at $\vec{X}_f$
Γ_d	is the surface on which ϕ_o is given
Γ_n	is the surface on which χ is given

(2.22)

2.2.1 Discretization and Singularity Distribution

To solve the integral equation for $\sigma(\vec{X}_s)$, the collocation method is used. Field points are chosen along the real boundary and sources are distributed outside the computational domain. A set of field points and the corresponding source points are chosen along the contours, S_f, S_b and S_h, as shown in Figure (2.2).

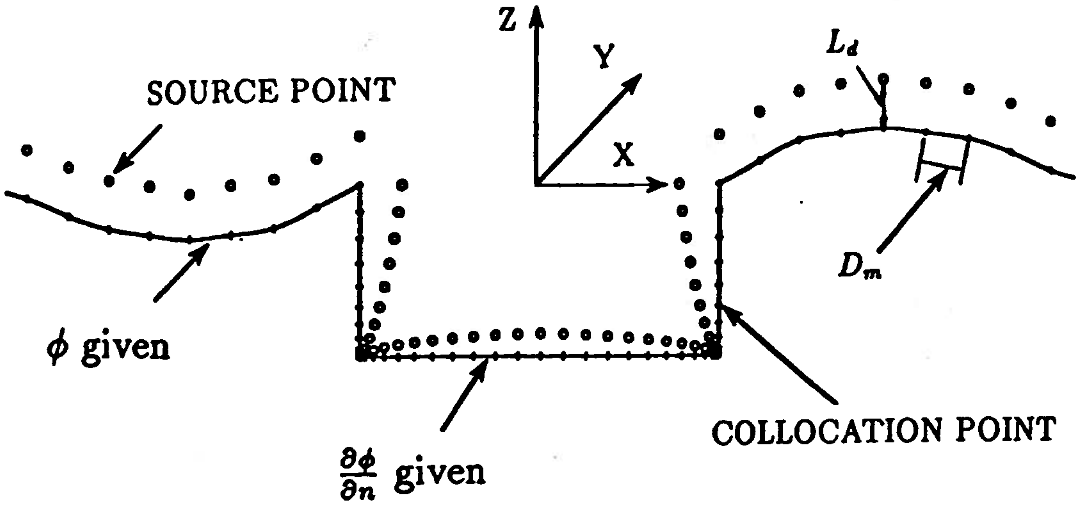

Figure 2.2: Model for numerical simulations

Usually, the integral equation can be discretized into a system of linear equations to be solved at each time step. In the desingularized method, the sources are distributed on the integration surface so that the source points never coincide with the field points and the integrals are nonsingular. In addition, because of the desingularization, simple isolated sources rather than a distribution can be used and the equivalent accuracy in the solution obtained.

The singularities are distributed above the field points on the free surface in the $+z$ direction. Inside the body, the isolated singularities are placed along the normal direction from the field points on the body surface. Numerical difficulties may occur in the vicinity of a sharp edge. One of the difficulties is due to the discontinuity in the unit normal of the surface. The other is that the singularity distribution may cross over the bisector of two body surfaces or even the other side of the body surface since the desingularization distance is proportional to the local surface grid size.

These types of difficulties can be avoided by careful discretization and desingularization. The desingularization distance near a sharp corner is modified so that the singularities are distributed on the bisector of the two body surfaces to avoid the cross over of the singularities beyond the centerline or the body surfaces.

If we establish that N_f , N_b , N_h and N_∞ are the numbers of the panels distributed on the free surface, the body surface, the bottom and the far field boundary respectively, the boundary conditions are

$$\begin{aligned}
\sum_{j=1}^{N_f+N_b+N_h+N_\infty} \sigma(\vec{X}_{sj})G(\vec{X}_{fi},\vec{X}_{sj}) &= \phi(\vec{X}_{fi}), \\
(for \;\; i=1 &\sim N_f) \qquad (2.23) \\
\sum_{j=1}^{N_f+N_b+N_h+N_\infty} \sigma(\vec{X}_{sj})\frac{\partial}{\partial n}G(\vec{X}_{fi},\vec{X}_{sj}) &= \vec{V}_b(\vec{X}_{fi})\cdot\vec{n}_b(\vec{X}_{fi}), \\
(for \;\; i=N_f+1 &\sim N_f+N_b) \qquad (2.24) \\
\sum_{j=1}^{N_f+N_b+N_h+N_\infty} \sigma(\vec{X}_{sj})\frac{\partial}{\partial n}G(\vec{X}_{fi},\vec{X}_{sj}) &= \vec{V}_h(\vec{X}_{fi})\cdot\vec{n}_h(\vec{X}_{fi}), \\
(for \;\; i=N_f+N_b+1 &\sim N_f+N_b+N_h) \qquad (2.25) \\
\sum_{j=1}^{N_f+N_b+N_h+N_\infty} \sigma(\vec{X}_{sj})\bigtriangledown G(\vec{X}_{fi},\vec{X}_{sj}) &= \vec{V}_\infty(\vec{X}_{fi}), \\
(for \;\; i=N_f+N_b+N_h+1 &\sim N_f+N_b+N_h+N_\infty) \qquad (2.26)
\end{aligned}$$

where,

$$G(\vec{X}_{fi},\vec{X}_{sj}) = \frac{1}{\left|\vec{X}_{fi}-\vec{X}_{sj}\right|}$$

ϕ	is the velocity potential
$\vec{X}_{fi}$	is the i^{th} field point on the boundaries
$\vec{X}_{sj}$	is the j^{th} source point outside the computational domain
$\vec{V}_b(\vec{X}_{fi})$	is the velocity of the i^{th} field point on the body surface
$\vec{n}_b(\vec{X}_{fi})$	is the inward unit normal vector to the body surface, out of fluid

$\vec{V}_h(\vec{X}_{fi})$	is the velocity of the i^{th} field point on the bottom
$\vec{n}_h(\vec{X}_{fi})$	is the outward unit normal vector to the bottom, out of fluid
$\vec{V}_\infty(\vec{X}_{fi})$	is the velocity of the i^{th} field point on the far field boundary and is assumed to be zero at all time

Combining equations (2.23), (2.24), (2.25) and (2.26), we obtain a linear system of **m** algebraic equations

$$\mathbf{A}_{m\times m} \cdot \vec{\mathbf{X}}_m = \vec{\mathbf{B}}_m \tag{2.27}$$

where,

m	is the total number of field points
$A_{m\times m}$	is the influence function matrix with $m \times m$ elements
$\vec{X}_m$	is the unknown source strength vector, $\sigma(\vec{X}_s)$, to be solved
$\vec{B}_m$	is the known vector which contains the values of ϕ at the field points on the free surface and the values of $\dfrac{\partial\phi}{\partial n}$ at the field points on the body surface and the bottom.

Once equation (2.26) is solved, $\nabla\phi$ can be evaluated on S_f, and the kinematic and dynamic conditions on the free surface can be integrated in time.

In order to solve the large scale linear equation system, a Generalized Minimized Residual (GMRES) algorithm (Saad and Schultz, 1986 and Olsen, 1989) with preconditioning developed by Cao (1992) is employed.

2.2.2 Free Surface Updating

A Runge-Kutta fourth-order scheme is used to update the potential and position of the field points on the free surface. The grid spacing on the body surface are then repanelized with a semi-cosine distribution due to the change of wave elevation at the intersection line. The collocation points distributed on the intersection line satisfy the free surface boundary conditions and are constrained to slide along the body surface.

2.2.3 Instability, Smoothing and Redistribution

Longuet-Higgins & Cokelet (1976) discuss a 'sawtooth' instability in their research with breaking waves. After careful study, they found the cause of the instability was partially numerical and partially physical. They used a smoothing technique to suppress the development of this instability. Baker *et al.* (1982) and Lin *et al.* (1984) both used a smoothing operator to reduce the instabilities when the waves became steep.

It is now believed that such high-wavenumber instabilities are related to the accuracy of the velocity calculations for the free surface particles. However, the real reasons which cause the instability are still not clear and may well depend on the numerical implementation used.

Dommermuth & Yue (1987) assumed that a root cause of the instability was the concentration of Lagrangian points in the region of higher gradients. They developed a regridding algorithm to eliminate the instabilities without using artificial smoothing. Dommermuth *et al.* found that the regridding technique was sufficient and conventional smoothing techniques were not necessary. The regriding could easily be applied at the body-free surface intersection line, and there was no need to find a smoothing formula for a particular problem.

In this thesis, a redistribution technique is used to suppress the possible numerical instabilities. After a certain number of time steps, the solution procedure is interrupted and the field points on free surface are redistributed using a cubic-spline technique. The calculations are then restarted with a continuation of the fourth-order Runge-Kutta evaluation.

2.3 Nondimensionalization

The fundamental variables, ρ, g and H are used to nondimensionalize all the other variables. ρ is the density of the fluid, g is the gravitational acceleration and H is the initial draught of the body. Thus,

$$\begin{aligned}
\bar{H} &= 1.0 && \text{is the nondimensional draught} \\
\bar{\vec{X}} &= \frac{\vec{X}}{H} && \text{is the nondimensional position vector} \\
\bar{R} &= \frac{R}{H} && \text{is the nondimensional radius} \\
\bar{D}_m &= \frac{D_m}{H} && \text{is the nondimensional panel size} \\
\bar{\omega} &= \omega\sqrt{\frac{H}{g}} && \text{is the nondimensional forcing frequency} \\
\bar{\vec{V}}_b &= \frac{\vec{V}_b}{\sqrt{gH}} && \text{is the nondimensional body velocity} \\
\bar{\vec{V}}_h &= \frac{\vec{V}_h}{\sqrt{gH}} && \text{is the nondimensional bottom velocity}
\end{aligned}$$

The nondimensionalized system, the bar system, will be used but bars on all the variables will be dropped from now on. The numerical results shown in this thesis are all based on nondimensionalized variables unless otherwise mentioned. Also, p_{air} is the air pressure and is taken as zero. Consequently, the nondimensional governing equation and boundary conditions are

$$\Delta\phi = 0 \qquad \text{(in } D\text{)} \tag{2.28}$$

and

$$\frac{D\vec{X}_f}{Dt} = \nabla\phi \qquad \text{(on S}_\mathrm{f}\text{)} \qquad (2.29)$$

$$\frac{D\phi}{Dt} = \frac{1}{2}\left|\nabla\phi\right|^2 - z_f \qquad \text{(on S}_\mathrm{f}\text{)} \qquad (2.30)$$

$$\frac{\partial\phi}{\partial n_b} = \vec{V}_b \cdot \vec{n}_b \qquad \text{(on S}_\mathrm{b}\text{)} \qquad (2.31)$$

$$\frac{\partial\phi}{\partial n_h} = \vec{V}_h \cdot \vec{n}_h \qquad \text{(on S}_\mathrm{h}\text{)} \qquad (2.32)$$

$$\nabla\phi \rightarrow 0 \qquad \text{(on S}_\infty\text{).} \qquad (2.33)$$

CHAPTER III

FAR FIELD BOUNDARY AND FAR FIELD BOUNDARY CONDITIONS

A proper treatment of the far field boundary is crucial to the study of wave propagation problems. Cost and data storage limitations dictate the use of a small computational domain which contains only a few dominant waves. One serious difficulty encountered is how to appropriately handle the far field boundaries during numerical simulations, so that the region of interest will not be contaminated by wave reflections and other effects, such as a free surface mean shift.

The free surface mean shift problem arises if the far field boundary condition is ignored. The initial boundary value problem becomes ill-posed and the solution of the boundary value problem is then not unique. A family of solutions may be obtained by adding homogeneous solutions to the exact solution. The added homogeneous solutions may introduce a positive or negative net flux into the fluid domain through the unspecified boundary surfaces. Consequently, the mean position of the free surface starts to move.

For forward speed problems, Cao, Schultz & Beck (1990) avoided the mean shift of the free surface by using a shifting window technique. For the upstream boundary, a calm water far field boundary condition was enforced. On the downstream side, one row of node points were dropped whenever the window was shifted. The treatment prevented wave reflection at the downstream boundary. For zero forward speed problems, the technique is not adaptable because there exists neither an upstream nor a downstream in the computational domain. The free surface mean shift problem can not be resolved due to the neglect of the far field boundary conditions.

Wave reflection is also a critical concern for problems with a truncated computational domain. A simple but effective treatment of the far field boundary should be set forth to delay the free surface mean shift and wave reflection from the truncation boundary. Therefore, numerical simulations can be carried out for a long enough time such that the convergence and stability properties of the DELTA method can be studied and the hydrodynamic forces and free surface wave profiles obtained.

3.1 Investigation of Free Surface Mean Shift and Wave Reflection in Two-Dimensions

Numerical investigations of the free surface mean shift and wave reflection are conducted. First, we consider a two-dimensional floating box undergoing vertical or lateral forced oscillations. A coordinate system with x positive to the right and z positive upward is used. Initially, a relatively small truncated computational domain (on the order of a wavelength) is chosen to investigate how the free surface behaves when the far field boundary condition is ignored.

The fluid is infinitely deep. The floating box has a breadth, B , and an initial draught, H , where B is equal to $2H$. The free surface is discretized in such a way that the variation of panel size near the intersection points is smooth.

Newman (1985) and Newman & Lee (1992) recommended a cosine distribution of the grid points on the body surface to anticipate the singular flow at the sharp corners. They compared solution accuracy of equal-spacing and cosine-spacing distributions; finding that more panels are necessary for the equal-spacing distributions to achieve the same accuracy.

In Chapter V, we show that the difference between the solutions obtained by a semi-cosine and cosine spacings is within 0.025 % when equal numbers of panels are used. But, the time step size used in cosine spacing should be much smaller than in semi-cosine spacing considering the stability of the numerical scheme near the intersection points. Therefore, a semi-cosine distribution with the smallest panel distributed near the corners is used to panelize the surface of the box.

The body is started from rest and oscillated vertically or horizontally. The velocity of the box is prescribed as

$$U(t) = \begin{cases} 0 & \text{if } t < 0 \\ \pm\,\omega a \; cos(\omega t) & \text{if } t \geq 0 \end{cases}$$

where

$$\begin{aligned} \omega &= \frac{\pi}{3} \text{ is the excitation frequency} \\ a &= 0.1 \text{ is the oscillation amplitude} \end{aligned}$$

Figures (3.1) and (3.2) show the time histories of the free surface when the box oscillates vertically and laterally, respectively. As can be seen, the mean position of the free surface shifts as the numerical simulation proceeds.

Wave reflection is also observed in figures (3.1) and (3.2). The wave amplitude is changed and the wave shape is distorted due to the reflection. Once the initial outgoing wave train reaches the truncation boundary, the waves reflect back and the solutions are contaminated. The wave reflection problem can be investigated by calculating some type of reflection coefficient. While wave reflection is physical, the mean shift is purely the consequence of the improper application of the far field boundary conditions. Both mean shift and wave reflection will contaminate the results in the inner domain.

3.2 Large Scale Outer Region

If it were possible to use an infinitely large computational domain, then there would be no problems with free surface mean shift and wave reflection because the far field boundary conditions would be satisfied. However, it is impossible to use an infinite computational domain in numerical calculations. In this thesis, a large scale outer region is proposed to postpone the free surface mean shift and wave reflection from the truncation boundary.

3.2.1 Free Surface Mean Shift

Forced periodic heaving motions of a floating box are used to investigate the free surface mean shift problem. In order to determine the proper scope of the outer region, five different sizes of the region are tested. The length of the outer region, L_{out} , of the first, second, third, fourth and fifth cases are 20λ , 40λ , 60λ , 80λ , 100λ respectively, where λ is the linear wavelength corresponding to the forcing frequency. In deep water, λ is determined by the dispersion relation, $\lambda = \frac{2\pi}{\omega^2}$.

Figure (3.3) shows the mean position of the free surface changing in time for swaying motions of a two-dimensional box. For each numerical simulation, the same initial condition is used but a different size of the computational domain is applied. The results show that the mean shift is detained as the range of computational domain is increased. When the length of the computational domain is greater than or equal to 80λ and the simulation time is less than 16 motion periods, the mean shifting rate of the free surface is about 6.7×10^{-7} per period. Therefore, the lower limit of the length of the computational domain is chosen to be 80λ .

3.2.2 Wave Reflection

A series of two-dimensional numerical experiments using a large outer region have been conducted and the parameters of the outer region selected.

In the numerical tests, the whole free surface domain is composed of two regions, an inner region (the domain of interest) and an outer region. The number of panels distributed in the outer region, N_{out} , is chosen to be 20. The length of the inner and outer region, L_{in} and L_{out} , are chosen to be 4λ and 80λ . A numerical wave probe, station A , is placed at a distance of 3λ away from the body. A total of 160 grid points are used on the body surface and free surface (20, 120 and 20 segments on the body surface, the inner and outer domains of the free surface, respectively). Uniform panel size, D_m , is used in most parts of the inner domain except in the region near the body-free surface intersection point. The variation of panel size should be smooth to reduce the numerical error caused by the change in panel size. On the body surface, a semi-cosine spacing distribution is applied.

In the outer region, 20 exponential-like grid spacings are distributed. The grid spacings D_{out} in the outer domain are designed to grow at a rate of γ with the largest spacing located at the far end of the outer region. The panel sizes in the outer region are

$$(D_{out})_N = (D_{o1}) \cdot (\gamma)^{N(N-1)/2} \tag{3.1}$$

for $N = 1 \sim N_{out}$

where

D_{o1} is the size of the first panel in the outer domain

γ is the distribution factor

The body is oscillated through one cycle and stopped. With good arrangement in panel size near the junction of the inner and outer domains, the radiating waves will transmit into the outer region and wave reflection is delayed. The effectiveness of the panel size arrangement near the junction can be examined by computing the contamination coefficient.

The contamination coefficient, C_c , is defined to be the normalized RMS difference of wave elevation between a contaminated wave elevation curve and the standard wave elevation curve, i.e.

$$C_c(T_o) = \frac{RMS_\eta}{\bar{\eta}_s} \tag{3.2}$$

where

$$RMS_\eta = \sqrt{\frac{\sum_{i=1}^{N}(\eta_c(i) - \eta_s(i))^2}{N}}$$

$$\bar{\eta}_s = \sqrt{\frac{\sum_{i=1}^{N}\eta_s(i)^2}{N}}$$

N the total number of points in the time record at station A

T_o the duration of the time history used in the calculation of C_c

$\eta_c(i)$ the i^{th} contaminated wave elevation record at station A

$\eta_s(i)$ the i^{th} standard wave elevation record at station A

A wave elevation curve is obtained by recording the time history of the wave elevation at station A . The standard wave elevation curve is shown in figure

(3.4) and is acquired by using a significantly larger inner domain in order to run the simulation without wave reflection arriving back at station A . The waves are produced by a single impulse of the body and the results are considered reliable as long as the domain is big enough and the simulation is stopped before the wave front reaches the border of the inner domain. The sizes of the inner and outer domains for the standard curve are $L_{in} = 40\lambda$ and $L_{out} = 80\lambda$, respectively. The panel number in the outer domain, N_{out} , is chosen to be 20.

An example of wave reflection from the outer domain is shown in figure (3.5). L_{in} and L_{out} are 4λ and 80λ while N_{out} is 20. The variation of panel size near the junction of the inner and outer domains is smooth, which will be shown in table (3.1) to be the optimum panel size arrangement in delaying wave reflection. Using the same initial waves as in figure (3.4), the outgoing waves reflect back from the outer domain after the time is greater than T_c . In other words, the outer domain essentially postpones but does not eliminate wave reflection. Waves reflection at station A is prevented until the simulation time is larger than T_c . It will also be shown in table (3.5) that $\frac{T_c}{period}$ is approximately independent of motion frequency. Therefore, for $L_{in} = 4\lambda$, $L_{out} = 80\lambda$ and $N_{out} = 20$, $\frac{T_c}{period} \approx 13$. Thus, if the simulation duration, T_o , is less than T_c , there will be less than 1% wave reflection for the optimum outer region configuration.

For perfect reflection, all of the outgoing waves are reflected from the junction of the inner and outer domains and pass station A . The wave elevation at station A will then include both the radiating and reflected waves. The reflected waves keep on traveling toward the body, bounce back from the body surface and cross station A again when time is T_1 where T_1 depends on the forcing frequency of the body, the

Table 3.1: The contamination coefficients and distribution factors for various D_{o1} on the free surface, $N_{out} = 20$, $L_{in} = 4\lambda$, $L_{out} = 80\lambda$, forcing frequency $= \frac{\pi}{3}$, motion amplitude = 0.1, $D_m = \frac{\lambda}{30}$, $\frac{T_o}{period} = 10$

D_{o1}	4λ	λ	$\lambda/2$	$\lambda/4$	$\lambda/8$	$\lambda/16$	$\lambda/30$	$\lambda/40$	$\lambda/50$	$\lambda/60$	$\lambda/70$	$\lambda/80$	$\lambda/100$	$\lambda/200$
γ	1.0000	1.0147	1.0201	1.0249	1.0295	1.0339	1.0378	1.0396	1.0409	1.0421	1.0430	1.0438	1.0451	1.0493
$C_c(T_o)$ %	94.23	60.79	38.62	22.75	10.88	2.98	0.49	1.12	5.75	15.97	28.78	39.21	61.24	92.37

location of the probe and the location of the reflecting boundary. The free surface elevation then includes the radiating waves, the first reflected waves and the second reflected waves.

If we want C_c to only measure the contamination due to reflection of the outer region and not include the reflection from the body, the duration of the wave elevation record at station A , T_o should be also less than T_1 . We place the wave probe near the junction of the inner and outer domains in order to make $T_c < T_1$, such that the contamination coefficient can be properly measured.

As the contaminated wave elevation is approximately the sum of the radiating waves plus the reflected waves, the contamination coefficient is around 1.0 for perfect wave reflection. When there are no reflected waves, η_c is always equal to η_s and the contamination coefficient will be 0.0. It should be noted that for highly nonlinear waves which significantly change shape upon reflection, C_c may become greater than 1.0 because it involves the square of the amplitude difference.

Table (3.1) shows the resulting contamination coefficients, C_c , for different values of D_{o1} . The panel size at the junction of the inner and outer domains, D_m , is $\frac{\lambda}{30}$. Figure (3.6) summarizes the results of the table (3.1) and some conclusions can be drawn.

It can be concluded from table (3.1) and figure (3.6) that a sharp discontinuity in panel size at the adjacent regions of the inner and outer domain result in significant wave reflection. A smooth variation in D_{out} with $D_{o1} \approx D_m$ works much better. Therefore, equation (3.4) can be rewritten as

$$(D_{out})_N = (D_m) \cdot (\gamma)^{N(N-1)/2} \quad \text{for } N = 1 \sim N_{out} \tag{3.3}$$

where

D_m is the panel size at the junction of the inner and outer domains

As shown in table (3.1), the use of $D_{o1} = D_m$ results in only about 0.49% wave contamination when $\frac{T_o}{period} = 10$. It should be noted that for fixed values of D_{o1} , N_{out} and L_{out} , there exists a single value of γ .

Figure (3.7) shows the waves generated by the heaving box using large and small computational domains and two types of outer region. The large domain is 40λ and is used to produce the standard wave elevation curve, η_s . The small domain is 4λ with D_m equal to $\frac{\lambda}{30}$. The outer region, L_{out} , is 80λ and N_{out} is 20. Two different values of D_{o1} are used, $D_{o1} = D_m$ and $D_{o1} = 120D_m$. Three curves are shown. The first curve, the dashed line, is the wave elevation curve at

Table 3.2: The contamination coefficient vs size of the outer region, $N_{out} = 20$, $D_m = \frac{\lambda}{30}$, forcing frequency $= \frac{\pi}{3}$, motion amplitude $= 0.1$, $L_{in} = 4\lambda$, $\frac{T_o}{period} = 10$

L_{out}	80λ	120λ	160λ	200λ	240λ	280λ	320λ	360λ
$C_c(T_o)$ %	0.49	0.63	0.82	1.34	4.15	7.98	17.28	26.53

station A computed using the large domain; the second one, the chain-dashed line, is the small domain curve with a good panel distribution ($D_{o1} = D_m$), and the third one is the small domain curve with a poor panel distribution ($D_{o1} = 120D_m$). The first and second curves are so close ($C_c = 0.49\%$) that their difference can not be seen in the figure. This suggests that the small domain results are acceptable as long as proper panel size distribution is used. The third curve shows how bad the small domain results are contaminated by wave reflection if improper values of the outer region parameters are used.

As concluded in the previous section, the outer region should be as large as possible so that the mean shift on the free surface can be postponed. However, there does exist an upper limit for the size of the region if only a fixed number of panels are to be distributed in it. Thus, as the region size grows, the panel sizes increase too fast and wave reflection occurs too early. Table (3.2) summarizes the contamination coefficients of different lengths of the outer region. D_m is set to be $\frac{\lambda}{30}$ and L_{in} is 4λ . For each case, a smooth spacing distribution is used in the outer domain with the first spacing equal to D_m . The results show that the most appropriate size of the outer region, L_{out} , should be less than or equal to 80λ . However, if L_{out} is smaller than 80λ , then the free surface mean shift is too large as shown in figure (3.3).

Table 3.3: The contamination coefficient vs size of the outer region, $D_m = 30$, forcing frequencies = $\frac{\pi}{6}$ and $\frac{2\pi}{3}$, motion amplitude = 0.1, $L_{in} = 4\lambda_{\omega_2}$, $L_{out} = 1280\lambda_{\omega_2}$, $\frac{T_o}{period} = 10$

N_{out}	20	22	24	26	28	30	32	34	36	38
$C_c(T_o)$ %	38.47	19.63	7.54	2.84	1.41	0.78	0.46	0.39	0.35	0.32

When multiple frequencies are presented in the forced motion, D_m should be set equal to the appropriate D_m of the highest frequency to properly represent the shortest waves, and L_{out} should be equal to the L_{out} of the lowest frequency to reduced the free surface mean shift. As an example, a two frequency motion system, $\omega_1 = \frac{\pi}{6}$ and $\omega_2 = \frac{2\pi}{3}$, is considered. The linear wavelengths of the two frequencies are λ_{ω_1} and λ_{ω_2} respectively. A two-dimensional box is oscillated with forcing frequencies, ω_1 and ω_2, and D_{o1} is set equal to D_m (i.e. $D_m = \frac{\lambda_{\omega_2}}{30}$). The lengths of the inner and outer regions, L_{in} and L_{out}, are $4\lambda_{\omega_1}$ and $80\lambda_{\omega_1}$ (i.e. $64\lambda_{\omega_2}$ and $1280\lambda_{\omega_2}$). Therefore, N_{out} is the only parameter to be determined to delay wave reflection.

The standard wave elevation curve for the double-frequency motion system is obtained by oscillating the box through one double-frequency cycle using a significant larger domain. The L_{in} and L_{out} are $40\lambda_{\omega_1}$ and $80\lambda_{\omega_1}$, respectively. Table (3.3) shows how the wave reflection corresponds to N_{out}. As shown, the contamination coefficient decreases as N_{out} increases. The contamination coefficient becomes less than 1% when N_{out} is greater than or equal to 30. We may conclude that N_{out} should be modified whenever L_{out} is changed. In order to effectively delay wave reflection, a greater N_{out} is necessary if a larger L_{out} is used.

Table (3.4) investigates the effectiveness of the outer region as the inner domain

Table 3.4: The two-dimensional distribution factor, γ, vs uniform panel sizes on the free surface, $N_{out} = 20$, $L_{in} = 4\lambda$, $L_{out} = 80\lambda$, forcing frequency = $\frac{\pi}{3}$, motion amplitude = 0.1, $\frac{T_o}{period} = 10$

D_m	$\lambda/20$	$\lambda/30$	$\lambda/40$	$\lambda/50$	$\lambda/60$	$\lambda/70$	$\lambda/80$
γ	1.0353	1.0378	1.0396	1.0409	1.0421	1.0430	1.0438
$C_c(T_o)$ %	0.42	0.49	0.53	0.59	0.66	0.72	0.77

panel size is varied. The contamination coefficient, C_c , remains small regardless of the uniform panel size, D_m . For a fixed N_{out} , C_c increases slightly because the growth rate of panel size in the outer region increases as $D_{o1} = D_m$ is decreased. This causes greater wave reflection. γ changes slightly even though D_m varies by a factor of 4.

The defined contamination coefficient is also used to investigate the performance of the outer region for different motion frequencies. The sizes of the inner and outer domains, L_{in} and L_{out} , are 4λ and 80λ respectively. The motion amplitude is 0.1; the frequency range is from $\frac{\pi}{6}$ to $\frac{4\pi}{6}$. As seen from table (3.5), the effectiveness of the outer region is not influenced by the frequency in the given range as long as the number of grid points per wavelength remains unchanged and the duration of the numerical simulation is less than T_c . It is also seen from table (3.5) that $\frac{T_c}{period}$ is approximately constant for the different frequencies and the given outer region parameters.

In conclusion, the calculations have shown that the outer region is effective in delaying mean free surface shift and wave reflection. The first panel size, D_{o1} , should be set equal to the last panel in the inner region. The panel number in the outer region, N_{out} , is critical. As L_{out} increases, N_{out} must also increase. With

Table 3.5: The contamination coefficient vs oscillating frequency, $N_{out} = 20$, $L_{in} = 4\lambda$, $L_{out} = 80\lambda$, motion amplitude = 0.1, $\frac{T_o}{period} = 10$

Forcing frequency	$\frac{\pi}{6}$	$\frac{2\pi}{6}$	$\frac{3\pi}{6}$	$\frac{4\pi}{6}$	$\frac{\pi}{6}$	$\frac{2\pi}{6}$	$\frac{3\pi}{6}$	$\frac{4\pi}{6}$
Panel number/ λ	20	20	20	20	30	30	30	30
Approx. $\frac{T_c}{period}$	13	13	13	13	13	13	13	13
$C_c(T_o)$ %	0.41	0.42	0.41	0.42	0.50	0.49	0.52	0.51

L_{out} equal to 80λ , a minimum of $N_{out} = 20$ has been found to be necessary. Using optimum values of L_{out} , D_{o1} and N_{out} , and limiting T_o to be less than T_c , the contamination coefficient, C_c , will be less than 1% regardless of frequency or wave amplitude. For all subsequent two-dimensional simulations in this thesis with single forcing frequencies, we shall use $D_{o1} = D_m$, $N_{out} = 20$ and $L_{out} = 80\lambda$, and the simulation duration should be less than $T_c = 13$ periods.

3.3 Investigation of Free Surface Mean Shift and Wave Reflection in Three Dimensions

In three dimensions, the wave amplitude of the radiating waves decays at least as fast as the square root of the radial distance whereas the energy density of the two dimensional radiating waves persists and does not change with the distance. The reflection effects and mean shift in three dimensions will therefore not be as bad as in two dimensions. Therefore, a smaller outer region with fewer grid points can be applied to examine the wave reflection in three-dimensions. The range of the outer region is thus chosen to be half that of the two-dimensional case and 10 rows of grid points are distributed in the region.

A right-handed rectangular coordinate system is used for the numerical simula-

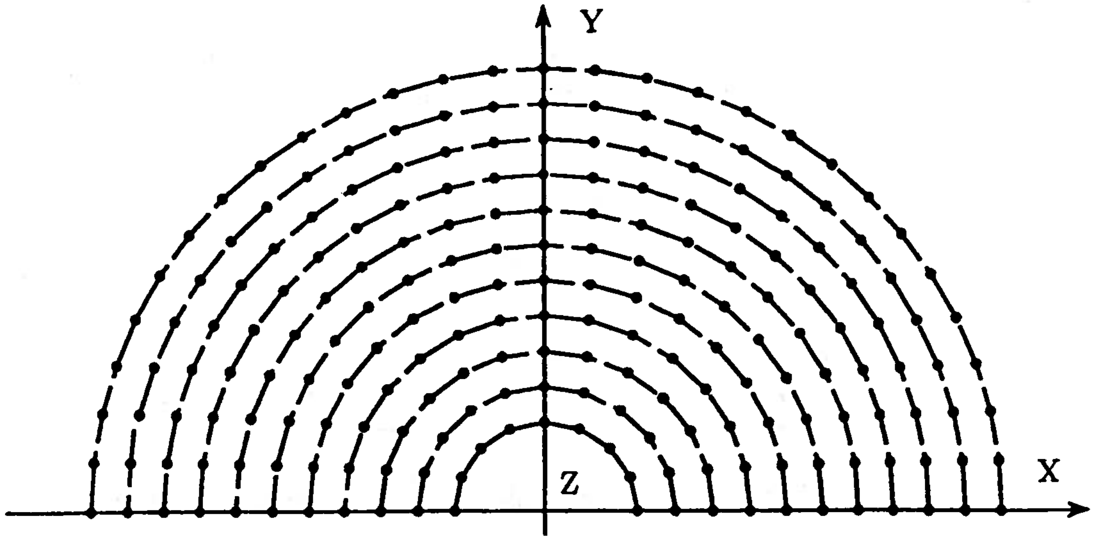

Figure 3.8: Collocation points distribution on the free surface in three dimensions

tions. The $x-$ and $y-$axis lay on the horizontal plane, and the $z-$axis is positive upward. A three-dimensional floating vertical cylinder undergoing forced oscillations is considered to investigate free surface mean shift and wave reflection when no far field boundary conditions are imposed.

The fluid field is assumed to be deep water and the cylinder is of radius R and of initial draught H . The oscillation amplitude is 0.1. The radius is equal to 1.0 and the initial draught is set equal to its radius.

The radius of the inner region is equal to 2λ and that of the outer region is chosen to be 40λ . The inner domain of the free surface is discretized into 60 uniform segments in the radial direction. In the outer domain, 10 ever-increasing grid spacings are employed in the radial direction. A semi-cosine distribution of 20 panels is used on the wall and bottom of the box. In the angular direction, uniform grid spacings are used for all three surfaces.

As shown in figure (3.8), the circumference of the i^{th} ring is larger than that of the $(i-1)^{th}$ one. The first ring, the body-free surface intersection line, is equally divided into N_b portions. In order to divide the free surface into panels with equal sizes, the i^{th} ring is uniformly allocated into $N_b + P_r(i-1)$ panels while the $(i-1)^{th}$ ring is equally apportioned into $N_b + P_r(i-2)$ panels. The P_r is an integer and is determined by

$$P_r = Integer(\frac{2\pi \triangle R}{\triangle C}) \tag{3.4}$$

where

$\triangle R$ is the radius difference for two sequential rings

$\triangle C$ is the arc length for any two successive grid points on the same ring

With $\triangle R = \triangle C$, P_r is found to be 6.

Figure (3.9) compares the mean shift on the free surface for swaying motions in two- and three-dimensions. The sizes of the outer regions are 80λ in two-dimensions and 40λ in three-dimensions. As shown, the free surface mean shift is slower in the three-dimensional cases even though a smaller outer region is used.

Table (3.6) shows the resulting contamination coefficients, C_c , for the different values of D_{o1} . The results of the numerical tests are shown in figure (3.10). When $D_{o1} = D_m$, only about 0.35% wave reflection results for $\frac{T_o}{period} = 5$.

Table (3.7) shows the contamination coefficient for a variety of inner domain panel sizes with $D_{o1} = D_m$. With these D_m , the variation of panel size in the outer region is smooth and the expected wave reflection is negligible.

The frequency sensitivity of the three-dimensional outer region is examined by calculating the contamination coefficient with different frequencies. The inner do-

Table 3.6: The contamination coefficients and distribution factors for various D_{o1} on the free surface, $N_{out} = 10$, $L_{in} = 2\lambda$, $L_{out} = 40\lambda$, forcing frequency $= \frac{\pi}{3}$, motion amplitude = 0.1, $D_m = \frac{\lambda}{30}$, $\frac{T_o}{period} = 5$

D_{o1}	4λ	λ	$\lambda/2$	$\lambda/4$	$\lambda/8$	$\lambda/16$	$\lambda/30$	$\lambda/40$	$\lambda/50$	$\lambda/60$	$\lambda/70$	$\lambda/80$	$\lambda/100$	$\lambda/200$
γ	1.0000	1.1387	1.1451	1.1499	1.1545	1.1622	1.1688	1.1695	1.1708	1.1720	1.1729	1.1737	1.1754	1.1796
$C_c(T_o)$ %	87.33	40.47	18.76	6.13	2.08	0.62	0.35	0.82	2.25	5.07	16.78	23.27	42.58	84.35

Table 3.7: The three-dimensional distribution coefficient, γ, vs panel sizes on the free surface, $N_{out} = 10$, $L_{in} = 2\lambda$, $L_{out} = 40\lambda$, forcing frequency $= \frac{\pi}{3}$, motion amplitude = 0.1, $\frac{T_o}{period} = 5$

D_m	$\lambda/20$	$\lambda/30$	$\lambda/40$	$\lambda/50$	$\lambda/60$	$\lambda/70$	$\lambda/80$
γ	1.1508	1.1688	1.1703	1.1765	1.1817	1.1860	1.1897
$C_c(T_o)$ %	0.33	0.35	0.38	0.42	0.47	0.54	0.60

Table 3.8: The contamination coefficient vs oscillating frequency, $N_{out} = 10$, $L_{in} = 2\lambda$, $L_{out} = 40\lambda$, motion amplitude = 0.1, $\frac{T_o}{period} = 5$

Forcing frequency	$\frac{\pi}{6}$	$\frac{2\pi}{6}$	$\frac{3\pi}{6}$	$\frac{4\pi}{6}$	$\frac{\pi}{6}$	$\frac{2\pi}{6}$	$\frac{3\pi}{6}$	$\frac{4\pi}{6}$
Panel number/ λ	20	20	20	20	30	30	30	30
$C_c(T_o)$ %	0.31	0.33	0.33	0.32	0.36	0.35	0.36	0.34

main is 2λ and the outer domain is 40λ . The D_m are used to determine the panel sizes in the outer domain. The frequency is changed from $\frac{\pi}{6}$ to $\frac{4\pi}{6}$ and the number of grid points in the inner domain are 40 and 60. As shown in table (3.8), the efficiency of the region is not a function of frequency if the number of grid points per wavelength remains unchanged and $\frac{T_o}{period} \leq 5$.

For all the three-dimensional numerical simulations performed later in this thesis, the outer region is chosen to be 40λ and 10 rows of grid points are distributed in the radial direction of the region. The D_{o1} is set equal to D_m and γ is determined from equation (3.3).

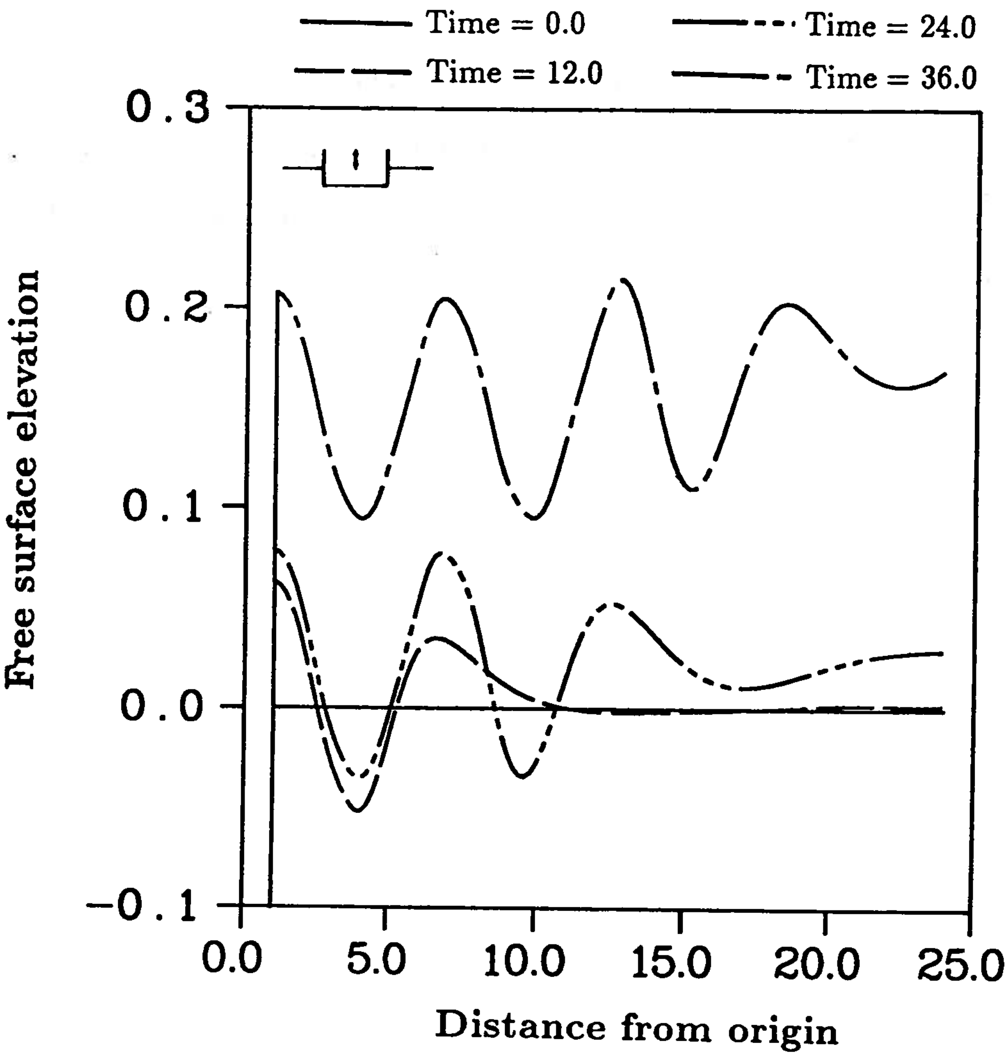

Figure 3.1: Time history of the free surface for a heaving two-dimensional box in infinite water depth, $B = 2.0$, $H = 1.0$, motion amplitude = 0.1

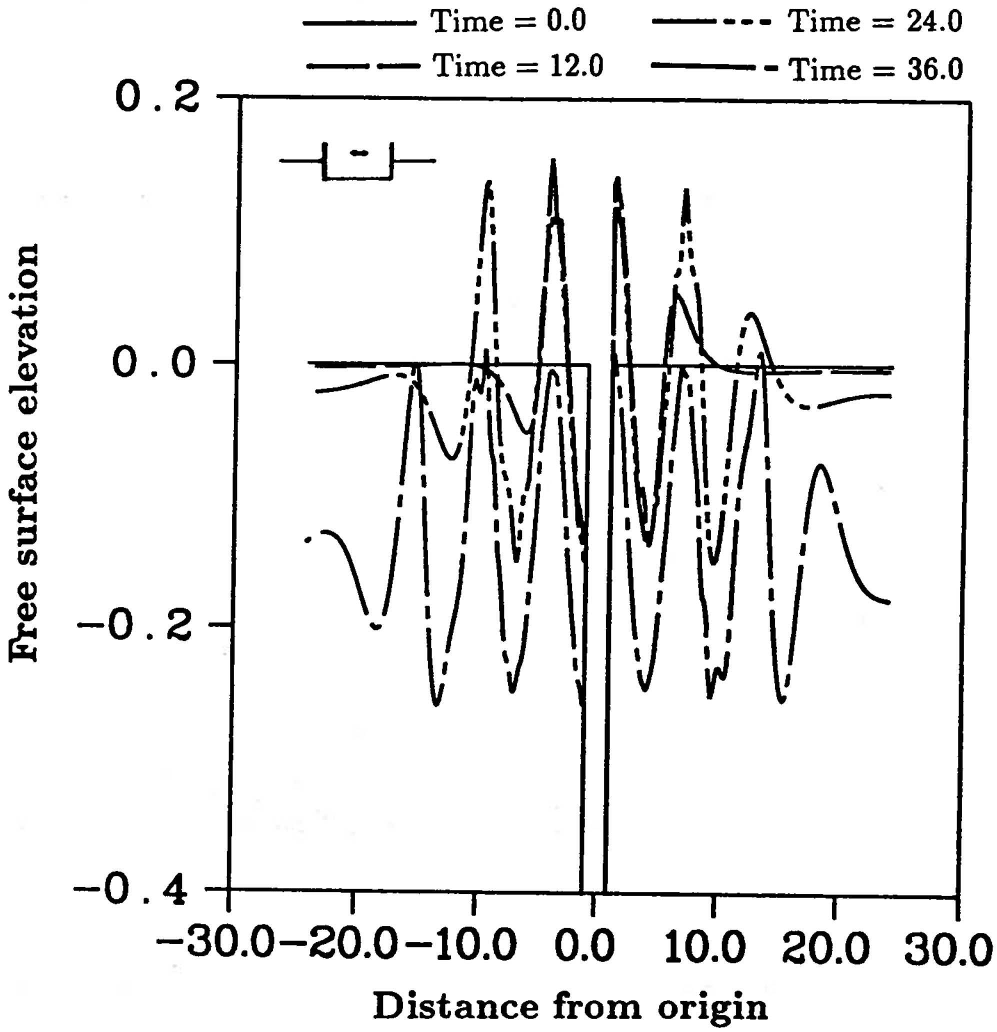

Figure 3.2: Time history of the free surface for a swaying two-dimensional box in infinite water depth, $B = 2.0, H = 1.0$, motion amplitude = 0.1

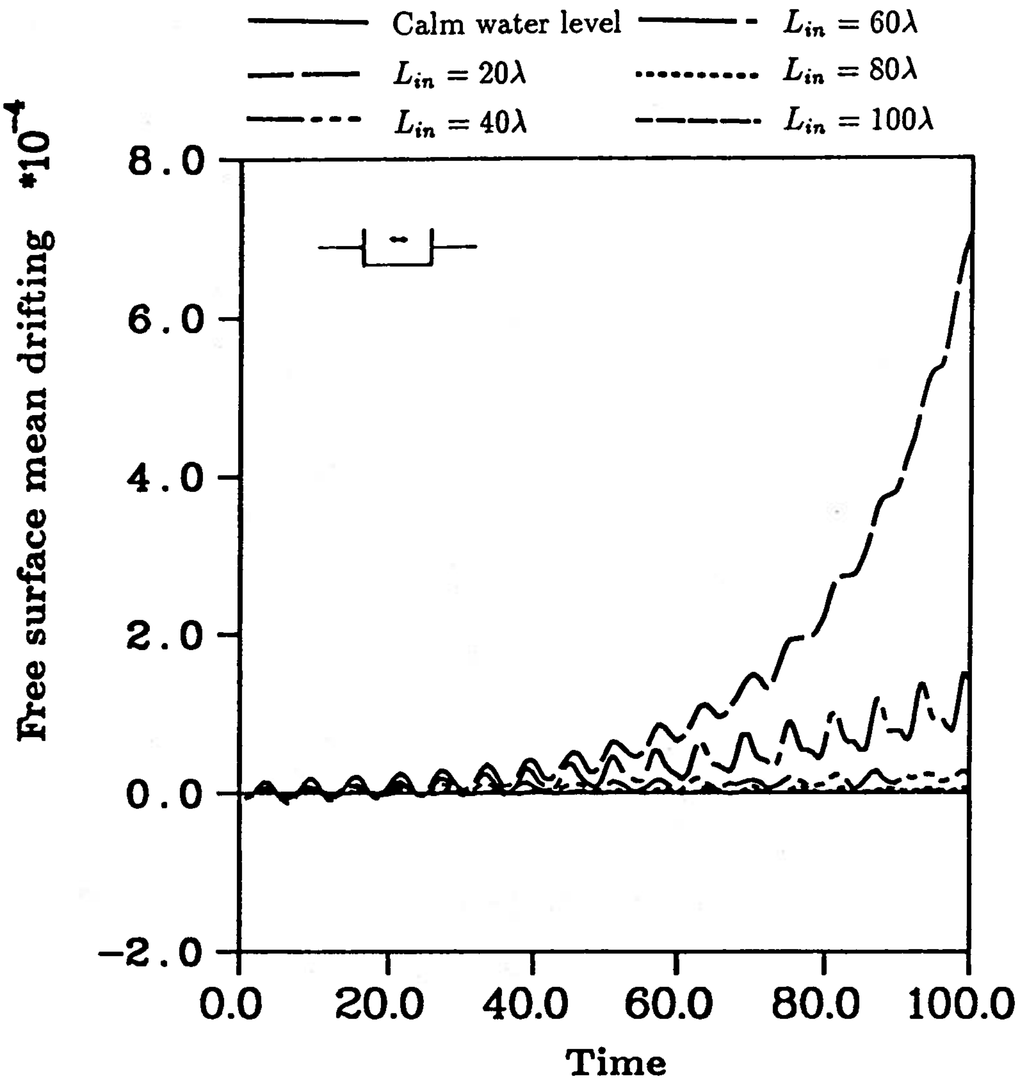

Figure 3.3: Mean position of the free surface shifting in time for sway motions of a two-dimensional box in infinite water depth, B = 2.0, H = 1.0, motion amplitude = 0.1, forcing frequency = $\frac{\pi}{3}$

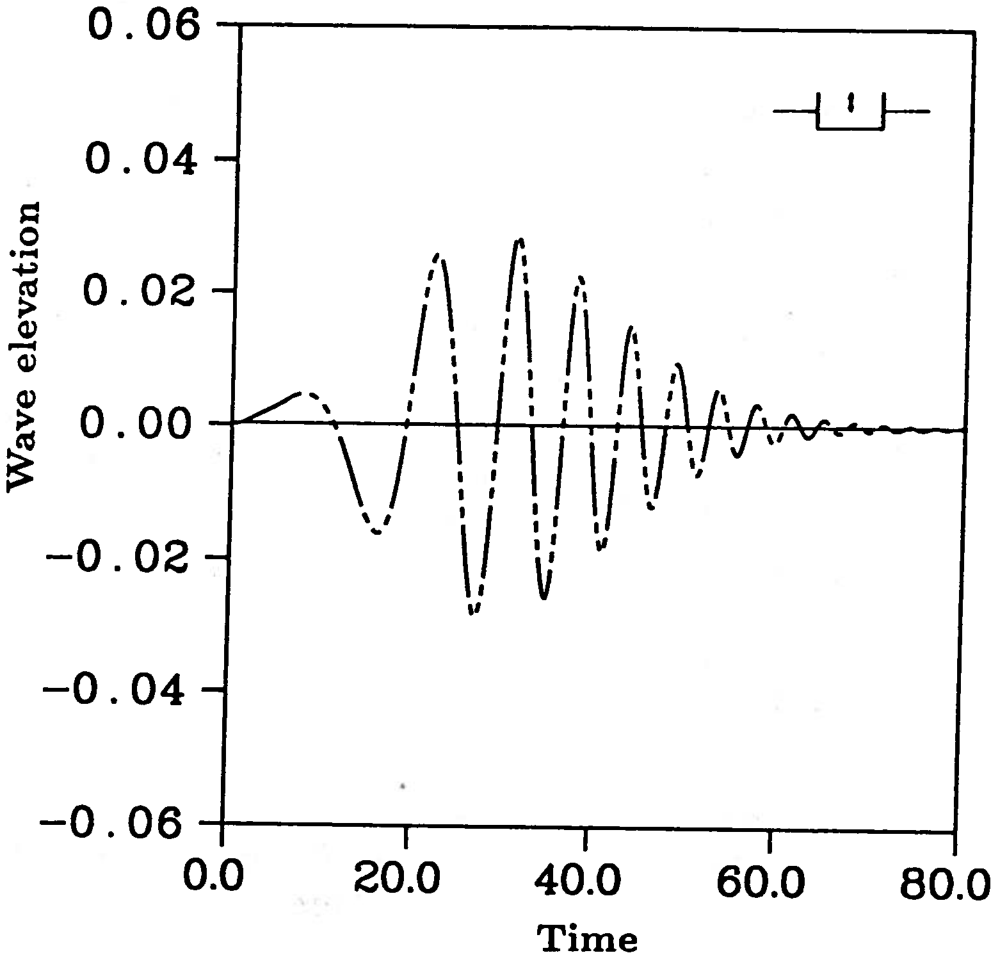

Figure 3.4: Standard wave elevation curve for a heaving two-dimensional box in infinite water depth, $B = 2.0$, $H = 1.0$, $L_{in} = 40\lambda$, panel size = $\frac{\lambda}{30}$, motion amplitude = 0.1, forcing frequency = $\frac{\pi}{3}$

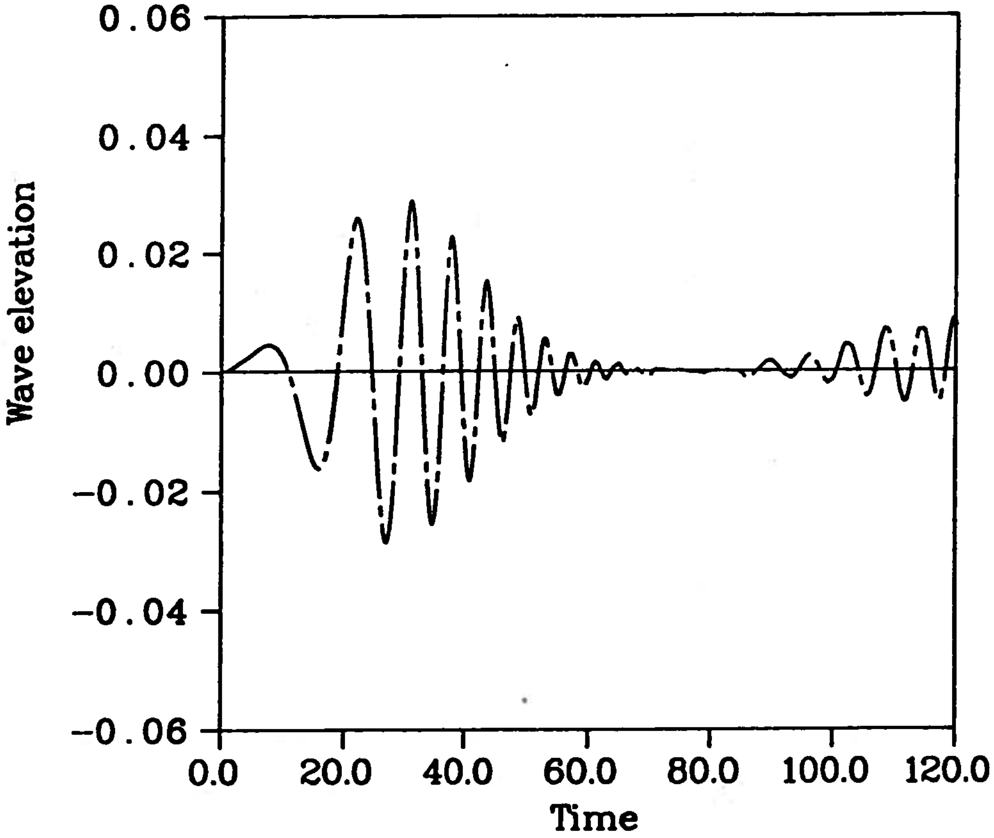

Figure 3.5: Wave elevation curve for a heaving two-dimensional box in infinite water depth, $B = 2.0$, $H = 1.0$, $L_{in} = 4\lambda$, panel size $= \frac{\lambda}{30}$, motion amplitude $= 0.1$, forcing frequency $= \frac{\pi}{3}$

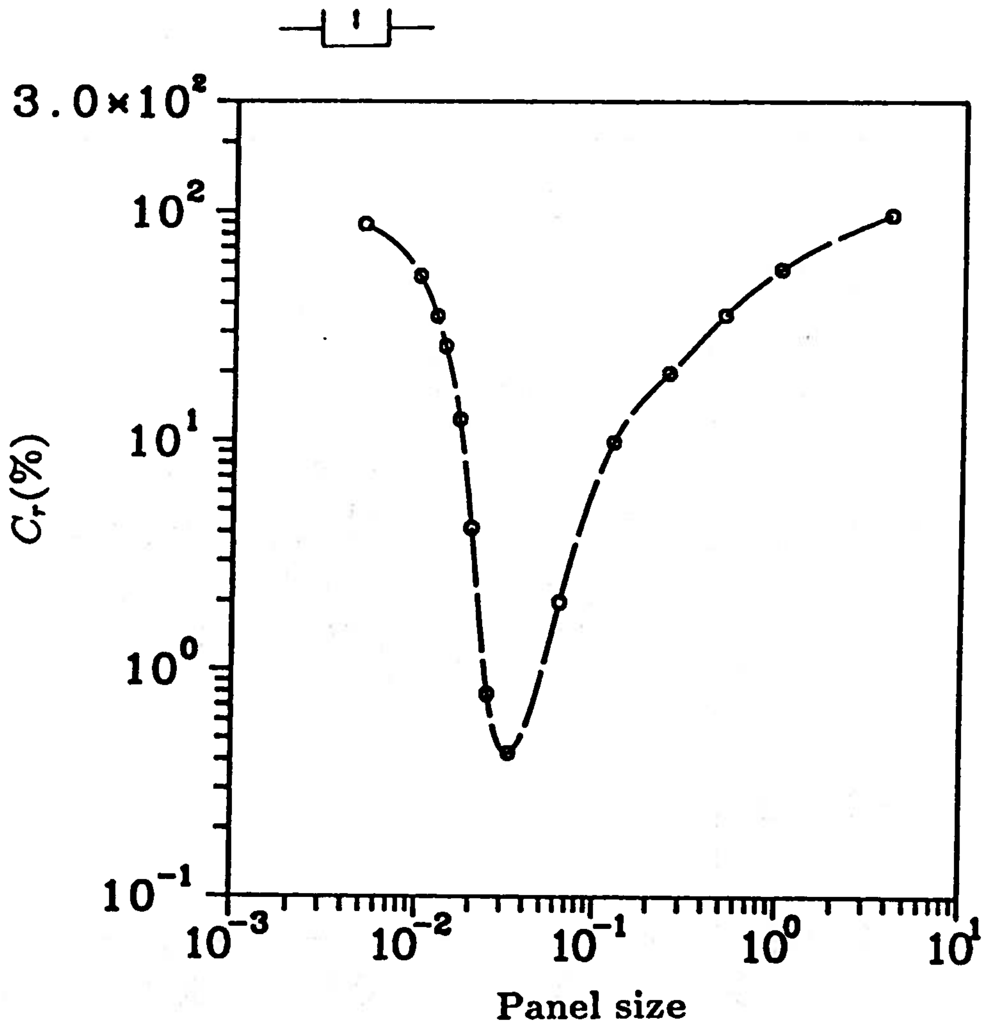

Figure 3.6: Contamination coefficient, (C_c), vs the first panel size in the damping region for a heaving two-dimensional box in infinite water depth, D_{o1}, $B = 2.0$, $H = 1.0$, $L_{in} = 4\lambda$, motion amplitude = 0.1, forcing frequency $= \frac{\pi}{3}$

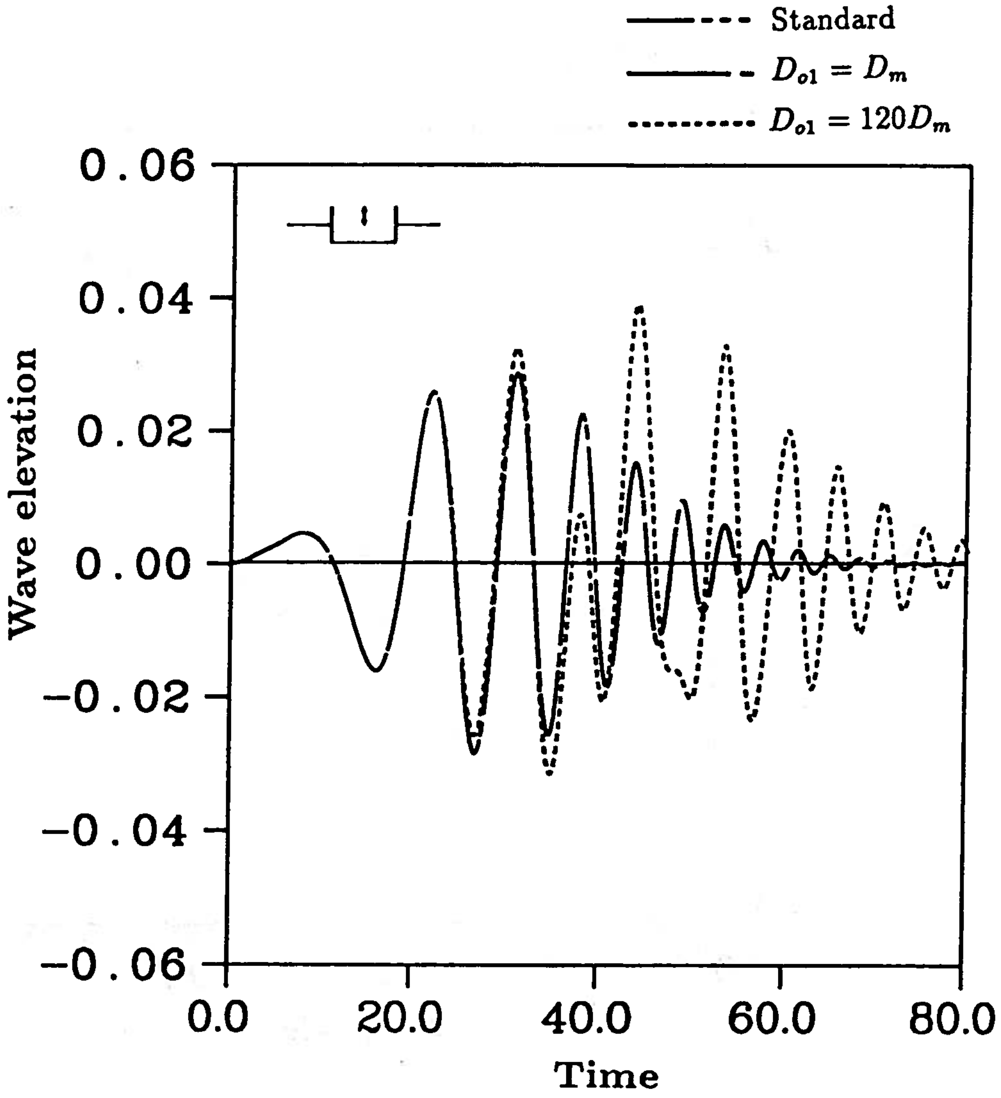

Figure 3.7: Comparison of the wave elevation curves at station A for a heaving two-dimensional box in infinite water depth, $B = 2.0$, $T = 1.0$, $L_{in} = 4\lambda$, motion amplitude = 0.1, forcing frequency = $\frac{\pi}{3}$

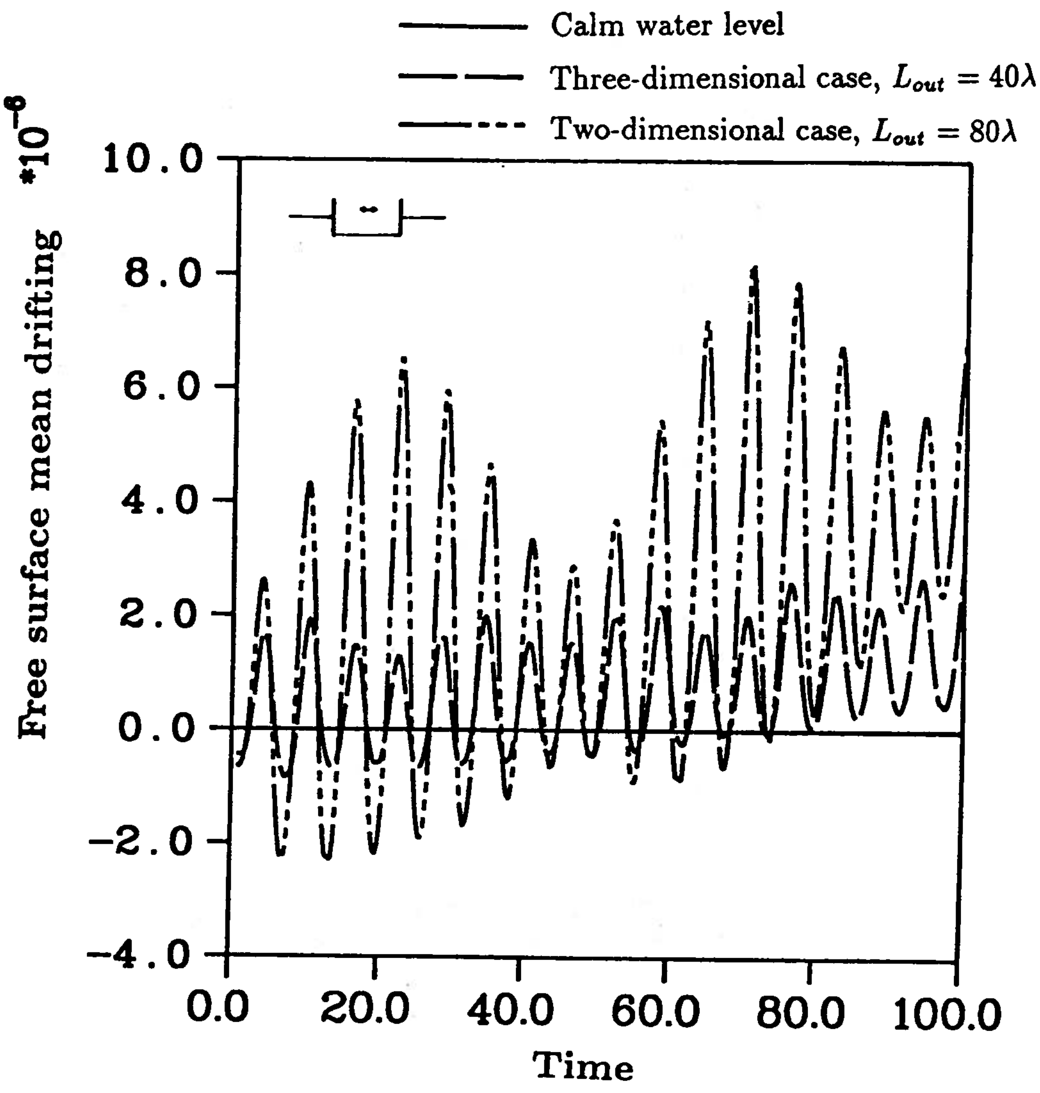

Figure 3.9: Comparison of the free surface mean shift of swaying motions in two- and three-dimensions, $L_{in} = 4\lambda$, motion amplitude = 0.1, forcing frequency = $\frac{\pi}{3}$

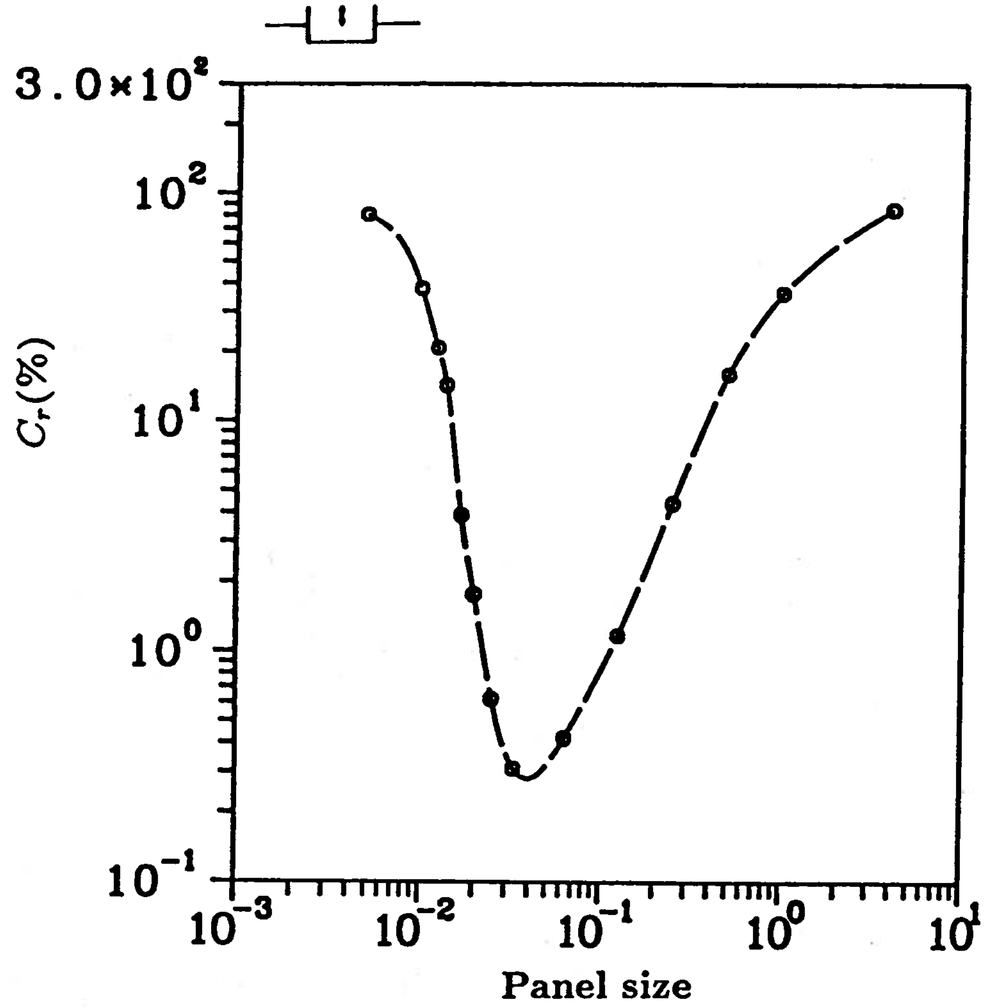

Figure 3.10: Contamination coefficient, (C_c), vs the first panel size in the damping region for a heaving three-dimensional cylinder in infinite water depth, R = 1.0, H = 1.0, D_{o1}, L_{in} = 2λ, motion amplitude = 0.1, forcing frequency = $\frac{\pi}{3}$

CHAPTER IV

CONVERGENCE AND STABILITY ANALYSES IN TWO DIMENSIONS

Primary convergence and stability analyses of the desingularized Eulerian-Lagrangian time-domain approach for two-dimensional surface-piercing bodies are conducted in this chapter. We consider a two-dimensional floating box undergoing forced periodic oscillations in deep water. The box has a breadth, B , and a initial draught, H . The inner domain of the free surface is divided into uniform grid spacings and a semi-cosine distribution of panel size is used on the box surface because of the singular flow at the corner. The outer region developed in the previous chapter is applied to absorb radiating waves generated by the motions of the body.

The box is started from rest and its velocity is prescribed by

$$U(t) = \begin{cases} 0 & \text{if } t < 0 \\ \pm\, \omega a \; sin(\omega t) & \text{if } t \geq 0 \end{cases}$$

where

ω is the forcing frequency

a is the oscillation amplitude.

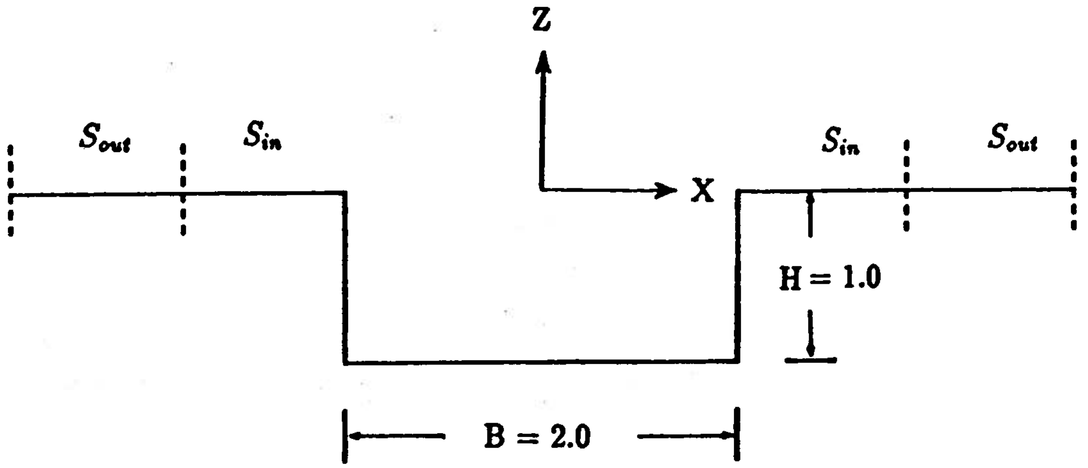

Figure 4.1: Problem definition and coordinate system

4.1 Convergence Analysis

The convergence of a numerical method requires that the numerical solution converge to the same solution as the computational grid spacing and time step are refined.

A total number of 120 fixed wave probes are uniformly distributed over S_{in} to serve as check points, such that the RMS of the free surface profiles can be calculated even when the free surface is discretized into a different number of panels. For each case, the cubic-spline method is used to interpolate the wave elevations, η, at check points from the computed values of η at the field points.

As no exact fully nonlinear solution is available, the relative RMS difference of wave profiles between cases is defined by

$$RMS^2_{k,k+1} = \frac{1}{a} \sum_{i=1}^{N_{rms}} \frac{(\eta(x_{i,k+1}) - \eta(x_{i,k}))^2}{N_{rms}} \tag{4.1}$$

where

$x_{i,k}$	is the location of the i^{th} check point in the k^{th} case
N_{rms}	is the number of check points
$\eta(x_{i,k+1})$	is the wave elevation at i^{th} check point in $(k+1)^{th}$ case
$\eta(x_{i,k})$	is the wave elevation at i^{th} check point in k^{th} case.

This error evaluation is then applied to analyze the convergency properties of the numerical techniques.

4.1.1 Heaving Motion

As shown in figure (4.1), the length of the inner domain, L_{in} , is 4λ and that of the outer domain, L_{out} , is 80λ for each side of the computational domain, when λ is the linear wavelength corresponding to the forcing frequency of the motion. For deep water, the linearized wave length is obtained by applying the dispersion relation, $\lambda = \frac{2\pi}{\omega^2}$.

For heaving motion in two dimensions, only one side of the computational domain needs to be computed because the fluid field is symmetric. Therefore, N_{in} grid points are uniformly distributed on the inner domain of the free surface S_{in} , and the outer domain S_{out} is divided into 20 panels by 20 grid points. Also, a semi-cosine spacing is used to discretize the side wall and bottom of the body surface into N_b panels.

Figure (4.2) shows the typical time histories of the free surface profile due to forced heaving motion of the body. The oscillating frequency is $\frac{\pi}{3}$, the motion amplitude is 0.1, the N_{in} is 120, and the duration of the motion is 10 periods.

Time is increasing from the bottom to the top of the figure. As shown, waves are successfully transmitted out of the inner domain and no wave reflection can be observed.

As N_{in} decreases, the uniform grid spacing D_m in the inner domain increases and the corresponding distribution factor γ is chosen to minimize possible wave reflection from the junction of the inner and outer domains. N_b should be determined in such a way that the size of the panel on the body near the intersection point is about the same as the uniform panel size on the free surface. Therefore, the variation in panel size is smooth near the intersection point. The least numerical error is encountered when the panel sizes around the intersection point are approximately the same.

Numerical tests are performed to check the convergence properties of the DELTA method with respect to the forcing frequency and the panel size on the free surface. N_{in} is increased from 60 to 300 in increments of 20. Three frequencies are chosen to be $\frac{\pi}{3}$, $\frac{\pi}{1.75}$ and $\frac{\pi}{1.25}$ and the corresponding linearized wavelengths are approximately equal to $3B$, B and $\frac{B}{2}$ respectively. The results of the relative RMS difference for the three frequencies are shown in figure (4.3). For all the three frequencies, the convergence rate is third-order.

The results of the present approach are compared with the theoretical solutions and the experimental results by Vugts (1968). In his work, a two-dimensional Lewis form and vertical cylinders were tested. The Vugts' solutions for heaving motion were computed by using the linearized free surface boundary conditions while the fully nonlinear free surface boundary conditions are applied in our calculations.

Three different stroke amplitudes, $\frac{a}{H}$ = 0.05, 0.10 and 0.15, are considered. A time history of the computed hydrodynamic force is plotted versus that of the motion. A phase shift between the two curves is found. When compared with the motion curve, the in-phase component of the computed force is used to obtain the added mass coefficient, and the 90 degree out of phase component of the computed force is utilized to get the wave damping coefficient.

The equations used to obtain the added mass and wave damping coefficients for heaving and swaying motions are

$$f = a \cdot (\omega^2 a_{zz} - i\omega b_{zz}) \tag{4.2}$$

where

f	is the computed hydrodynamic force
a	is the oscillation amplitude
ω	is the oscillation frequency
a_{zz}	is the added mass coefficient
b_{zz}	is the wave damping coefficient

(4.3)

Figures (4.4 ~ 4.6) show the comparisons of added mass coefficients from the present method and the results of Vugts (1968). The breadth-to-draught ratio, $\frac{B}{H}$, is equal to 2.0. The added mass coefficients were plotted versus the forcing frequency. The comparisons of wave damping coefficients are shown in figures (4.7 ~ 4.9).

Figure (4.10) presents the convergence of the added mass coefficient versus panel number with the heaving amplitude equal to 0.15. As panel number increases, the nonlinear solution converges to a value that falls between the experimental results and the linear solution.

4.1.2 Swaying Motion

The whole computational domain shown in figure (4.1) is considered for the numerical simulations of swaying motion because the symmetry of the fluid field is no longer valid. A total of ($2N_{in} + 40 + 2N_b$) grid points are distributed on the inner and outer domain of the free surface and the body surface, respectively.

Typical time histories of the free surface profiles due to forced swaying motions of the body are shown in figure (4.11). The uniform panel size in the inner domain is $\frac{\lambda}{30}$ and the panel number in each side of the domain is equal to 90. The motion is simulated up to 10 periods.

Thirteen cases are tested. $2N_{in} = 60$ is the first case and $2N_{in} = 300$ is the last. Grid points are uniformly distributed on S_{in} and the corresponding N_b are determined accordingly. The size of the inner domain is 2λ each side. With 60 fixed wave probes evenly spaced at each side of the computational domain, a total of 120 probes are set up to be check points in order to compute the relative RMS difference. As shown in figure (4.12), a third-order convergence is obtained.

We compare the fully nonlinear results of the DELTA method with the linear theoretical solutions and the experimental results of Vugts (1968). Fifteen cases with three swaying amplitudes and five forcing frequencies are tested. The amplitudes are 0.05, 0.10 and 0.15, and the frequencies are 0.25, 0.5, 0.75, 1.0, 1.25 and 1.5. The breadth-to-draught ratio $\frac{B}{H}$ is equal to 2.0. Figure (4.13 $\sim$ 4.18) present the results of the comparison.

The convergence of the added mass coefficient versus panel number for swaying motion is shown in figure (4.19). The oscillation amplitude is equal to 0.15 in this case. When the panel number increases, the numerical solution moves toward the experimental results. The computed solutions might not coincide with the experimental results due to the neglect of fluid viscosity effects.

When the oscillation amplitude and forcing frequency of motion increases, the nonlinearity becomes important and the discrepancy between the linear and nonlinear solutions increases. This phenomenon can be demonstrated by comparing the computational results in figures (4.4) and (4.6) for heaving motion and figures (4.13) and (4.15) for swaying motion. The results of the comparisons are shown in figures (4.20) and (4.21).

4.2 Stability Analysis

The stability of a numerical scheme demands that the accumulated numerical error does not increase during the process of simulation. The Free Surface Stability number (the FSS number) introduced by Park & Troesch (1992) is used as a guideline for the stability analysis of the DELTA method. The resulting FSS number is also compared with the stability criteria, the Courant condition, derived by Dommermuth and Yue (1986).

The FSS number is defined as

$$FSS = \pi g \frac{(\Delta t)^2}{\Delta x} \tag{4.4}$$

where

g is the gravitation acceleration

Δt is the time step size

Δx is the panel size

Therefore, the Courant condition with an expression of $(\Delta t)^2 \leq \frac{8}{\pi}\frac{\Delta x}{g}$ has corresponding FSS number equal to 8.

Park & Troesch (1992) derived the FSS number by using the linearized free surface boundary conditions in initial boundary value problems. The conventional boundary integral equation method was used to solve the problem in two and three dimensions. Even when the nonlinear free surface boundary conditions were considered, Park *et al.* still used the linearized stability criteria to analyze the nonlinear results. A Green's function constant, c , was used to improve the condition of the matrix of influence functions. They found that the conditioned numerical scheme was much more stable than the unconditioned one. The stability of the scheme became much better when c was chosen to be less than or equal to 0.02. When no treatment was made on the matrix (i.e. $c = 1.0$), there existed a very limited stability region in which the numerical scheme of the conventional boundary integral equation method was stable.

We employ the fully nonlinear free surface boundary conditions to investigate the stability properties of the desingularized Eulerian-Lagrangian time-domain approach. No Green's function constant is used in our approach. The two primary parameters for stability analysis are the spatial and the temporal increments, Δx and Δt respectively.

A two-dimensional box is initially at rest. When time is greater than zero, the body is oscillated periodically. The inner domain is 4λ and the outer domain is 80λ . The amplitude of body motion, $\frac{a}{H}$, is 0.1. Eight series of numerical experiments are then carried out. In the first four series of tests, the time step size is varied. In the other four sets, the panel size is changed. The forcing frequency, ω, for the first, the fourth, the fifth and the eighth series is $\frac{\pi}{3}$. For the second and the sixth series, ω is $\frac{\pi}{1.75}$,f and ω is $\frac{\pi}{1.25}$ for the third and the seventh series. All series are for heaving motions except the fourth and the eighth series which are for swaying motions.

4.2.1 Time Step Size, Δt

In the first sequence of investigations, 120 grid points are equally distributed in the inner domain (i.e. $\Delta x = \frac{\lambda}{30}$) when the size of time step varies. Nine cases are tested and results are examined. The number of time steps in one period, N_{time}, is increased from 30 to 150, and the increment between two consecutive cases is 15. The relative RMS difference between the cases are shown in figure (4.22), and the convergence rate of the numerical solutions show third-order convergence.

The numerical scheme becomes unstable if $\Delta t > \frac{T}{25}$. Figure (4.23) shows the time history of the wave profiles when $\Delta t = \frac{T}{25}$ and $\Delta x = \frac{\lambda}{30}$ are used. As shown, the instability grows as the numerical procedure progresses. Eventually, the scheme will break down due to the accumulated numerical error caused by the improper time step size.

By keeping the size of uniform panels in the inner domain at $\frac{\lambda}{30}$, a critical time step size is found to be $\Delta t = 0.041T$. The corresponding critical FSS number is equal to 9.76. The numerical scheme for heaving motions will be stable if the FSS number is less than the critical FSS number.

The second and the third series of tests follow the same analysis algorithm used in the first series. 120 grid points are uniformly distributed in the inner domain of the free surface for both series. It is found that the critical FSS number is 9.58 for

$\omega = \frac{\pi}{1.75}$ and is 9.53 for $\omega = \frac{\pi}{1.25}$.

In the fourth series, the distribution of grid points for swaying motions is similar to that in the last three sets of the investigations. The time step changes as the panel size stays fixed, and nine cases are tested using the same set of time step sizes as that in the first series. The values of the relative RMS difference are shown in figure (4.24), and a third-order convergence of the numerical results is found.

The instability also appears in the numerical simulations of swaying motion when Δt is greater than $\frac{T}{26}$. The instability increases as the calculation proceeds. Finally, the accumulated numerical error becomes too large to proceed with the computations. By adjusting the size of the time step, the numerical scheme becomes stable again when the time step is $0.039T$. The critical FSS number here is 8.83.

4.2.2 Panel Size, Δx

In the fifth set of tests, the number of panels in the inner region changes as time step size is fixed and equal to $\frac{T}{30}$. The period of heaving motion is 6 while the corresponding frequency is $\frac{\pi}{3}$ for all cases. The size of the uniform panels in the inner domain decreases from $\frac{12\lambda}{240}$ to $\frac{5\lambda}{240}$, and the amount of decrement is equal to $\frac{\lambda}{240}$.

The scheme is stable for the first 7 cases in which panel sizes are larger than $\frac{5\lambda}{240}$. The convergence rate of the wave profiles is found to be the same as that obtained in the convergence analysis for heaving motion, a third-order convergence.

In order to investigate the stability properties of the DELTA method in the sense of panel size, the time step size used in this series remains unchanged and the panel size is adjusted between $\frac{5\lambda}{240}$ and $\frac{6\lambda}{240}$. When panel size is smaller than or equal to 0.0233λ, instability occurs. This leads to an FSS number equal to 9.22 which is slightly smaller than the critical FSS number obtained in the stability analysis for time step size.

The same process for stability analysis used in the fifth series of numerical experiments is applied in the sixth and the seventh, and the fixed time step size is $\frac{T}{30}$ for both series. Note that the oscillating period, T , is equal to $\frac{2\pi}{\omega}$. Therefore, different values of ω result in different fixed time step sizes. After modifying the panel size on the free surface, the critical FSS number is 9.17 for $\omega = \pi 1.75$ and is 9.20 for $\omega = \pi 1.25$.

In the eighth series of numerical experiments, all of the parameters are the same as those in the fifth set of tests except the motion is a swaying motion instead of a heaving motion. The numerical schemes of the first 7 cases are found to be stable. The instability occurs as the size of uniform panels become too small to meet the stability criteria for swaying motions. The scheme remains unstable until panel size is greater than or equal to 0.0248λ. The corresponding critical FSS number is 8.66.

4.3 Discussion

The convergence and stability properties of the DELTA method are cross-examined by using the panel and time step size analyses. The numerical results show that the scheme does converge, and a third-order convergence is found for a two-dimensional floating box.

Overall, the fully nonlinear solutions agree well with the experimental results by Vugts (1968). The results are compared when the forcing frequency is $0.5 \leq \omega \leq 1.5$. With a moderate oscillating frequency and motion amplitude, all the results coincide with each other. However, some differences are found. On the low frequency side, the discrepancy between the experimental results and the nonlinear solutions may be due to the inviscid fluid assumption. Also, this discrepancy may be due to numerical errors because it is very difficult to measure added mass and wave damping at low frequencies. The nonlinearity of the numerical results becomes stronger as the strength of the disturbance gets bigger. On the high frequency side, the results of the fully nonlinear model approach the experimental results as the motion amplitude increases.

Piling up of the field points on the free surface occurs in the vicinity of the intersection points when the Lagrangian description is used to update the free surface position. The numerical error may arise due to the irregularity of the panel size. In addition, the numerical scheme might become unstable because the piling up reduces the local panel size and forces the local FSS number to exceed the critical FSS number. Therefore, it is necessary to redistribute the field points when the situation occurs.

After closely studying the convergence rate of the relative RMS difference of all numerical simulations, it is found that the rate for the sway motions is slightly lower than that for the heaving motions. The reason for the variance may be because the singularity at the body-free surface intersection points is more crucial for swaying motions. The argument is confirmed by testing the convergence rate of the results of a submerged two-dimensional cylinder oscillating both laterally and vertically. As shown in figure (4.25), the rate is the same for the two motions.

The results of the numerical experiments suggest that the convergence rate is not affected by the value of the oscillating frequency. A third-order convergence is achieved for the three frequencies tested and the FSS number is relatively independent of forcing frequency. The results of the numerical experiments suggest that the frequency is not a crucial factor for the convergence and stability of the DELTA method.

The numerical scheme is slightly more stable in the analysis of time step size than in the analysis of panel size. In other words, the stability of the DELTA method is more sensitive to the change of panel size than that of time step size although the same order of convergence is achieved in both analyses.

The critical FSS numbers are 9.17 for heaving motion and 8.67 for swaying motion in two dimensions. Both of them fall in the unstable region of Dommermuth & Yue (1986). For heaving motions, the resulting critical FSS number of the DELTA method shows a similar stability limit as Park & Troesch (1992) when the Green's function constant $c = 0.02$ is applied in their computations. They have shown that a proper value of the constant can improve the condition of the matrix of shape functions substantially. However, no special treatment is employed in the DELTA method to modify the condition of the matrix. This indicates that the stability of the indirect version of the DELTA method may be surperior to that of the conventional numerical methods used and tested in the work of Park & Troesch (1992) and Dommermuth & Yue (1986).

Even with the small differences in the convergence rate and the FSS number, the singularity at the body-free surface intersection point does not stop the DELTA method from solving the boundary value problem and obtaining correct results. No special treatment is necessary to take care of the intersection points. Without exceeding the stability limits of the method, the numerical scheme is stable and the computational results converge. So far, the DELTA method has shown good ability to manage the singularity at the intersection points for motion where the velocity is low enough such that there is no spray root.

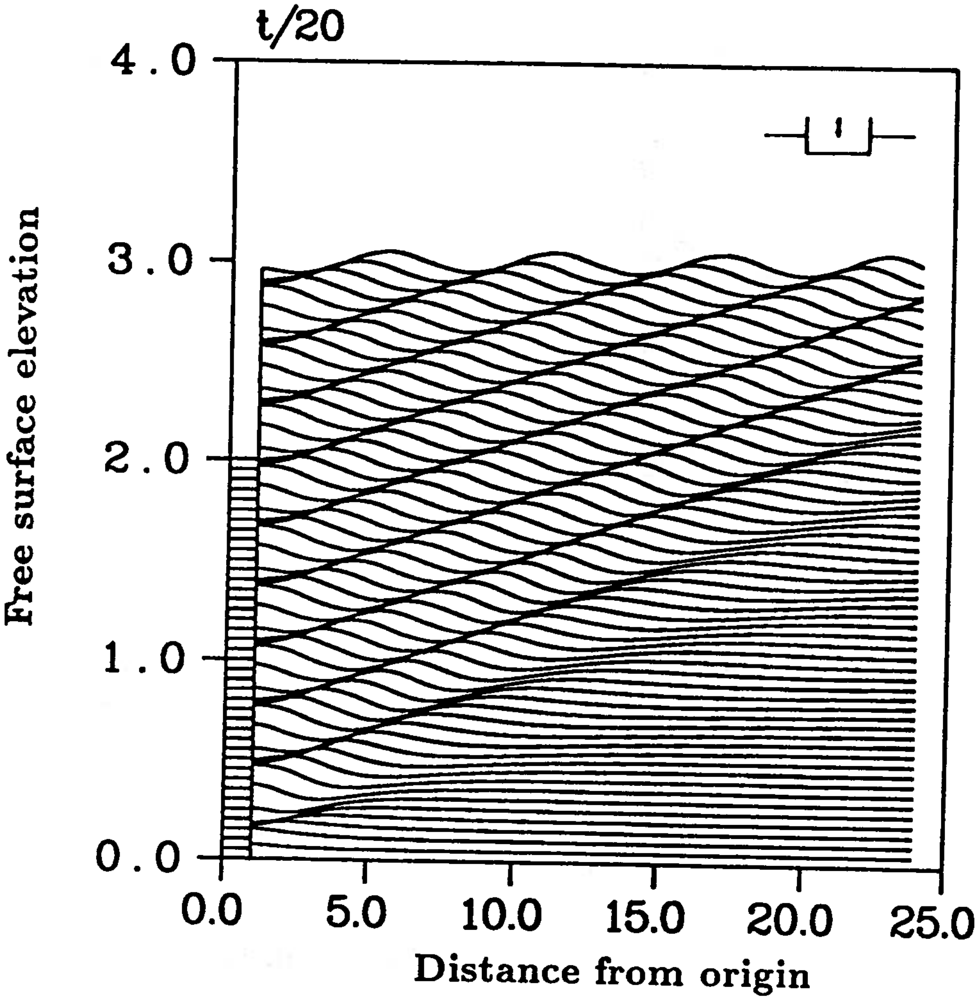

Figure 4.2: Time history of the free surface profile for a heaving two-dimensional box. in infinte water depth, $B = 2.0$, $H = 1.0$, $L_{in} = 4\lambda$, $L_{out} = 80\lambda$, panel size $= \frac{\lambda}{30}$, motion amplitude $= 0.1$, forcing frequency $= \frac{\pi}{3}$

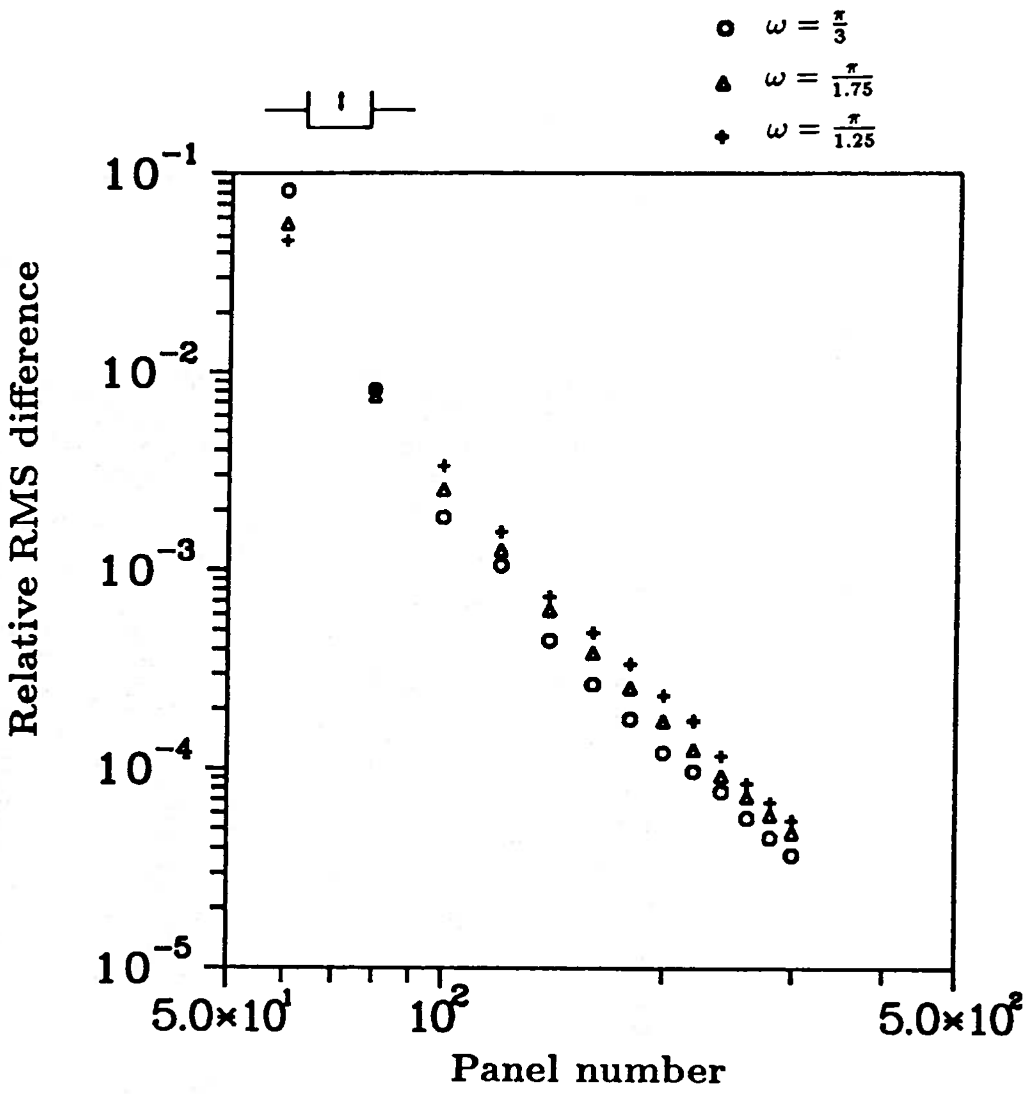

Figure 4.3: Convergencce of RMS error in free surface elevations for a heaving two-dimensional box in infinite water depth, $B = 2.0$, $H = 1.0$, $L_{in} = 4\lambda$, $L_{out} = 80\lambda$, motion amplitude = 0.1

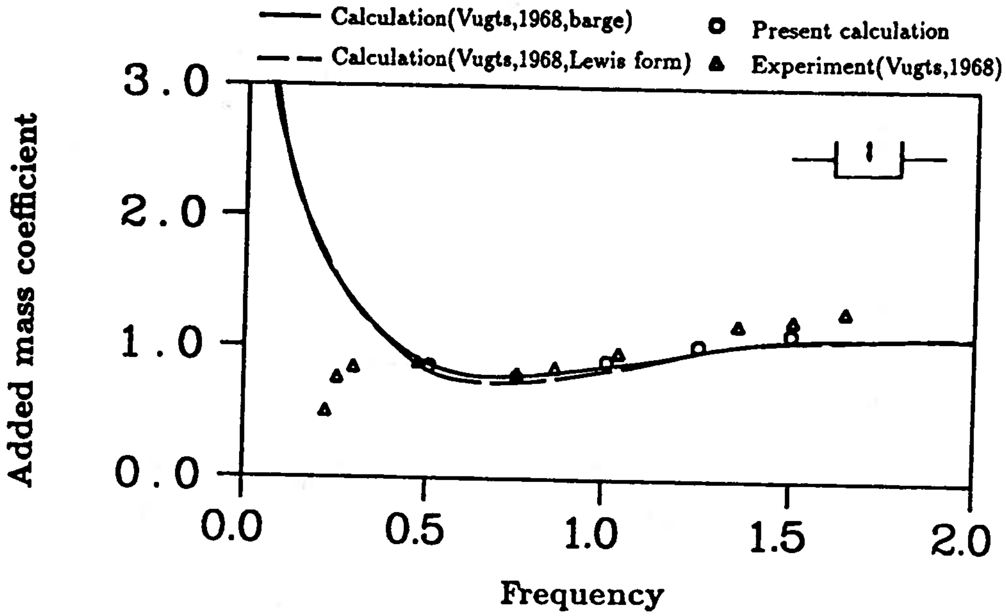

Figure 4.4: Added mass coefficient vs frequency for a heaving two-dimensional box in infinite water depth, $B = 2.0$, $T = 1.0$, $L_{in} = 4\lambda$, $L_{out} = 80\lambda$, motion amplitude = 0.05, panel size = $\frac{\lambda}{30}$

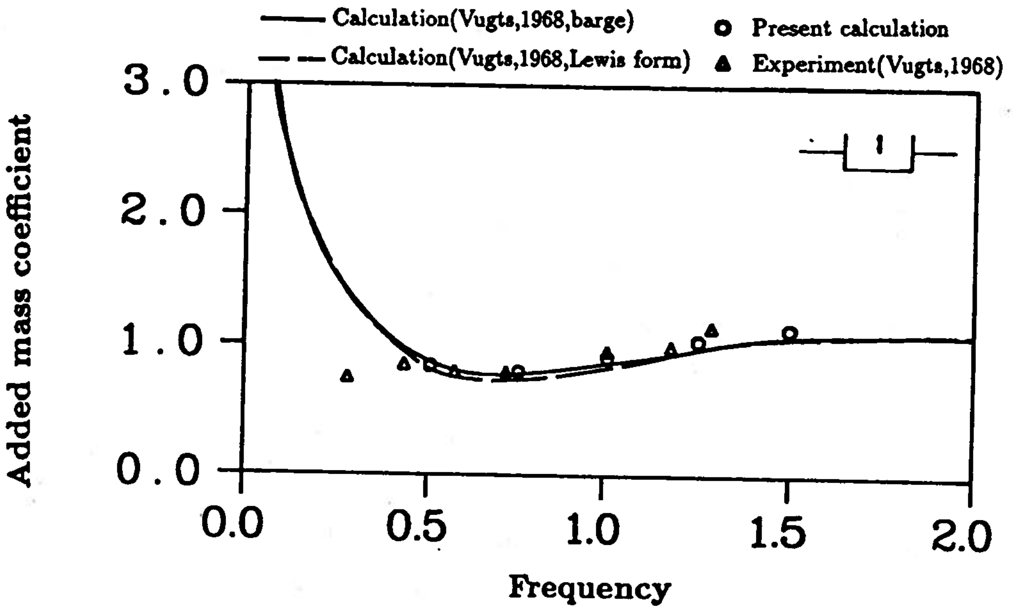

Figure 4.5: Added mass coefficient vs frequency for a heaving two-dimensional box in infinite water depth, $B = 2.0$, $H = 1.0$, $L_{in} = 4\lambda$, $L_{out} = 80\lambda$, motion amplitude = 0.10, panel size = $\frac{\lambda}{30}$

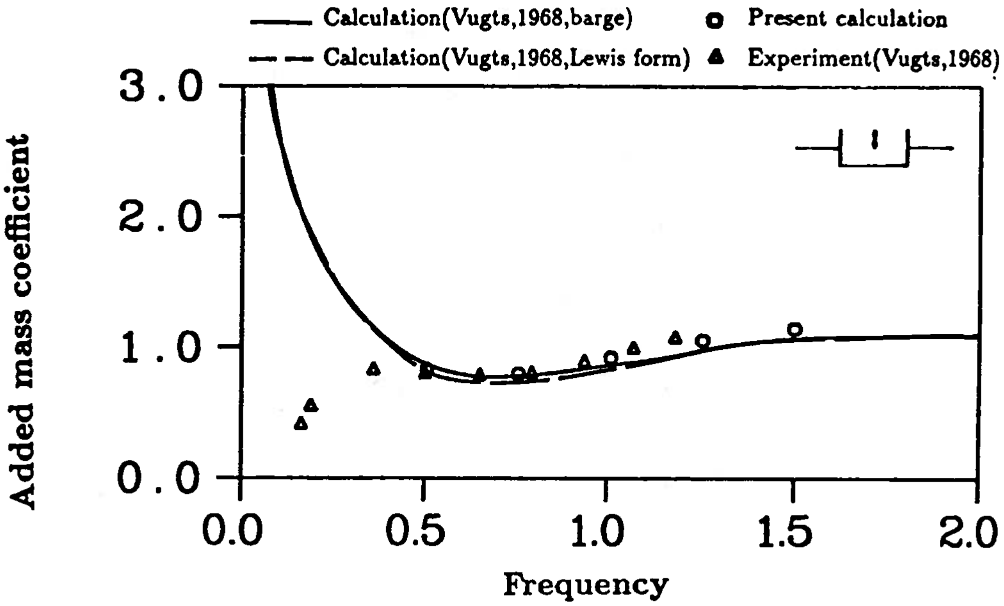

Figure 4.6: Added mass coefficient vs frequency for a heaving two-dimensional box in infinite water depth, $B = 2.0$, $T = 1.0$, $L_{in} = 4\lambda$, $L_{out} = 80\lambda$, motion amplitude = 0.15, panel size = $\frac{\lambda}{30}$

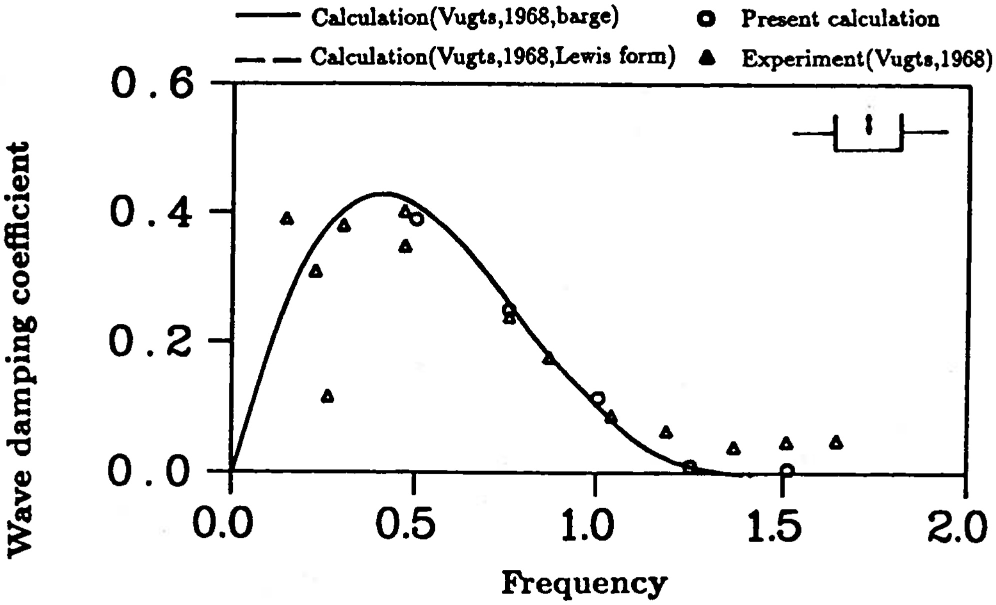

Figure 4.7: Wave damping coefficient vs frequency for a heaving two-dimensional box in infinite water depth, $B = 2.0$, $H = 1.0$, $L_{in} = 4\lambda$, $L_{out} = 80\lambda$, motion amplitude = 0.05, panel size = $\frac{\lambda}{30}$

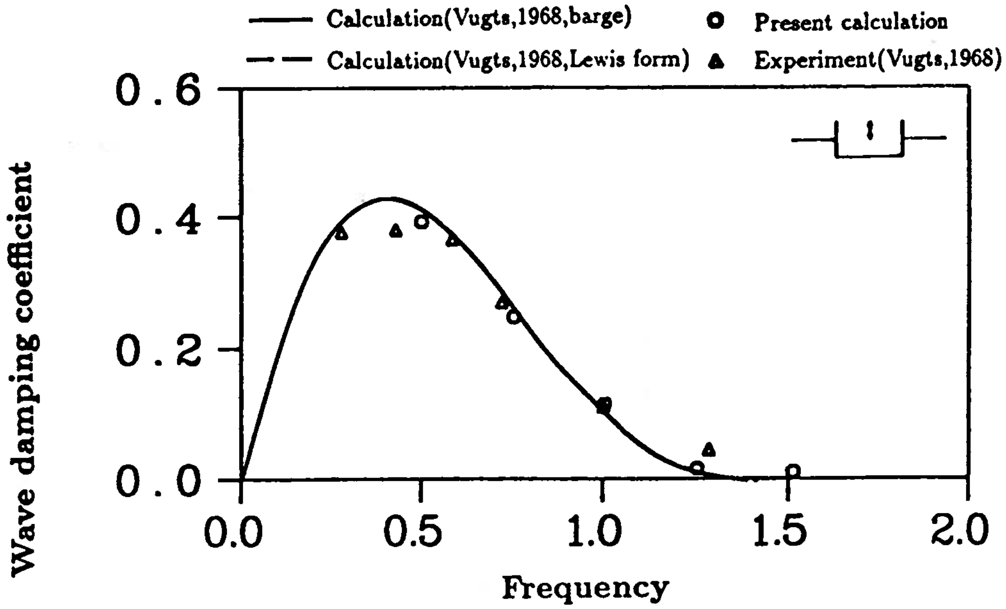

Figure 4.8: Wave damping coefficient vs frequency for a heaving two-dimensional box in infinite water depth, $B = 2.0$, $T = 1.0$, $L_{in} = 4\lambda$, $L_{out} = 80\lambda$, motion amplitude = 0.10, panel size = $\frac{\lambda}{30}$

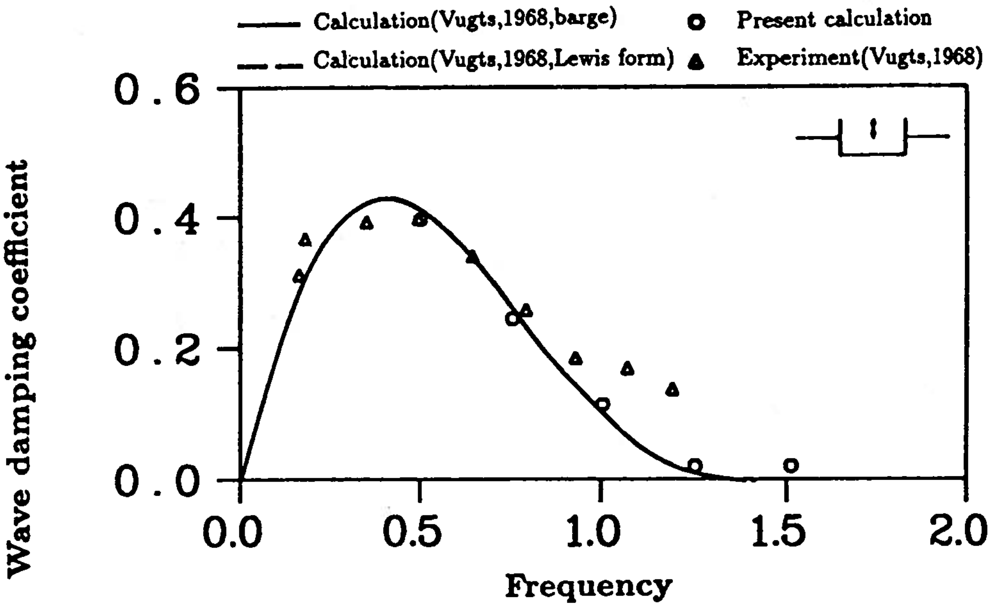

Figure 4.9: Wave damping coefficient vs frequency for a heaving two-dimensional box in infinite water depth, $B = 2.0$, $H = 1.0$, $L_{in} = 4\lambda$, $L_{out} = 80\lambda$, motion amplitude = 0.15, panel size = $\frac{\lambda}{30}$

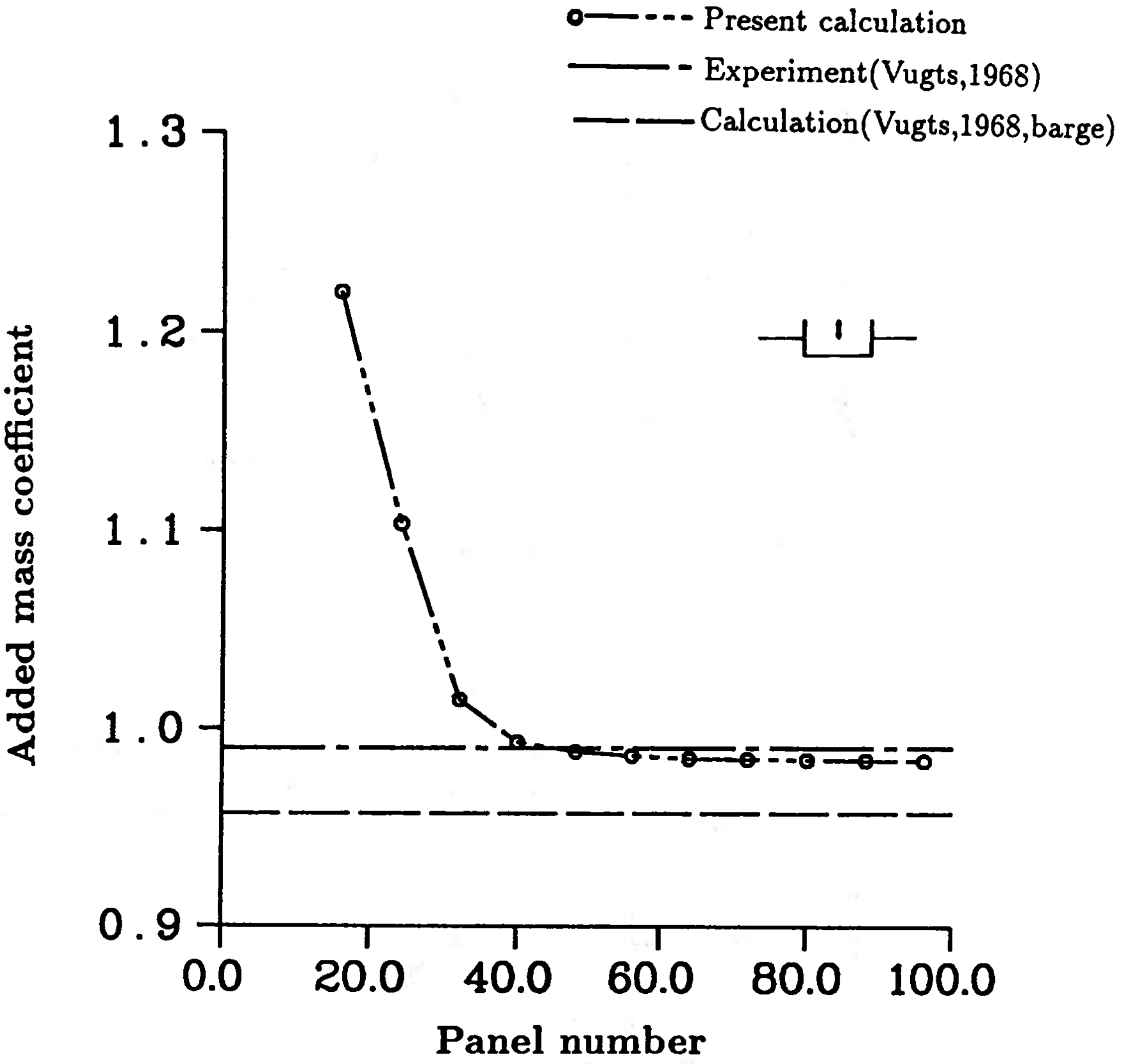

Figure 4.10: Added mass coefficient vs panel number on the inner domain of the free surface for a heaving two-dimensional box in infinite water depth, $B = 2.0$, $H = 1.0$, $L_{in} = 4\lambda$, $L_{out} = 80\lambda$, motion amplitude = 0.15, forcing frequency = $\frac{\pi}{3}$, panel size = $\frac{\lambda}{30}$

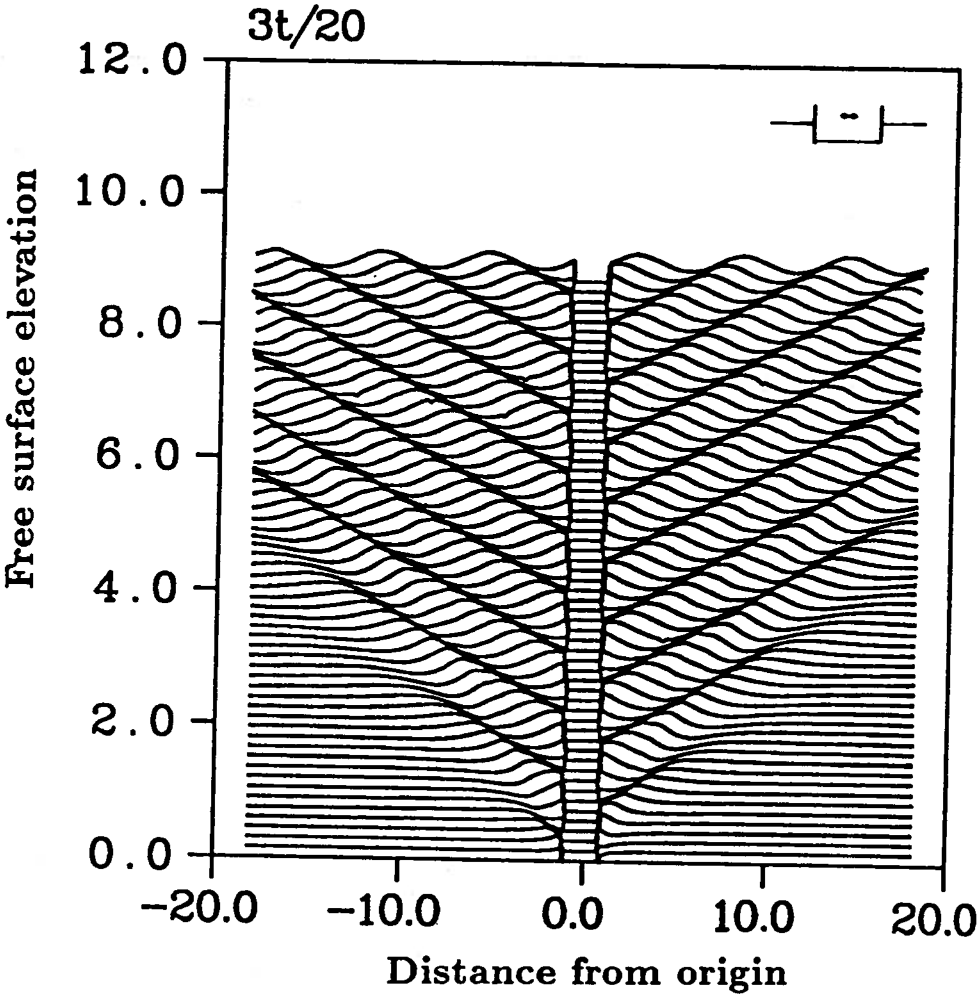

Figure 4.11: Time history of the free surface profile for a swaying two-dimensional box in infinte water depth, $B = 2.0$, $H = 1.0$, $L_{in} = 3\lambda$, $L_{out} = 80\lambda$, motion amplitude = 0.1, forcing frequency = $\frac{\pi}{3}$, panel size = $\frac{\lambda}{30}$

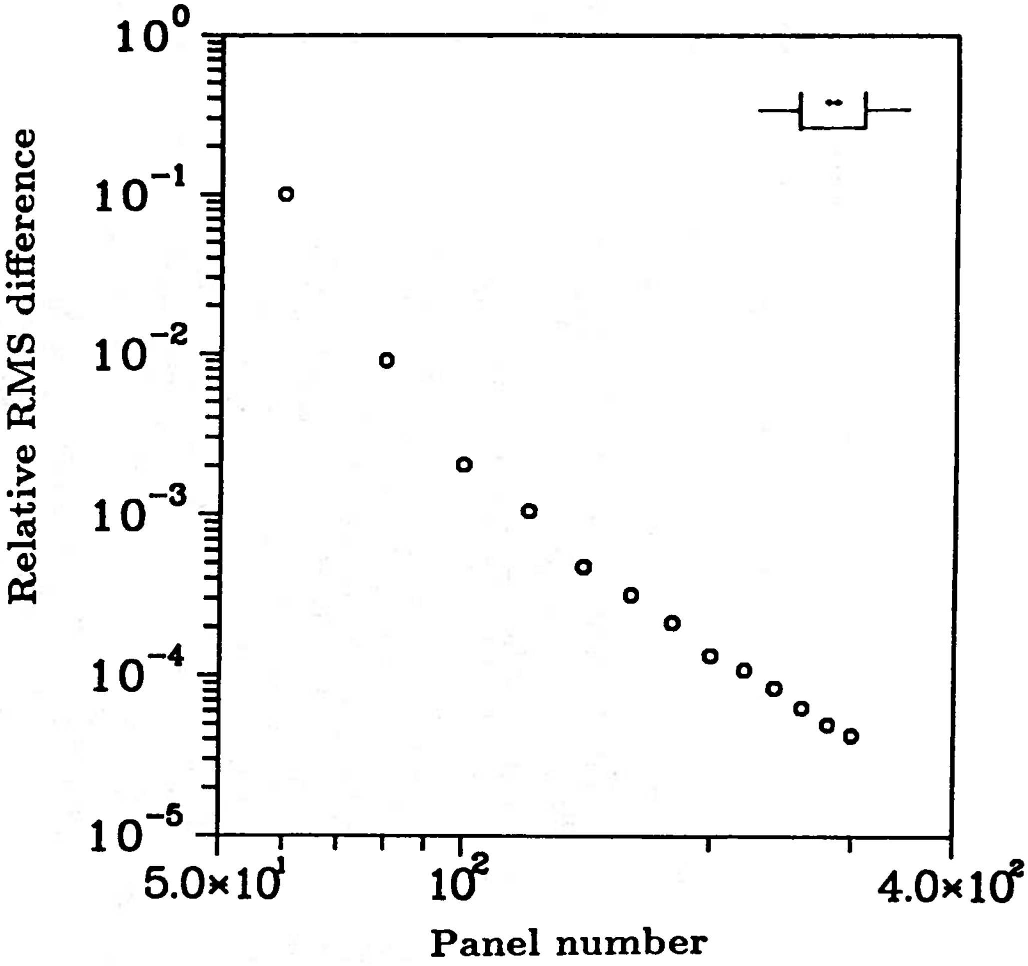

Figure 4.12: Convergencce of RMS error in free surface elevations for a swaying two-dimensional box in infinite water depth, $B = 2.0$, $H = 1.0$, $L_{in} = 2\lambda$, $L_{out} = 80\lambda$, motion amplitude = 0.1, panel size = $\frac{\lambda}{30}$

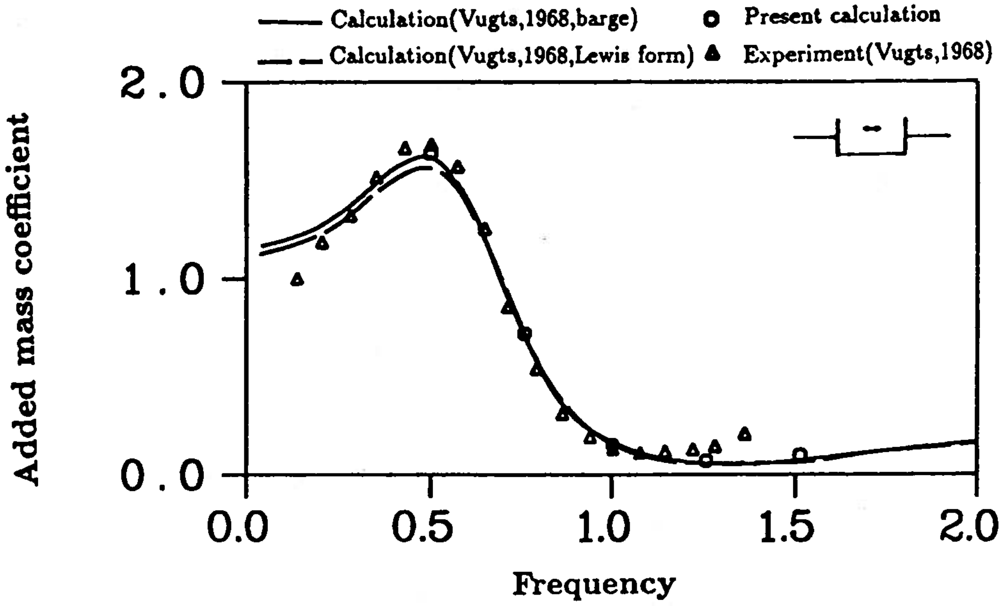

Figure 4.13: Added mass coefficient vs frequency for a swaying two-dimensional box in infinite water depth, $B = 2.0, T = 1.0, L_{in} = 2\lambda, L_{out} = 80\lambda$, motion amplitude = 0.05, panel size = $\frac{\lambda}{30}$

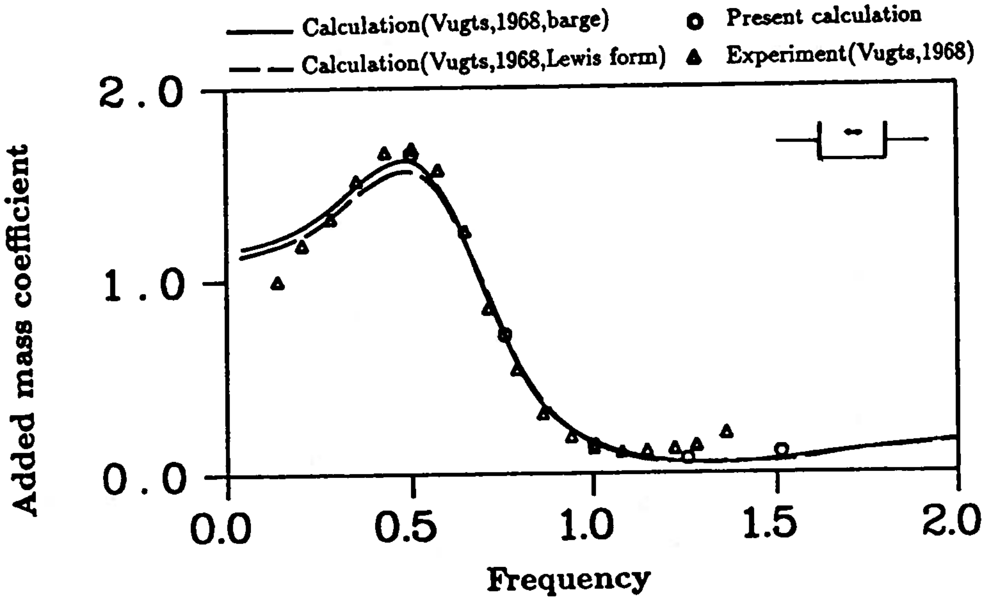

Figure 4.14: Added mass coefficient vs frequency for a swaying two-dimensional box in infinite water depth, $B = 2.0, H = 1.0, L_{in} = 2\lambda, L_{out} = 80\lambda$, motion amplitude = 0.10, panel size = $\frac{\lambda}{30}$

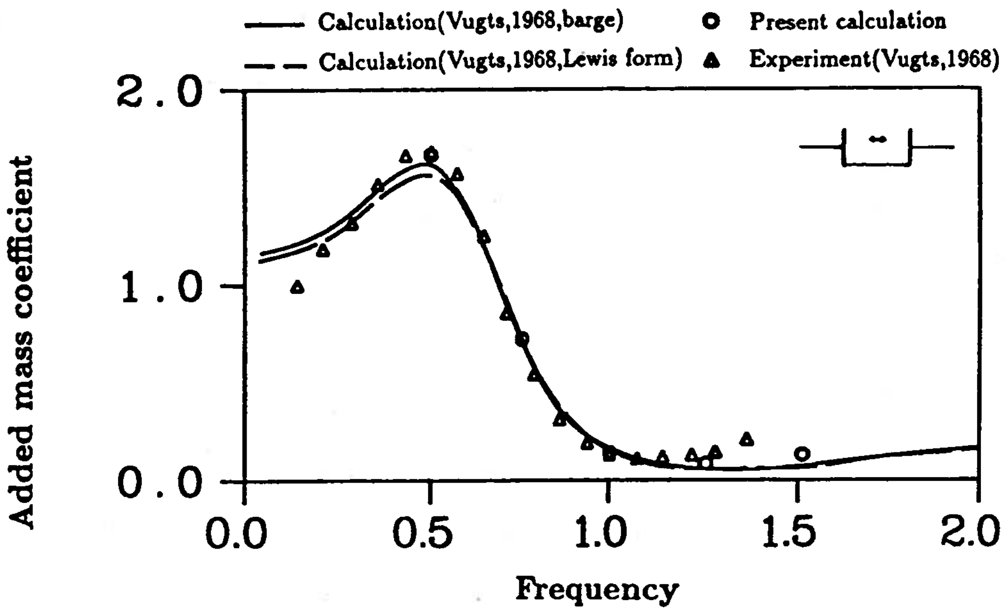

Figure 4.15: Added mass coefficient vs frequency for a swaying two-dimensional box in infinite water depth, $B = 2.0, T = 1.0, L_{in} = 2\lambda, L_{out} = 80\lambda$, motion amplitude = 0.15, panel size = $\frac{\lambda}{30}$

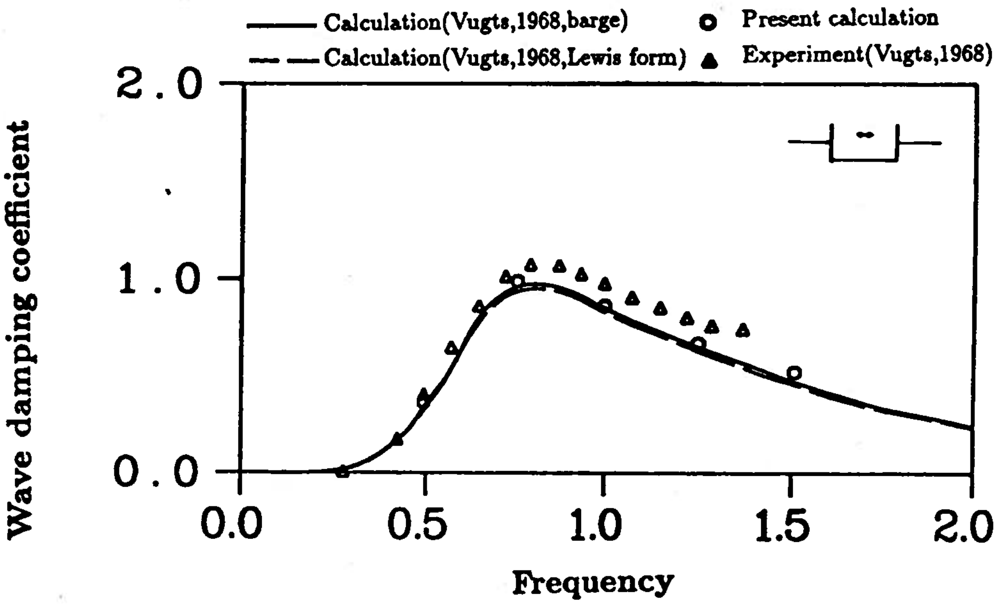

Figure 4.16: Wave damping coefficient vs frequency for a swaying two-dimensional box in infinite water depth, $B = 2.0$, $H = 1.0$, $L_{in} = 2\lambda$, $L_{out} = 80\lambda$, motion amplitude = 0.05, panel size = $\frac{\lambda}{30}$

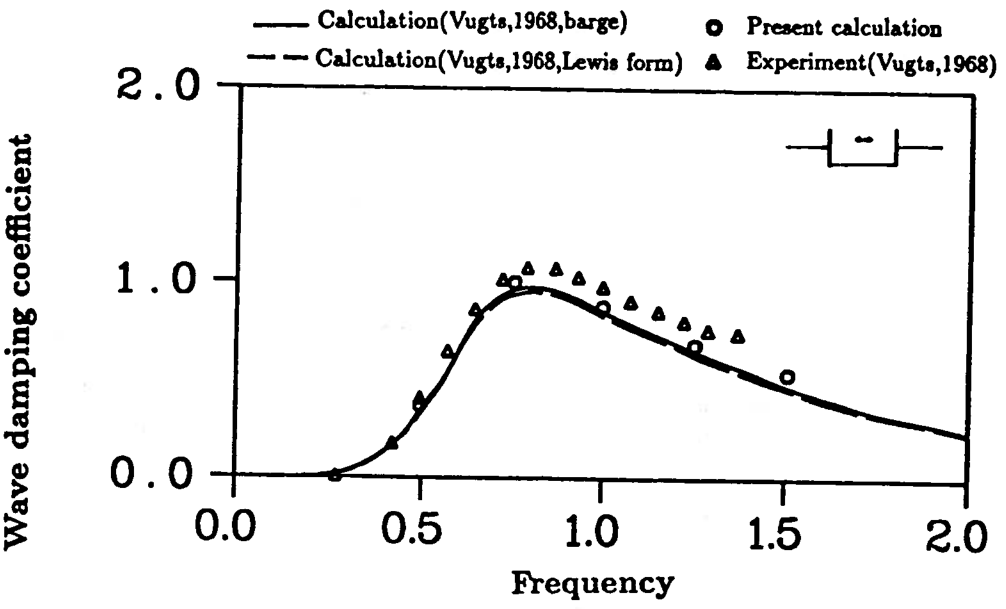

Figure 4.17: Wave damping coefficient vs frequency for a swaying two-dimensional box in infinite water depth, $B = 2.0$, $T = 1.0$, $L_{in} = 2\lambda$, $L_{out} = 80\lambda$, motion amplitude = 0.10, panel size = $\frac{\lambda}{30}$

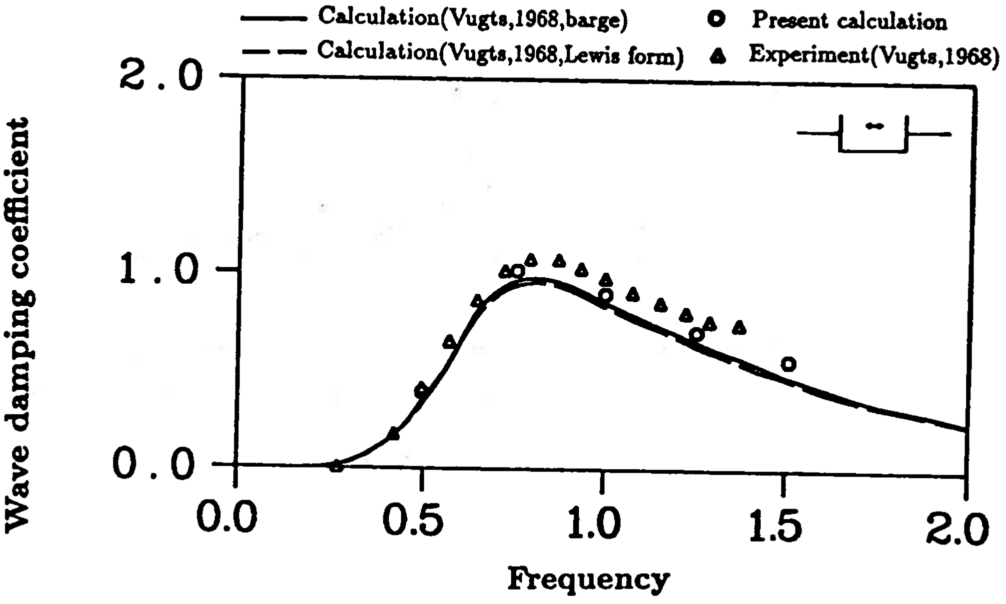

Figure 4.18: Wave damping coefficient vs frequency for a swaying two-dimensional box in infinite water depth, $B = 2.0, H = 1.0$, $L_{in} = 2\lambda$, $L_{out} = 80\lambda$, motion amplitude = 0.15, panel size = $\frac{\lambda}{30}$

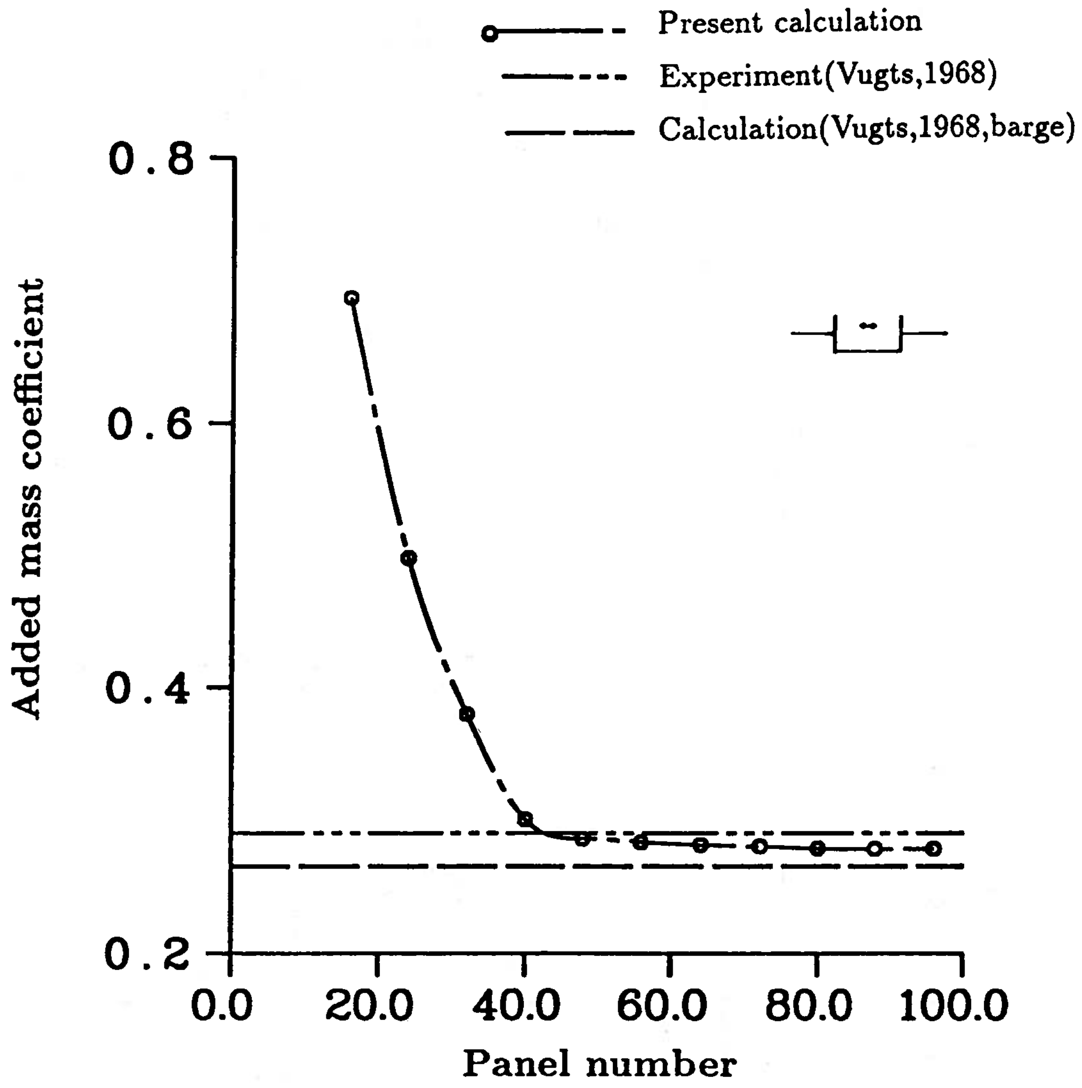

Figure 4.19: Added mass coefficient vs panel number on the inner domain of the free surface for a swaying two-dimensional box in infinite water depth, $B = 2.0$, $H = 1.0$, $L_{in} = 2\lambda$, $L_{out} = 80\lambda$, motion amplitude = 0.15, forcing frequency = $\frac{\pi}{3}$, panel size = $\frac{\lambda}{30}$

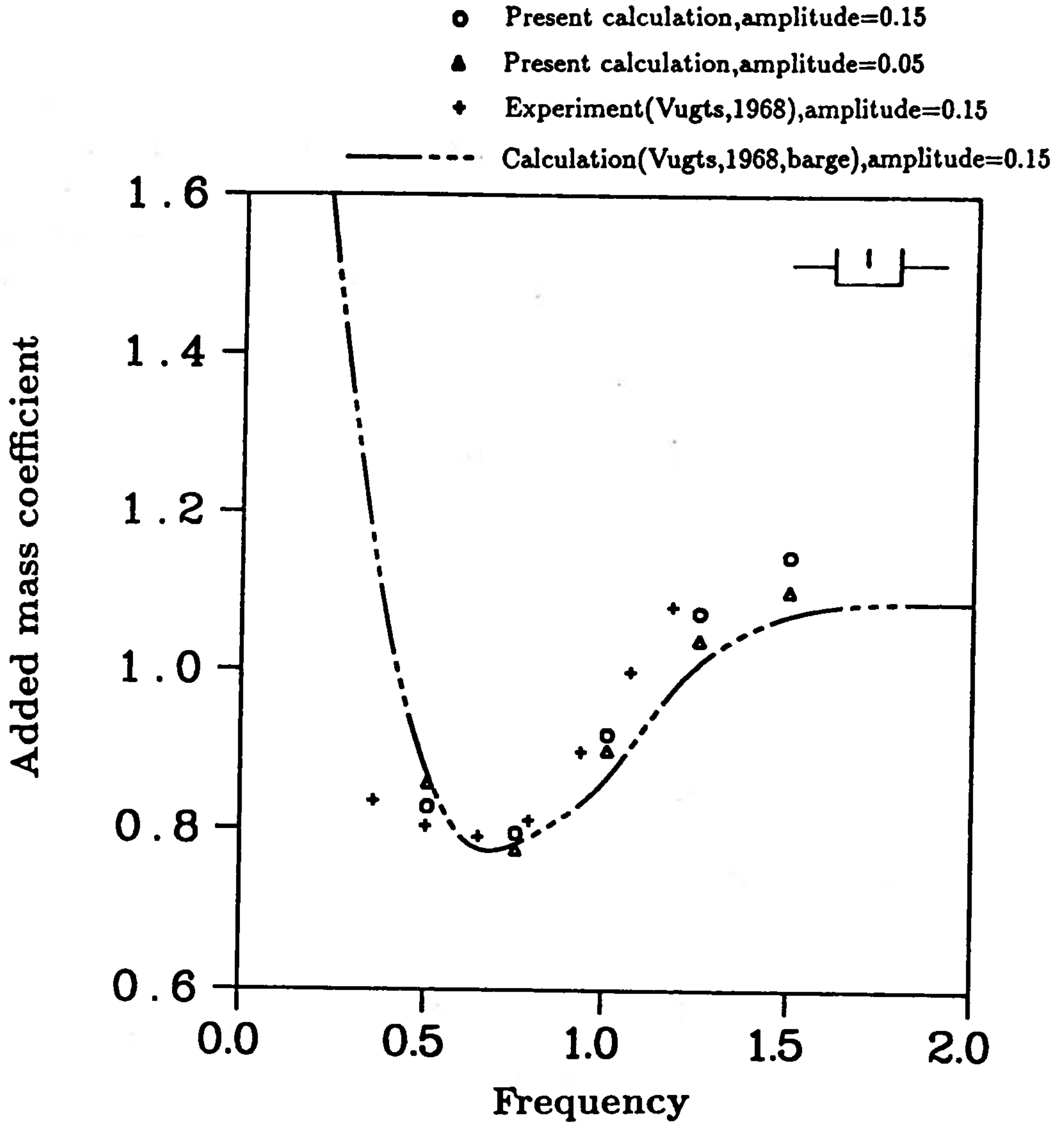

Figure 4.20: Comparison of added mass coefficient for a heaving two-dimensional box in infinite water depth, $B = 2.0$, $H = 1.0$, $L_{in} = 2\lambda$, $L_{out} \doteq 80\lambda$, panel size $= \frac{\lambda}{30}$

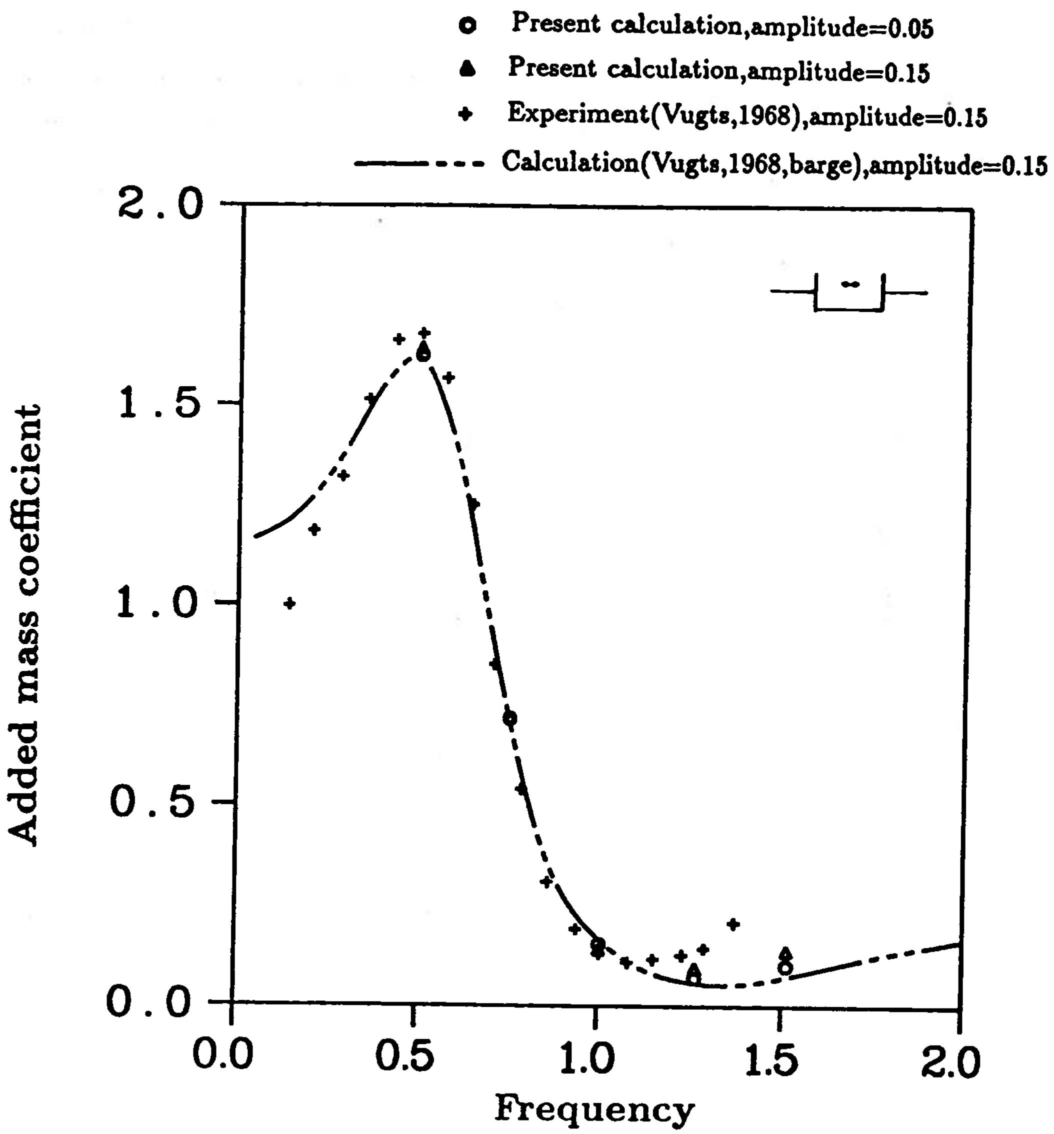

Figure 4.21: Comparison of added mass coefficient for a swaying two-dimensional box in infinite water depth, $B = 2.0$, $H = 1.0$, $L_{in} = 2\lambda$, $L_{out} = 80\lambda$, panel size = $\frac{\lambda}{30}$

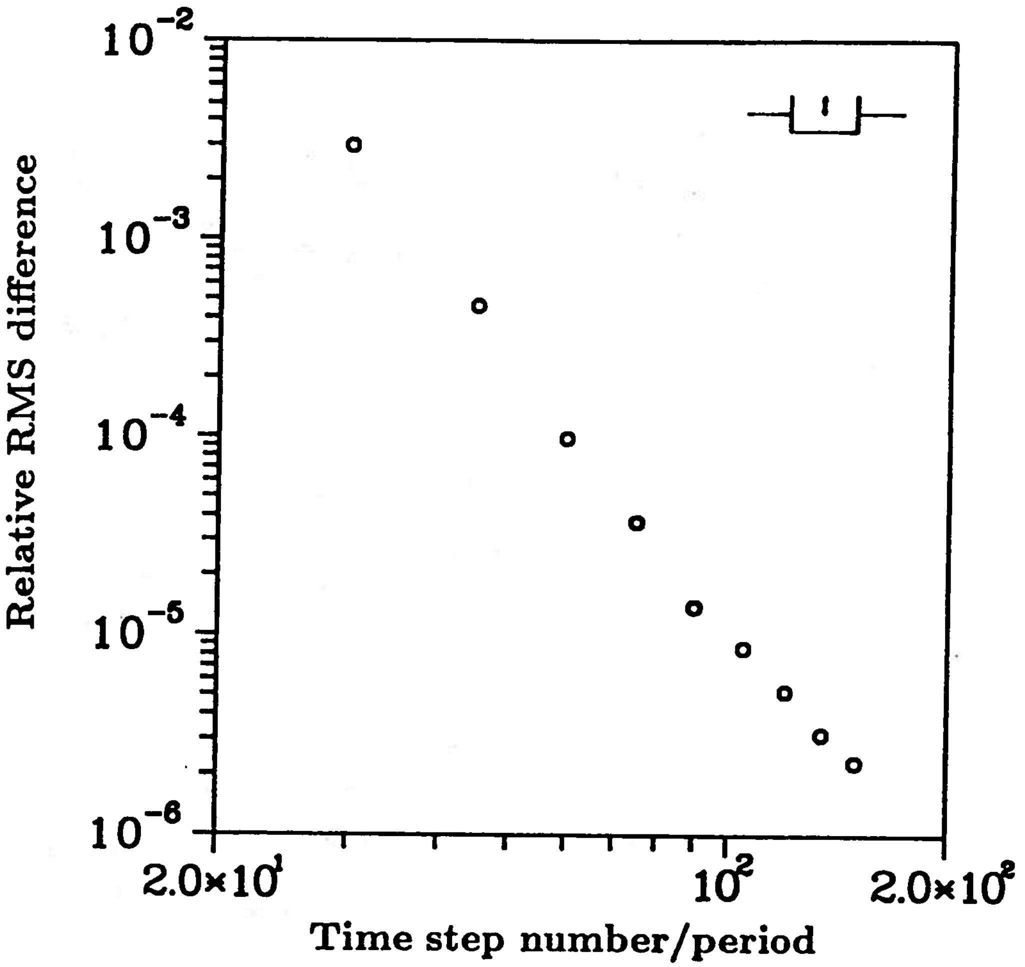

Figure 4.22: Convergencce of RMS error in free surface elevations for a heaving two-dimensional box in infinite water depth, $B = 2.0, H = 1.0$, $L_{in} = 2\lambda$, $L_{out} = 80\lambda$, motion amplitude = 0.1

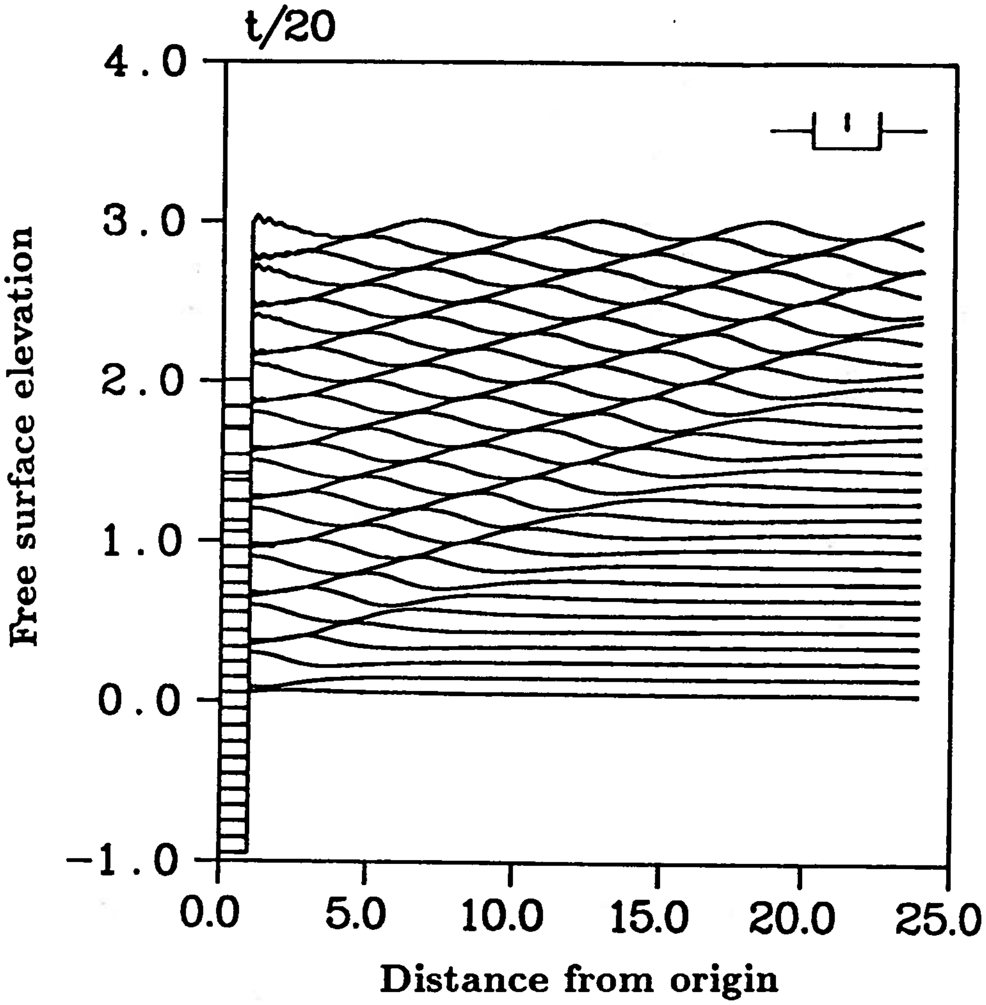

Figure 4.23: Time history of the unstable free surface profile for a heaving two-dimensional box in infinte water depth, $B = 2.0$, $H = 1.0$, $L_{in} = 3\lambda$, $L_{out} = 80\lambda$, motion amplitude = 0.1, forcing frequency = $\frac{\pi}{3}$, panel size = $\frac{\lambda}{30}$

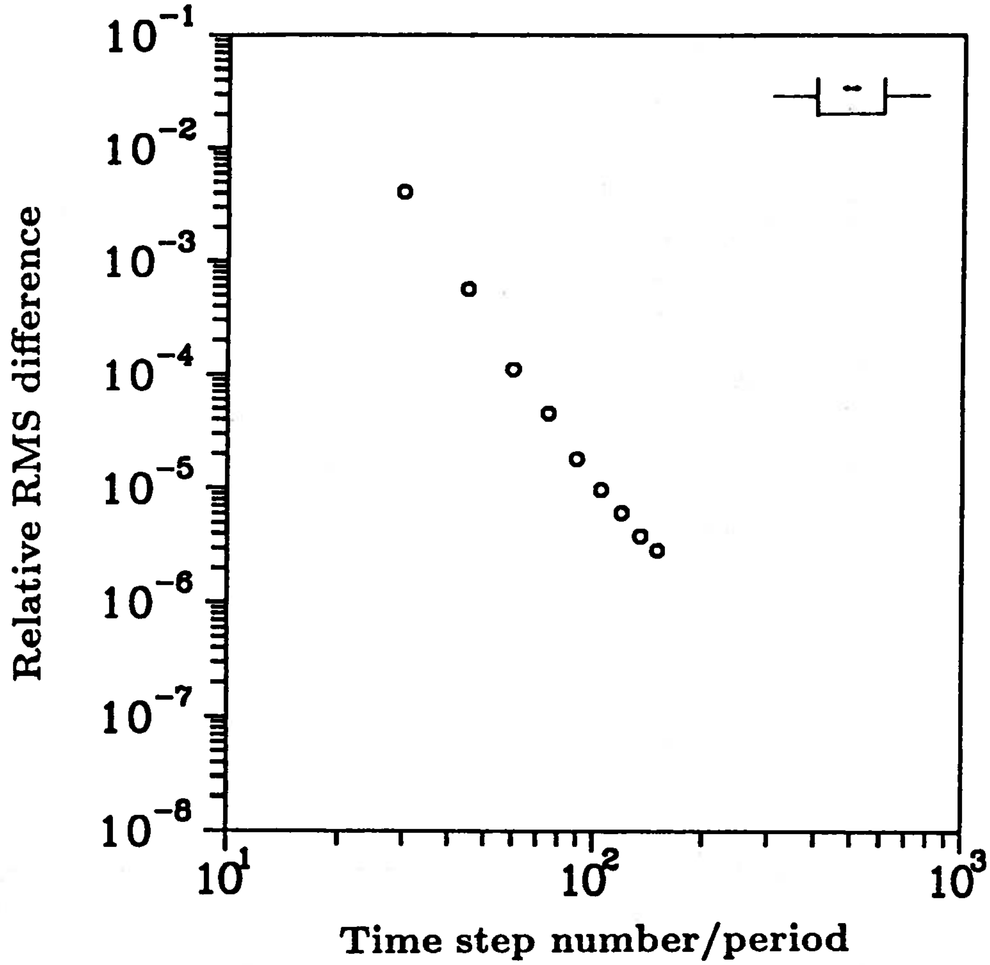

Figure 4.24: Convergencce of RMS error in free surface elevations for a swaying two-dimensional box in infinite water depth, $B = 2.0$, $H = 1.0$, $L_{in} = 2\lambda$, $L_{out} = 80\lambda$, motion amplitude = 0.1

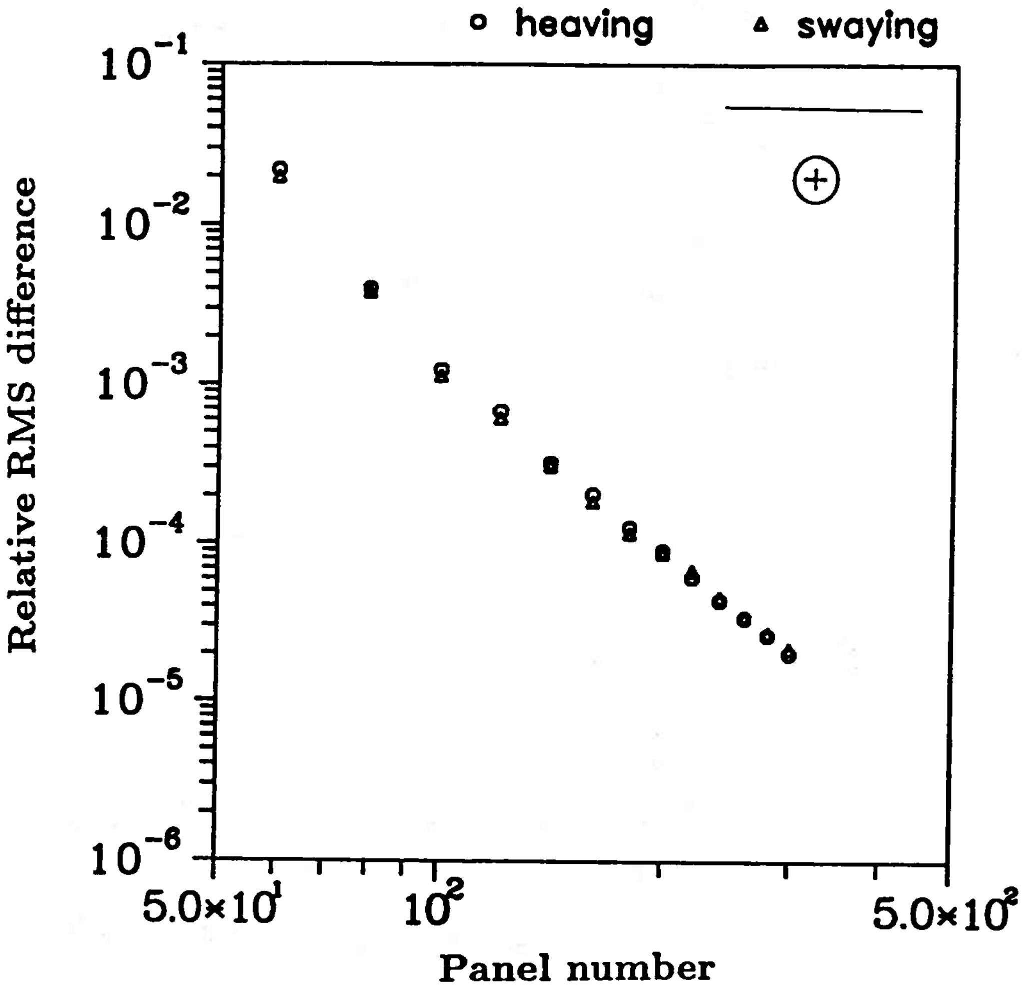

Figure 4.25: Convergencce of RMS error in free surface elevations for a submerged two-dimensional cylinder in infinite water depth, $R = 1.0$, $H = 1.0$, submerged depth $= 4R$, $L_{in} = 2\lambda$, $L_{out} = 80\lambda$, motion amplitude = 0.1

CHAPTER V

CONVERGENCE AND STABILITY ANALYSES IN THREE DIMENSIONS

In this chapter, the desingularized Eulerian-Lagrangian time-domain approach (the DELTA method) is extended to initial boundary value problems in three dimensions. The properties of convergence and stability of the method are analyzed by considering a three-dimensional surface-piercing body oscillating horizontally or vertically. The coordinate system is a right-handed rectangular system with the $x-$ and $y-$axis in the horizontal plane, and the $z-$axis vertically upward. The assumptions are the same as in the two-dimensional case, i.e. the flow is ideal, incompressible and irrotational. The surface tension and fluid viscosity are neglected.

The convergence of the DELTA method for a submerged disturbance with forward speed in three dimensions was investigated by Cao, Schultz & Beck (1991a). In their study of the truncation effect of a infinitive plane, the computational domain was extended by adding uniformly sized panels and a quadratical convergence was found. When keeping the computational domain unchanged but reducing the panel size (therefore, increasing the panel number), they found that the numerical scheme converged linearly.

The indirect version of the DELTA method is applied to solve problems in which unbounded boundaries are taken into consideration. The system of equations is solved iteratively by using the GMRES method (Saad & Schultz, 1986 and Olson, 1989). A fourth-order Runge-Kutta method is also applied to march the solution procedure forward in time. A cubic-spline technique is utilized to regrid the field point distribution on the free surface. This lessens the numerical instability in the vicinity of steep water profiles or the intersection line where grid points may accumulate.

We consider a three-dimensional floating vertical cylinder periodically oscillating in deep or shallow water. The radius of the cylinder is R and the initial draught is H . The cylinder is started from rest and oscillated vertically or laterally. The velocity of the body is prescribed as

$$U(t) = \begin{cases} 0 & \text{if } t < 0 \\ \pm\, \omega a\; cos(\omega t) & \text{if } t \geq 0 \\ \pm\, \omega a\; sin(\omega t) & \text{if } t \geq 0 \end{cases}$$

where

ω is the forcing frequency

a is the oscillating amplitude

A cosine start introduces a large impulse into the fluid field because of a step in body velocity of $\pm\, \omega a$. On the other hand, a sine start has a zero initial velocity but a step in acceleration. Numerical experiments using both types of starts are conducted. The results of a cosine heaving motion are compared with those by Dommermuth & Yue (1987), and the two types of starts are used in both heaving and swaying cases to study the convergence and stability of the DELTA method.

The convergence and stability analyses of the DELTA method have been numerically investigated for a three-dimensional floating body with zero forward speed.

The size of the mesh and the time steps are two principle parameters in the tests. The results are presented and discussed in the following sections.

5.1 Heaving Motion

For heaving motions of three-dimensional axisymmetric bodies, the fluid field is circumferentially symmetric. This property is then used to reduce the size of the computational domain required to solve the initial boundary value problem. Three simplified numerical schemes are plausible.

5.1.1 Simplification of Axisymmetry Problems in Three Dimensions

The first scheme is to reduce the order of dimensions from three dimensions to two dimensions. Rankine ring sources can be used in a Green's theorem boundary integral formulation to solve the field equation (Dommermuth & Yue, 1987). The approach was used to study the growth and collapse of a vapour cavity near the free surface; the heaving of an inverted vertical cone starting from rest and a floating upright cylinder also starting from rest. This approach will be called Dommermuth's method hereafter.

The second scheme is to compute only one quarter of the whole computational domain due to the feature of symmetry in the fluid field. The free surface profiles and hydrodynamic forces are obtained by summing up the effects from the four portions. This method is most commonly used. Simple bodies such as the hemisphere and cylinder have been studied by Beck & Liapis (1987) and others. Complicated structures such as the Tension Leg Platforms (TLP) with four or six columns were investigated in both the frequency- and time-domains by Korsmeyer *etal.* (1988).

The third scheme is an extension of the second approach with more symmetry planes applied. In the second method, only two symmetry planes, $x = 0$ and $y = 0$, are used to divide the whole domain into four symmetrical sub-domains. As the number of symmetry planes increases, the number of sub-domains grow. By keeping the total number of field points constant, the number of grid points distributed in one single sub-domain decreases accordingly. Consequently, the size of the influence matrix that need to be solved is greatly reduced.

A. Numerical Implementation

In this thesis, the second and third approaches are applied to obtain the wave profiles caused by forced periodic heaving motions of a floating vertical cylinder. The results of these two approaches are compared, and the RMS of the resulting wave profiles are computed.

The draught-to-radius ratio, $\frac{H}{R}$, of the cylinder is 1.0. A deep water case is considered, and the size of the inner domain is 2λ , where the λ is the linear wavelength corresponding to the forcing frequency of the motion and is obtained by applying deep water dispersion relation, $\lambda = \frac{2\pi}{\omega^2}$. The oscillation amplitude, $\frac{a}{H}$, is 0.1, and the forcing frequency, ω , is chosen to be $\frac{\pi}{3}$.

Similar to the two-dimensional cases, the free surface is divided into two regions, an inner domain and an outer domain. In the radial direction, the spacings are uniform in the inner domain while exponential-like spacings are distributed in the outer domain. The first spacing of the outer domain is placed right next to the border of the inner domain, and its size is set equal to the uniform panel size in the inner domain, D_m . The size of the i^{th} spacing is equal to $D_m \cdot (\gamma)^{i(i-1)/2}$ (see equation 3.4). The distribution factor γ is then determined by the D_m and the scope of the outer region, 40λ . The singular flow at the sharp edge of the body is anticipated by using a semi-cosine distribution on the side wall and bottom of the cylinder.

In the second approach, the uniform panel size is $\frac{\lambda}{30}$ for the inner domain of the free surface. A total of 60 rows of field points with N_{cir} grid points on each row equally spaced in the angular direction are distributed on one quarter of the free surface. The outer domain contains 10 rows of grid points. N_b rows of grid points with N_{cir} points on each row are allocated on one-fourth of the body surface.

The same arrangement of grid points on the surfaces in the second method are used in the third method. But, instead of distributing N_{cir} points on each row and using 2 symmetry planes, only one point is located on each row and $\frac{N_{cir}}{2}$ symmetry planes are applied.

In order to determine a proper number of symmetry planes to obtain accurate results, the relative RMS difference of free surface profiles at the end of the tenth period for different numbers of symmetry planes are calculated. The relative RMS difference is defined in the fourth chapter (equation 4.1). Figure (5.1) shows the convergence of the relative RMS difference versus symmetry plane number. The results of the numerical experiments suggest that the number of symmetry planes should be greater than or equal to 60 such that the relative RMS difference is less than 10^{-5} . Figure (5.2) shows typical time histories of the wave profiles for a heaving vertical cylinder when 60 symmetry planes are used. The time is increasing from the bottom to the top of the figure, and the temporal increment is $\frac{\Delta t}{T} = 0.8$.

A proper discretization scheme should be determined to panelize the body surface so that accurate computational results can be obtained. A uniform spacing scheme is one obvious option.

With the size of panels proportional to the cosine of equally-spaced increments along a circular arc, a cosine spacing distribution was suggested by Newman (1985) and Newman & Lee (1992). When a cosine spacing scheme is used to discretize the body surface, the smallest panels are distributed at the sharp corners and the body-free surface intersection line in order to anticipate the singular flows.

A semi-cosine spacing distribution is another plausible consideration, in which the idea of the cosine spacing is followed but only half of the circular arc is used. The smallest panels are distributed near the sharp corners of the body, and the largest panels are placed near the intersection line.

A series of tests with panel size, Δx, equal to $\frac{\lambda}{12}$, $\frac{\lambda}{15}$, $\frac{\lambda}{18}$, $\frac{\lambda}{20}$, $\frac{\lambda}{25}$, $\frac{\lambda}{30}$, $\frac{\lambda}{40}$ and $\frac{\lambda}{60}$ are conducted, and the size of the inner domain is chosen to be 2λ. A cosine start is used, and the motion amplitude is 0.25. The number of symmetry planes is 60, and the forcing frequency is $\frac{\pi}{3}$.

A total number of 120 fixed wave probes are uniformly distributed over the free surface to serve as check points, such that the relative RMS difference of free surface profiles can be calculated even when the free surface is discretized into different number of panels. For each case, the cubic-spline method is used to interpolate the wave elevations, η , of the check points from the computed values of η at the field points on the free surface.

Figure (5.3) shows the convergence of free surface elevations of a heaving three-dimensional vertical cylinder. The three discretization schemes are tested, and both deep water and shallow water cases are studied. For shallow water, the relative RMS differences are higher than those of deep water due to the existence of the bottom. The discrepency in the relative RMS differences of the three discretizations decreases as the size of panels is reduced. However, the resulting convergence rates are independent of the bottom condition.

Both semi-cosine and cosine spacings are superior to uniform spacing. When the desingularized method is tested, no significant difference (within 0.025 %) between the numerical results of semi-cosine and cosine discretization schemes is found. However, the local FSS number near the intersection line is much higher for cosine spacing distribution when time step size is the same for the two distributions. This is because the mesh size at the intersection line is much smaller in cosine spacing than in semi-cosine spacing. In other words, bigger time step size can be used to obtain an accurate solution and keep the numerical scheme stable when semi-cosine distribution is utilized. Therefore, the semi-cosine spacing is applied to discretize the body surface in z direction for both heaving and swaying motions hereafter.

Figure (5.4) shows the comparison of the wave profiles of the second and third methods at different periods for a forced heaving motion of the body. 60 symmetry planes are used and the computation is carried up to 10 periods. Table (5.1) shows the relative RMS difference of free surface profiles of the two methods at the end of every period. As shown, the results of the two approaches agree with each other very well, and the largest relative RMS difference computed is 4.73×10^{-6} at the fifth period.

The relative RMS difference does not increase as the simulation continues. However, the numerical effort for the calculations in the third method is much less than that in the second method. This is expected because the matrix size of the second method is much bigger than that of the third method. Therefore, the third method, the symmetry plane approach, is preferable and used for further calculations for heav-

Table 5.1: The relative RMS difference of the free surface elevation at the end of each period of the second and third methods

$Time$	$2T$	$3T$	$4T$	$5T$	$6T$	$7T$	$8T$	$9T$	$10T$
$RMS(\times 10^6)$	3.93	4.15	4.32	4.73	4.58	4.61	4.70	4.67	4.69

ing motion in three dimensions. Using the third approach in the DELTA method, the shallow water results are then compared with those obtained by Dommermuth & Yue (1987).

The number of symmetry planes used for the simulation is 90 and the draught-to-radius ratio, $\frac{H}{R}$, of the cylinder is 0.5. A finite depth case is considered in order to compare with the results of Dommermuth & Yue (1987). The water depth is h, where $\frac{h}{R} = 1$. Two sizes of the inner domain, L_{in} , are used, $L_{in} = 4R$ and $L_{in} = 9R$. The oscillation amplitude, $\frac{a}{H}$, is 0.5, and the forcing frequency, ω , is chosen to correspond to an Airy wavelength λ of $2R$, i.e. $\omega^2 = 3.13$.

Figure (5.5) presents time histories of the nonlinear vertical force on the cylinder computed by Dommermuth's method and the third method. As shown, steady state for the nonlinear force is reached within two periods in both cases. The two nonlinear forces show good agreement considering that two completely different numerical techniques are used.

Figure (5.6) compares the wave profiles of Dommermuth's approach and the third approach at the specific instants, $\frac{t}{T}$ = 4, 8 and 10 for $\frac{a}{H} = 0.5$. Generally, the results of the two methods show good agreement. However, no instability near the intersection line is observed in the results of the DELTA method while irregularity is seen in the results of Dommermuth's approach. The occurrence suggests that the

DELTA method is more stable than the conventional boundary integral equation method used by Dommermuth & Yue (1987).

From all the comparisons made above, the multiple symmetry plane approach is shown to be reliable and promising in obtaining correct solutions to initial boundary value problems. Therefore, the method is utilized to analyze the convergence and stability properties of the DELTA method for heaving motions in three-dimensions.

5.1.2 Convergence Analysis

The convergence characteristics of the desingularized Eulerian-Lagrangian time-domain approach are examined using two analysis parameters, time step size and panel size. When one of the two parameters changes, the other one stays fixed. The outer region is 40λ and the inner domain is 2λ . Both shallow water and deep water cases are tested. The heaving amplitude is equal to $0.25H$ where H is the draft of the body. The period of oscillations, T , is equal to 6 and the corresponding frequency is equal to $\frac{\pi}{3}$.

N_{in} grid points are distributed in the inner domain of the free surface, S_{in} , and the number of the grid points on the outer domain, S_{out} , is 10. The distribution factor γ is determined by equation (3.3) to discretize S_{out} such that wave reflection from the junction of the inner and outer domains is minimized. 90 symmetry planes are applied, and the uniform segment length in the inner domain is equal to $\frac{2\lambda}{N_{in}}$.

60 fixed wave probes are equally spaced in the inner region and utilized to compute the relative RMS difference of the instantaneous free surface positions at the end of the sixth period. By using the cubic-spline technique, the position of the check points are interpolated from the computed values of the free surface elevations of the field

points at each instant of time.

A. Panel Size, Δx

Nine numerical experiments are carried out with the number of grid points, N_{in} , increasing from 20 to 100 in S_{in} . The increment of grid points of the two successive cases is 10. The outer region, S_{out}, is divided into 10 panels, and the panel sizes in the region increase with an order of γ. The time step size is set equal to $\Delta t = 0.025T$ for all cases in this series of numerical experiments.

Figure (5.7) shows the relative RMS difference of the cases with different numbers of grid points in the S_{in} for deep water. The first case has N_{in} equal to 20, and N_{in} is 100 in the ninth case. The convergence rate is found to be second-order.

Also shown in figure (5.7) are shallow water results. The relative RMS difference is bigger in the low panel number side and the solution converges slower than those in deep water case. However, the final converge rates of deep and shallow water cases are the same.

B. Time Step Size, Δt

Time step size is the principle variable in this sequence of tests with the panel size fixed at $\frac{\lambda}{30}$. The number of time steps in one period is increased from 25 to 80 with an increment of 5 for the twelve cases. Figure (5.8) shows the relative RMS differences of the deep and shallow water cases and a small discrepancy is observed when the time step size is larger. The numerical solution convergences with a second-order convergence for both deep and shallow water cases.

The analysis is extended to check the relation between the forcing frequency and the convergency of the desingularized scheme in deep water. Time step size is the principle analysis parameter. Three frequencies, $\omega = \frac{\pi}{3}$, $\omega = \frac{\pi}{1.75}$ and $\omega = \frac{\pi}{1.25}$, are used. As shown in figure (5.9), the convergence rates of the relative RMS difference are the same for the three frequencies, a second-order convergence.

5.1.3 Stability Analysis

The FSS number defined by Park & Troesch (1992) is used to analyze the stability criteria of the DELTA method for heaving motions in three dimensions. The critical FSS number obtained by Park & Troesch (1992) and Dommermuth & Yue (1986) are 9.33 and 8 respectively.

Two series of numerical experiments are conducted for two variables, time step size and panel size. The outer domain is 40λ . The inner domain is 2λ for the analysis in time step size, and 1λ for panel size analysis. The same oscillation period and oscillating amplitude as those in the panel size analysis are used.

A. Panel Size, $\triangle x$

In this set of investigations, panel size is the principle analysis variable. Time step size is equal to $\frac{T}{30}$ and remains unchanged through the series of tests. S_{in} is divided into 10, 20, 30, 40, 50 and 60 uniform panels.

The results of the tests in deep water show that the scheme is stable for the first five cases in which the sizes of the panels are large enough to keep the numerical scheme stable. For the sixth case, the instability grows as the computations continue. By adjusting panel size to regain stability, the critical panel size is found to be 0.0181λ and the corresponding FSS number is 11.87. The same tests are conducted for shallow water cases and the same stability number is achieved.

With the cylinder oscillating in deep water, the stability of the numerical scheme is also tested at two other frequencies, $\omega = \frac{\pi}{1.75}$ and $\omega = \frac{\pi}{1.25}$. It is found that the critical FSS number for $\omega = \frac{\pi}{1.75}$ and $\omega = \frac{\pi}{1.25}$ are 11.76 and 11.80 respectively.

B. Time Step Size, Δt

The primary analysis parameter is the time step size in this series of tests. The size of the panel is chosen to be $\frac{\lambda}{30}$, and the time step size is increased from $\frac{T}{120}$ to $\frac{T}{20}$. Seven cases are tested and the temporal increment is equal to $\frac{T}{120}$.

The simulation process becomes unstable in the last case, $\Delta t = 0.05T$, and the time histories of the wave profiles is shown in figure (5.10). The instability clearly starts at the body-free surface intersection line. The simulation is finally forced to stop because of the improper time step size. Stable computations are possible when the time step size is less than or equal to $0.0468T$. The critical FSS number is then determined to be 12.71 for both shallow and deep water.

The dependency between the forcing frequency and the numerical stability is investigated at two other frequencies, $\omega = \frac{\pi}{1.75}$ and $\omega = \frac{\pi}{1.25}$. The fluid field is assumed to be infinitely deep. When forcing frequency equal to $\omega = \frac{\pi}{1.75}$, the critical FSS numbers is 12.58. The FSS number is 12.63 as the frequency is $\omega = \frac{\pi}{1.25}$.

The results for heaving motion show no difference in stability criteria and convergence rate regardless of the presence of the bottom. As the bottom effects are more crucial in heaving motions than in swaying motions, the numerical tests for stability and convergence analyses in swaying motions will be conducted in deep water only.

5.2 Swaying Motion

For sway motions of a three-dimensional axisymmetric floating body, the fluid field is symmetric only in the direction of the body motion. The Rankine ring source and multiple symmetry plane approaches are not suitable for swaying motion simulations due to the lack of a circumferential symmetry property in the fluid flow. Therefore, the only plane of symmetry is the $o-x-y$ plane.

It is important to remember that the DELTA method has no difficulty in handling irregular meshes because the method does not require surface integrals over panels. A series of fictious concentric rings are applied on the free surface. As shown in figure (3.8), the rings are of different radius and distributed in the radial direction.

The free surface is divided into two regions, an inner domain and an outer domain. The radius of the inner region, R_{in}, is equal to 1λ , and that of the outer domain is chosen to be 40λ . In the r direction, the inner domain of the free surface is discretized into N_{in} rings with an uniform interval, $\triangle r_{in} = \frac{R_{in}}{N_{in}}$, between rings. The outer domain is distributed with 10 rings of field points, and the spacings between two succesive rings in the region grows with an order of γ . As in the two-dimensional problems, the panel size of the first ring of panels in the outer region is set equal to the last ring size in the inner region ($\triangle r_{in}$).

The circumference of each ring is increasing as R increases. Therefore, the larger ring is equally divided by more grid points so that the arc length of any two successive grid points on the same ring is equal to $\triangle r_{in}$. For example, the first ring, the ring on the body surface, is evenly allocated into N_b panels and the i_{th} ring has $N_b + P_r(i-1)$ uniform panels where P_r is found to be 6 in Chapter III. The total number of grid points on the whole free surface is $\frac{(2N_b+6(N_{in}-1))\cdot N_{in}}{2}$. N_b is decided after N_{in} is determined so that the arc lengths and the uniform ring interval are about the same.

5.2.1 Convergence Analysis

The convergence properties of the DELTA method in swaying motions is studied by two series of numerical experiments in which different panel sizes and time step sizes are used as the investigation parameters. The numerical experiments for the initial boundary value problem in deep water are conducted.

A system of check points is set up on the free surface by using 60 symmetry planes with 40 fixed wave probes equally distributed on each plane in the radial direction. Therefore, a total number of 2400 check points are used to calculate the relative RMS difference of the numerical results.

Before any relative RMS difference can be computed, the free surface elevations of the check points should be obtained. The variation of wave elevation in one mesh is assumed to be bilinear so that the elevations of the check points is obtained by interpolating the positions of the field points. However, the error in approximating wave elevations at the check points may exist because of the bilinear assumption. The error is reduced as the number of field points is increased.

A. <u>Panel Size, $\triangle x$</u>

The number of rings in the inner domain is increased from 10 to 50 with an increment of 5 for nine numerical simulations. The N_{in} and N_b in the first case are equal to 10 and 10 respectively. The N_{in} is 50 in the ninth case and the corresponding N_b is equal to 55. The relative RMS difference of the nine cases is plotted in figure (5.11). As shown, the results converge faster when the grid points are few, for example $N_{in} = 10$, 15 and 20. The convergence rate of the numerical solutions becomes stable when the mesh size becomes smaller, and a second-order convergence is the ultimate convergence rate.

B. Time Step Size, Δt

Figure (5.12) shows the relative RMS difference of the ten cases. With the $N_{in} = 30$, the number of time step sizes in one period is changed from 80 to 25. The decrement of the time step number per period is 5. The convergence rate is also second-order.

5.2.2 Stability Analysis

The length of the inner domain is $1\ \lambda$ and that of the outer domain is $40\ \lambda$. The period of oscillation, T, is equal to 6 and the corresponding frequency is equal to $\frac{\pi}{3}$. The definition of the FSS number by Park & Troesch (1992) is again used to investigate the stability properties of the DELTA method for fully nonlinear three-dimensional swaying motions.

A. Panel Size, Δx

In this series of numerical experiments, time step size is set equal to $\frac{T}{20}$ through the series of the experiments. The N_{in} is increased from 6 to 24 with an increment of 3. The scheme is stable for all the cases but the last one, $N_{in} = 24$. By keeping the size of time step unchanged, the proper Δr_{in} is found to be 0.0432λ to keep the numerical scheme stable, and the corresponding FSS number is 11.20.

B. Time Step Size, Δt

The number of time steps per period is changed from 60 to 20 with a decrements equal to 5. The N_{in} is set equal to 30. During the numerical experiments, the scheme remains stable until the time step size exceeds $\frac{T}{25}$. At this time step size, the irregularity shows on the free surface profile. The stability can be recovered by reducing the time step size to $0.0456T$. The corresponding FSS number is found to be 12.07.

5.3 Discussion

The convergence properties of the DELTA method in three-dimensions is investigated. The convergency rate for swaying motions is slightly lower than that for heaving motions. It is difficult to isolate the reason for this discrepancy. However, one of the most important causes may be because of the existence of the body-free surface intersection line. The singularity is more crucial for swaying motions.

The critical FSS numbers of the DELTA method for the heaving and swaying motions of a three-dimensional vertical cylinder are greater than the limit of the FSS number of Park & Troesch (1992) and the Courant condition of Dommermuth & Yue (1986). This result suggests that the indirect version of the DELTA method has better stability properties than the conventional boundary integral equation method. In the stability analysis of both motions, the critical FSS number for the time step size analysis is slightly larger than that in the panel size analysis.

Three forcing frequencies, $\omega = \frac{\pi}{3}$, $\omega = \frac{\pi}{1.75}$ and $\omega = \frac{\pi}{1.25}$, are used to investigate the frequency dependence of the numerical scheme. Table (5.2) lists the convergence rate and the critical FSS number for the three frequencies. The results show that the convergency and stability of the numerical scheme is relatively independent of the forcing frequencies used in our numerical experiments.

Table 5.2: The convergence rate and the stability number for the tested forcing frequencies

forcing frequency	$\frac{\omega}{3}$	$\frac{\omega}{1.75}$	$\frac{\omega}{1.25}$
convergence rate	second-order	second-order	second-order
stability number (Δx)	11.87	11.76	11.80
stability number (Δt)	12.71	12.58	12.63

The existence of the bottom does not affect the stability of the numerical scheme when the forcing frequency is $\frac{\pi}{3}$. The convergence rate is also the same in shallow and deep water cases. Therefore, a conclusion based on our numerical results is that the stability and convergence of the DELTA method are not affected by water depth, H , for forcing frequencies higher than $\frac{\pi}{3}$. For lower forcing frequencies, the $\frac{\lambda}{H}$ ratio is larger and the bottom effect may be stronger, and the above conclusions may have to be modified.

The body-free surface intersection line does not cause difficulties in solving boundary value problems when the DELTA method is applied. The expected singularity at the intersection line was smoothed out by the properties of desingularization.

The field points in the vicinity of the intersection line tend to pile up on the upstream side and to scatter on the downstream side for swaying motions. In order to avoid numerical errors caused by the grouping, the field points on the symmetry plane of the motion were redistributed where necessary. While there is no upstream nor downstream for heaving motion, the regridding technique is still used to reduce numerical instabilities.

The results of the quarter plane method and the multiple symmetry plane method show good agreement. The two results agree up to 5 significant digits when the number of symmetry planes is equal to 60. However, the computing time used for simulations is much less when the multiple symmetry plane method is used. Therefore, the multiple symmetry plane approach is preferable for the simulation of an axisymmetry body experiencing heaving motion.

The same initial boundary value problem is solved by using the DELTA method and the conventional boundary integral equation method by Dommermuth & Yue (1987). The comparison between the two numerical results show good agreement. The linear force is also compared with the two nonlinear hydrodynamic forces. As shown in figure (5.5), at the downstroke of the heaving cycle, the discrepancy between the linear and nonlinear forces is small because the bottom is far away from the free surface. A significant difference during the upstroke of the motion is shown between the linear and nonlinear forces. This is because the vertical force is obtained by integrating pressure over the bottom of the cylinder which is close to the free surface during the upward part of a heave cycle. Nonlinear effects strongly dominate the results, and non-sinusoidal waves appear. The nonlinear forces have mean shifts and are much larger than the linear force. The results show that the nonlinear calculations have avoided the need to calculate the first, second and higher order forces or the slowly varying forces separately. That is, nonlinear computations determine the total effect of all components of hydrodynamics forces without extra programming and computational effort.

The vertical force acting on an upright cylinder with a larger bottom has also been computed. The radius of the lower cylinder is 1.5 and the radius of the upper cylinder is 1.0. The depth of the upper cylinder is equal to its radius and is 2 times the depth of the lower cylinder. Two cases with heaving amplitude equal to 0.25 and 0.5 are examined. The time histories of the hydrodynamics forces and the heaving amplitudes are shown in figures (5.13) and (5.14). In figure (5.13), nonlinear effects are not obvious and the mean shift is small because the amplitude of motion is modest. When the motion amplitude is increased, the nonlinearity increases and the mean shift becomes large as shown in figure (5.14). At the peak of the force curve, the vertical force is well in phase with the motion because the bottom of the cylinder is deeply submerged under the free surface. The force is almost a pure added mass effect. As the cylinder moves upward, however, the bottom is closer to the free surface and a phase difference appears between the curve of the force and the motion. This is a consequence of wave damping. The results demonstrate the power of the DELTA method and are promising for offshore applications.

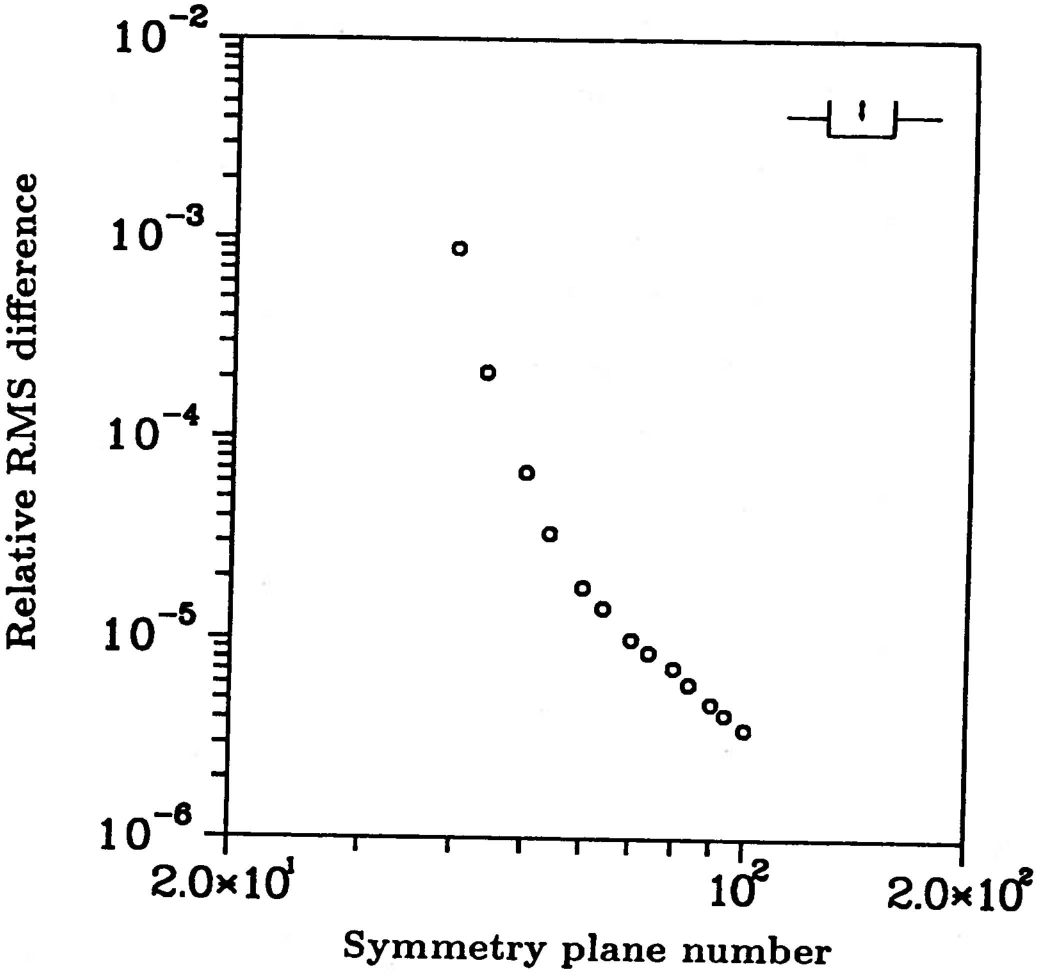

Figure 5.1: Convergencce of RMS error in free surface elevations for a heaving three-dimensional cylinder in infinite water depth, $R = 1.0$, $H = 1.0$, $L_{in} = 2\lambda$, $L_{out} = 40\lambda$, motion amplitude = 0.1

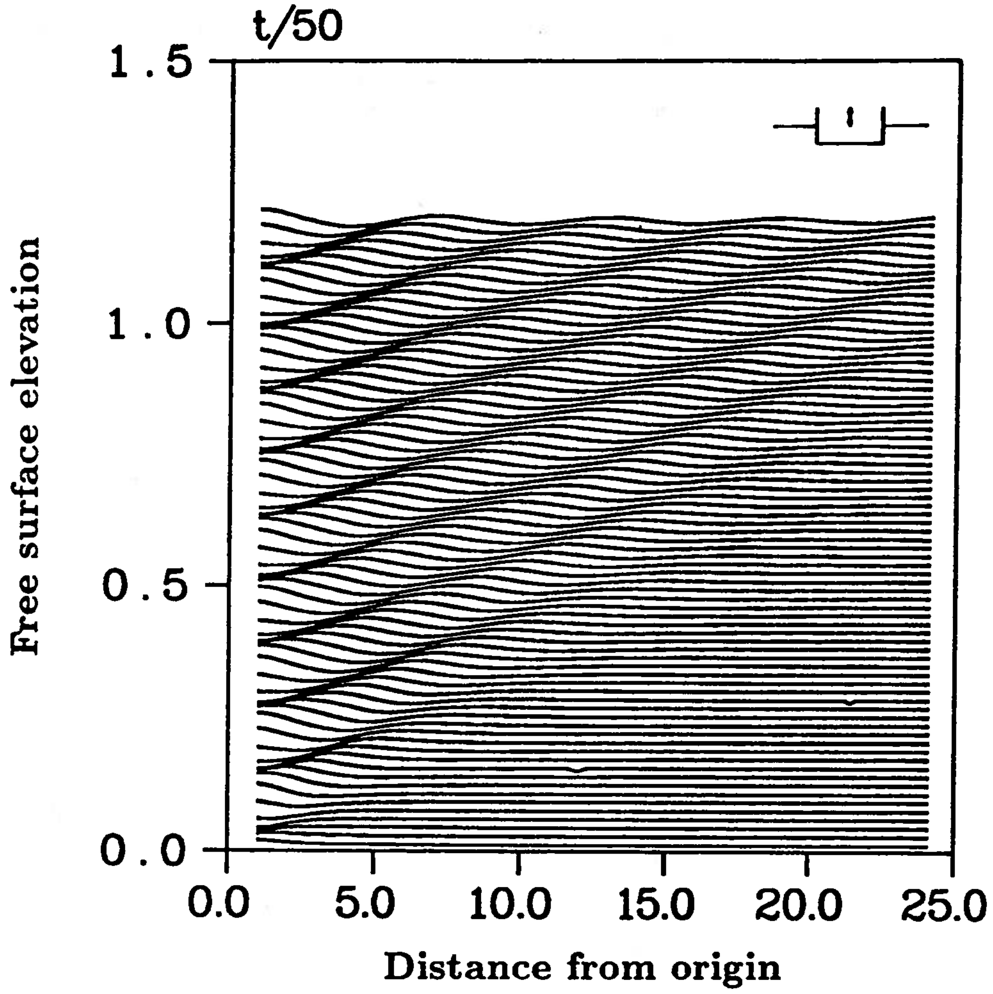

Figure 5.2: Time history of the free surface profile for a heaving three-dimensional cylinder in infinte water depth, $R = 1.0$, $H = 1.0$, $L_{in} = 2\lambda$, $L_{out} = 40\lambda$, panel size $= \frac{\lambda}{30}$, motion amplitude $= 0.1$, forcing frequency $= \frac{\pi}{3}$, symmetry plane number $= 90$

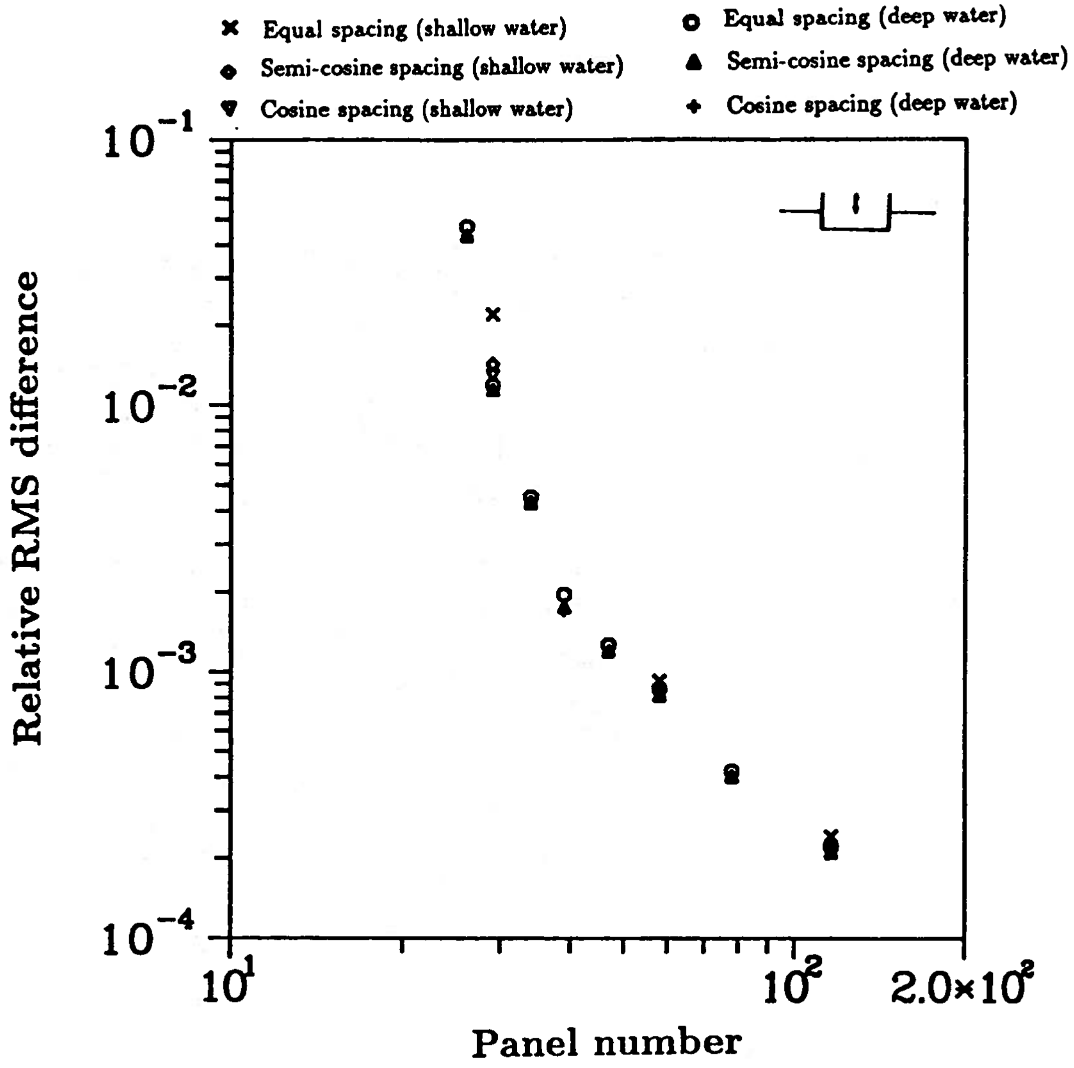

Figure 5.3: Convergencce of RMS error in free surface elevations for a heaving three-dimensional cylinder in infinite water depth, $R = 1.0$, $H = 0.5$, $L_{in} = 2\lambda$, $L_{out} = 40\lambda$, motion amplitude = 0.25, forcing frequency = $\frac{\pi}{3}$, symmetry plane number = 60

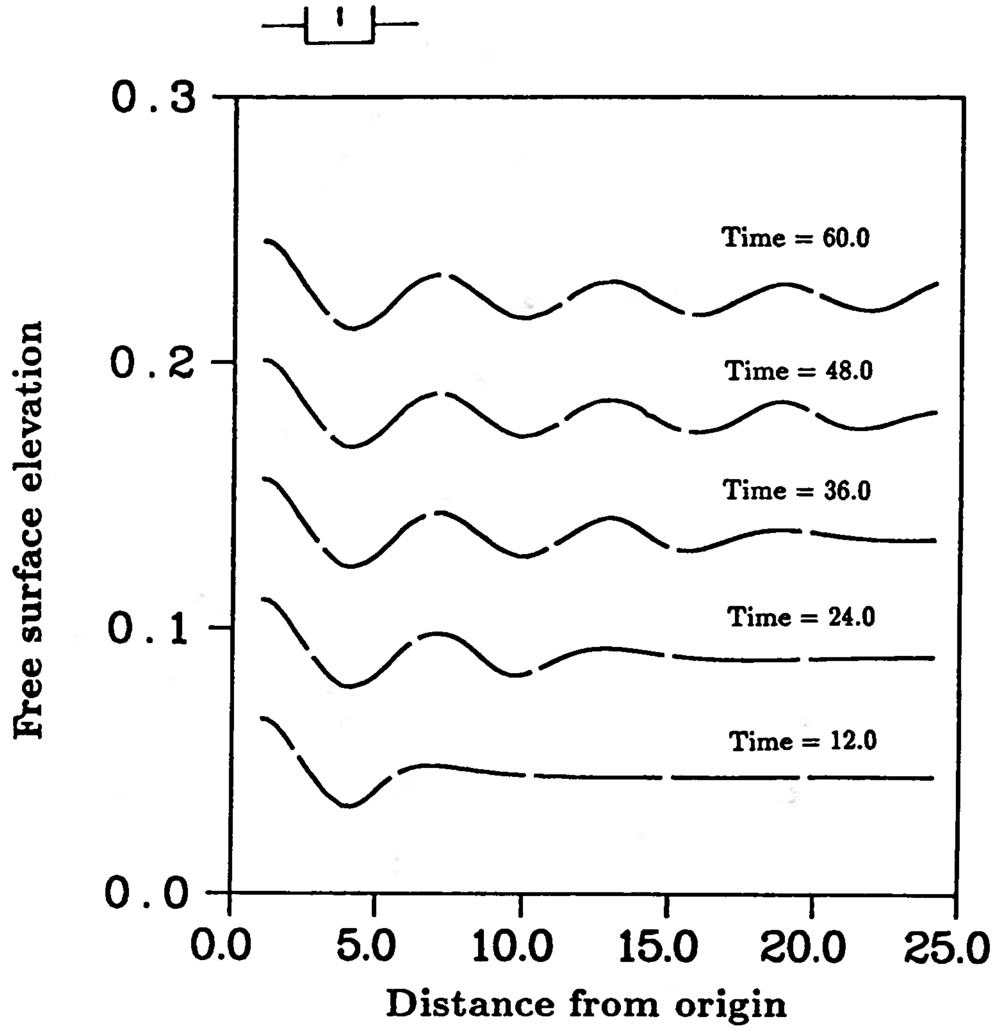

Figure 5.4: Comparison of the wave profiles of the second and third methods at the end of different periods for a heaving three-dimensional cylinder in infinite water depth, $R = 1.0$, $H = 1.0$, $L_{in} = 4\lambda$, $L_{out} = 40\lambda$, motion amplitude = 0.1, forcing frequency = $\frac{\pi}{3}$, symmetry plane number = 60

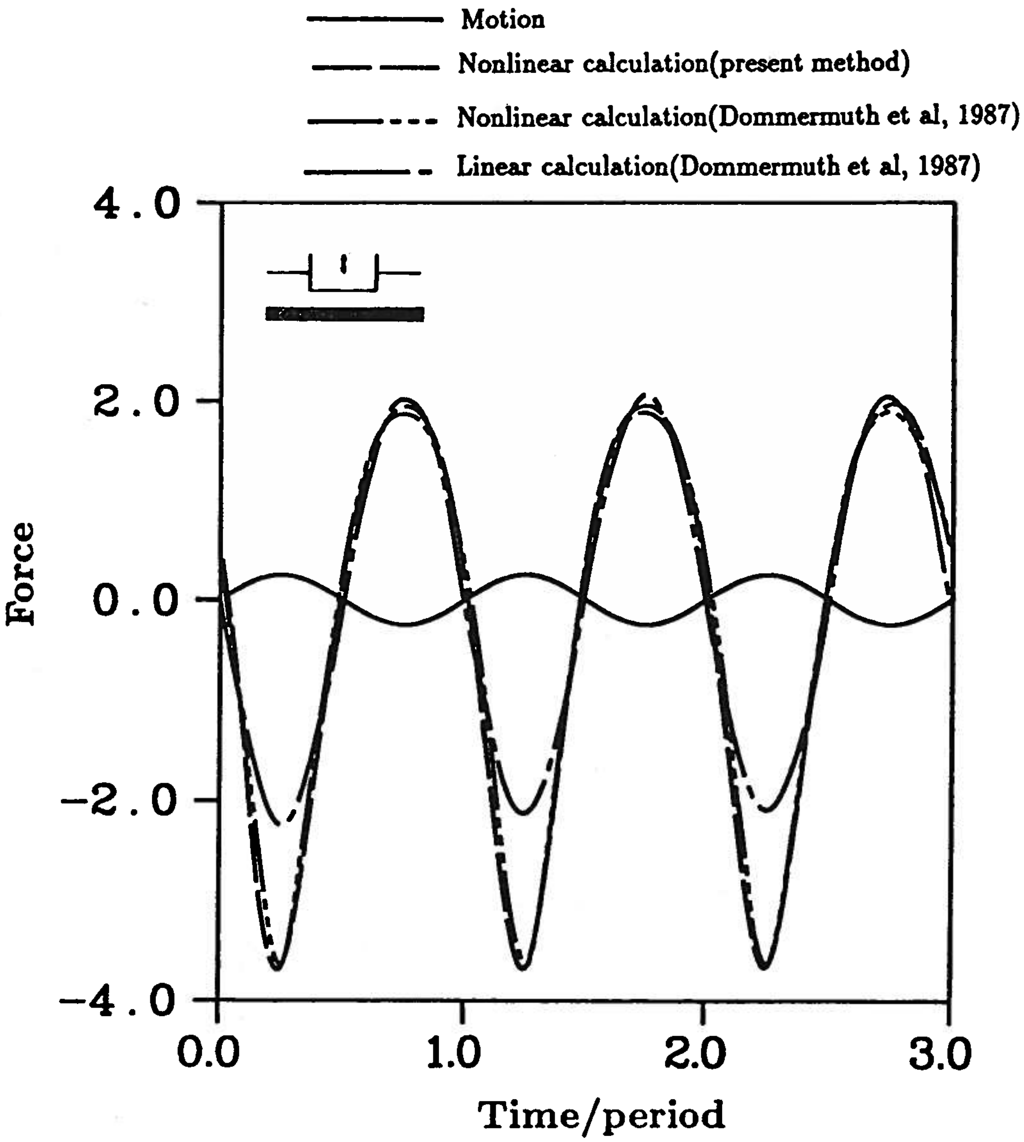

Figure 5.5: Time history of the vertical force for a heaving three-dimensional cylinder in finite water depth equal to the radius, $R = 1.0$, $H = 0.5$, $\lambda = 5R$, $L_{in} = 2\lambda$, $L_{out} = 40\lambda$, motion amplitude = 0.25, symmetry plane number = 60

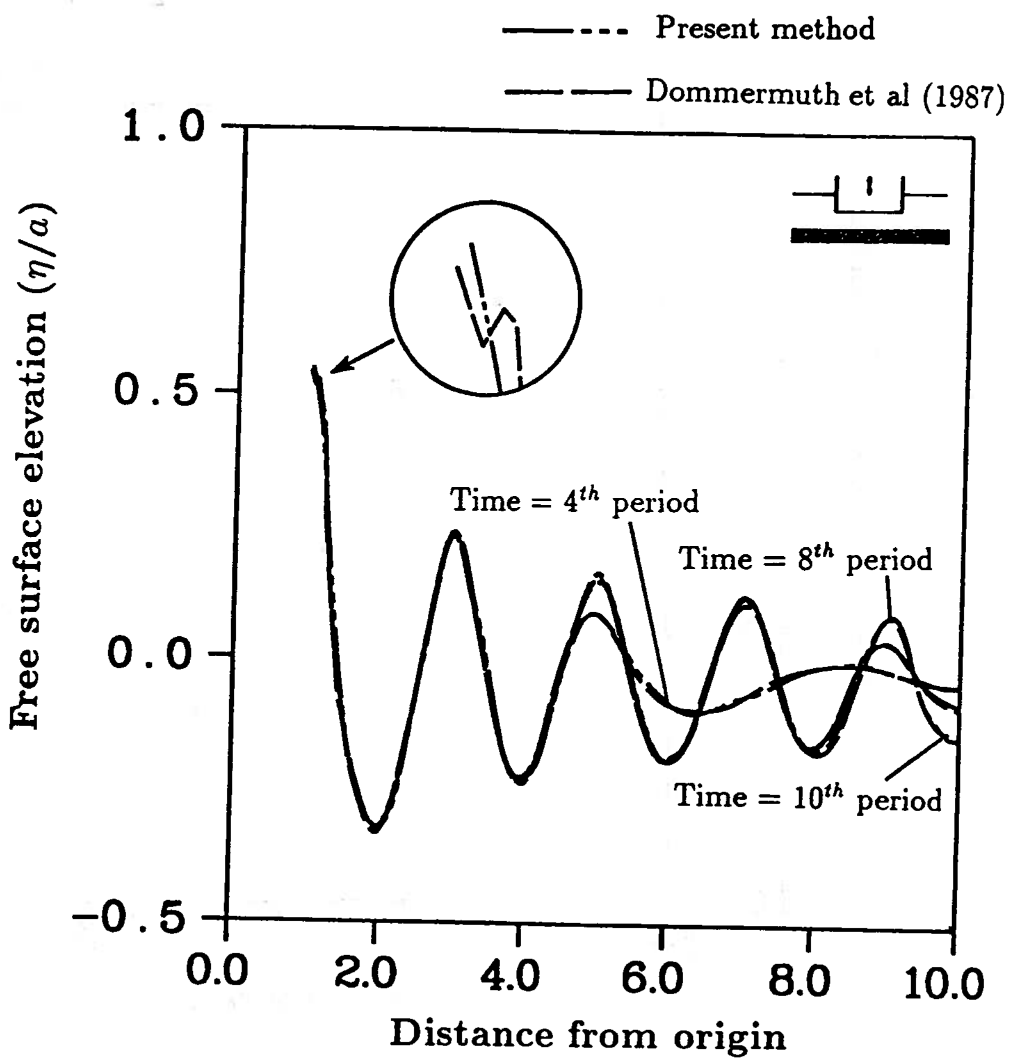

Figure 5.6: Comparison of the instaneous wave profiles of the Dommermuth's method and the third method, $R = 1.0$, $H = 0.5$, $\lambda = 5R$, $L_{in} = 4.5\lambda$, $L_{out} = 40\lambda$, motion amplitude = 0.25, symmetry plane number = 60

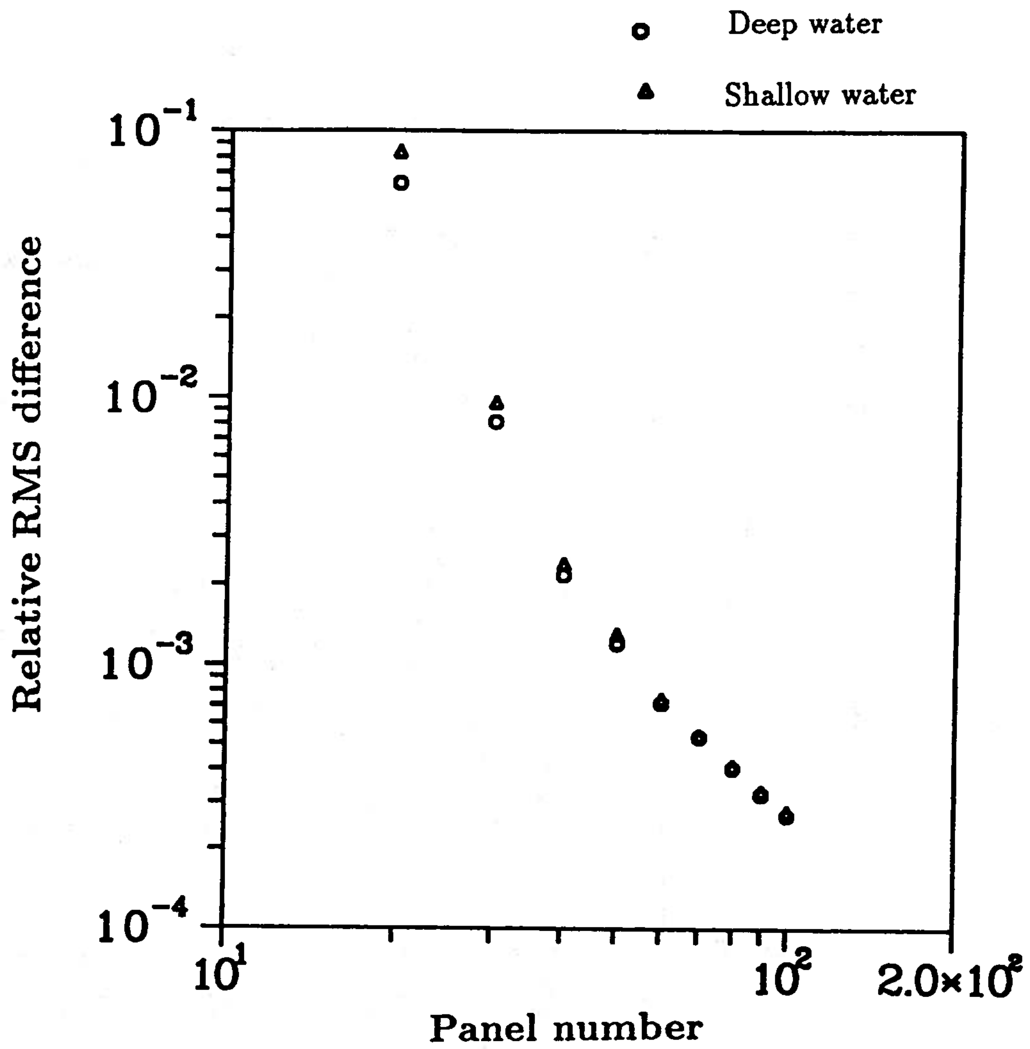

Figure 5.7: Convergencce of RMS error in free surface elevations for a heaving three-dimensional cylinder, $R = 1.0$, $H = 1.0$, $L_{in} = 2\lambda$, $L_{out} = 40\lambda$, motion amplitude = 0.1

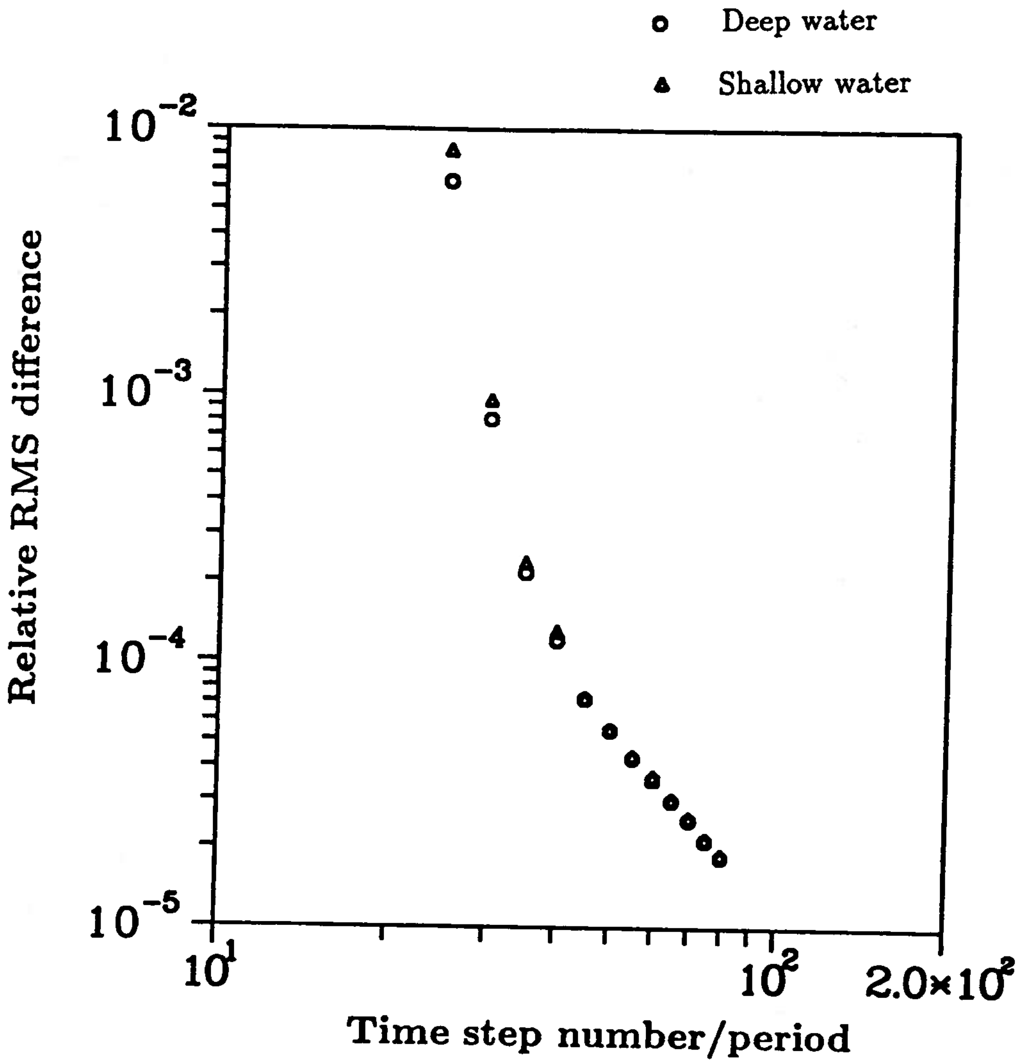

Figure 5.8: Convergencce of RMS error in free surface elevations for a heaving three-dimensional cylinder, $R = 1.0$, $H = 1.0$, $L_{in} = 2\lambda$, $L_{out} = 40\lambda$, motion amplitude = 0.1

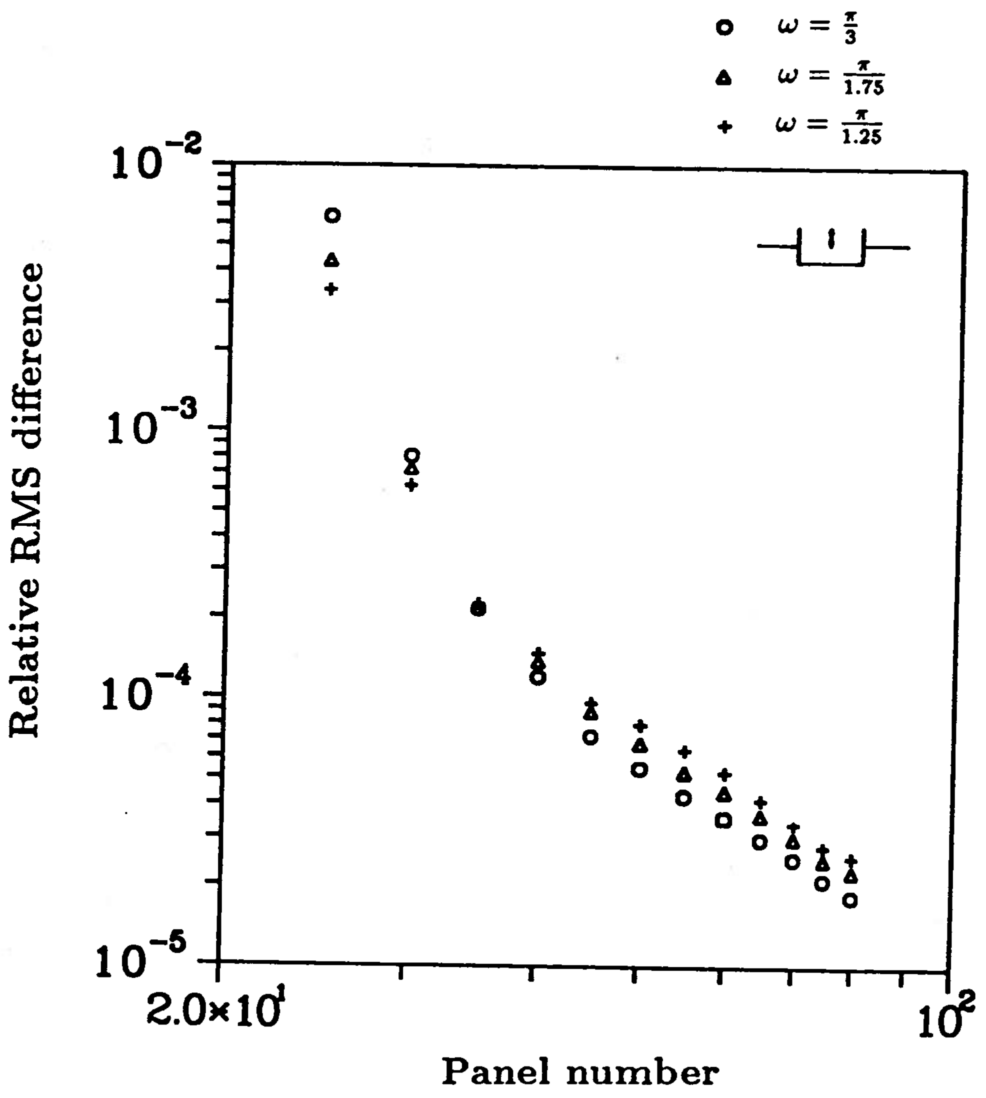

Figure 5.9: Convergencce of RMS error in free surface elevations for a heaving three-dimensional cylinder in infinite water depth, $R = 1.0$, $H = 1.0$, $L_{in} = 2\lambda$, $L_{out} = 40\lambda$, motion amplitude $= 0.25$

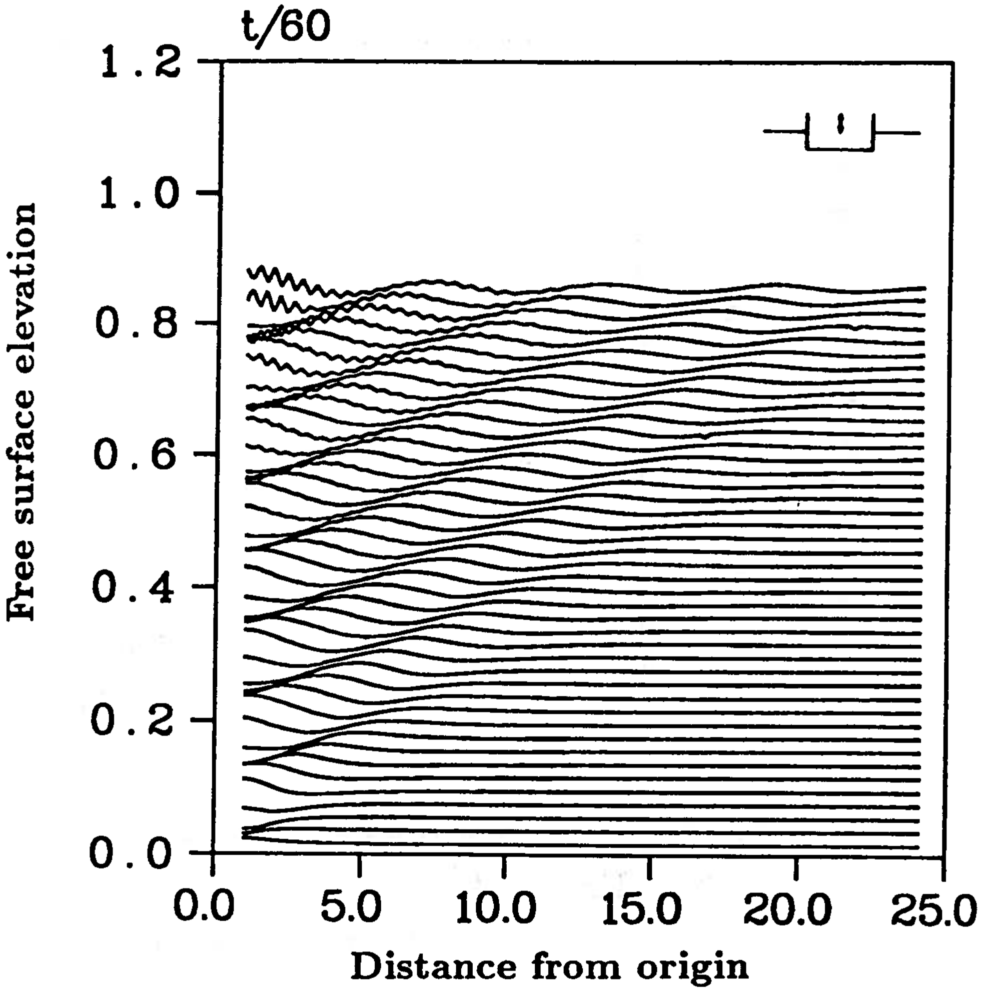

Figure 5.10: Time history of the unstable free surface profile for a heaving three-dimensional cylinder in infinte water depth, $R = 1.0$, $H = 1.0$, $L_{in} = 4\lambda$, $L_{out} = 40\lambda$, motion amplitude = 0.1, forcing frequency = $\frac{\pi}{3}$, panel size = $\frac{\lambda}{30}$

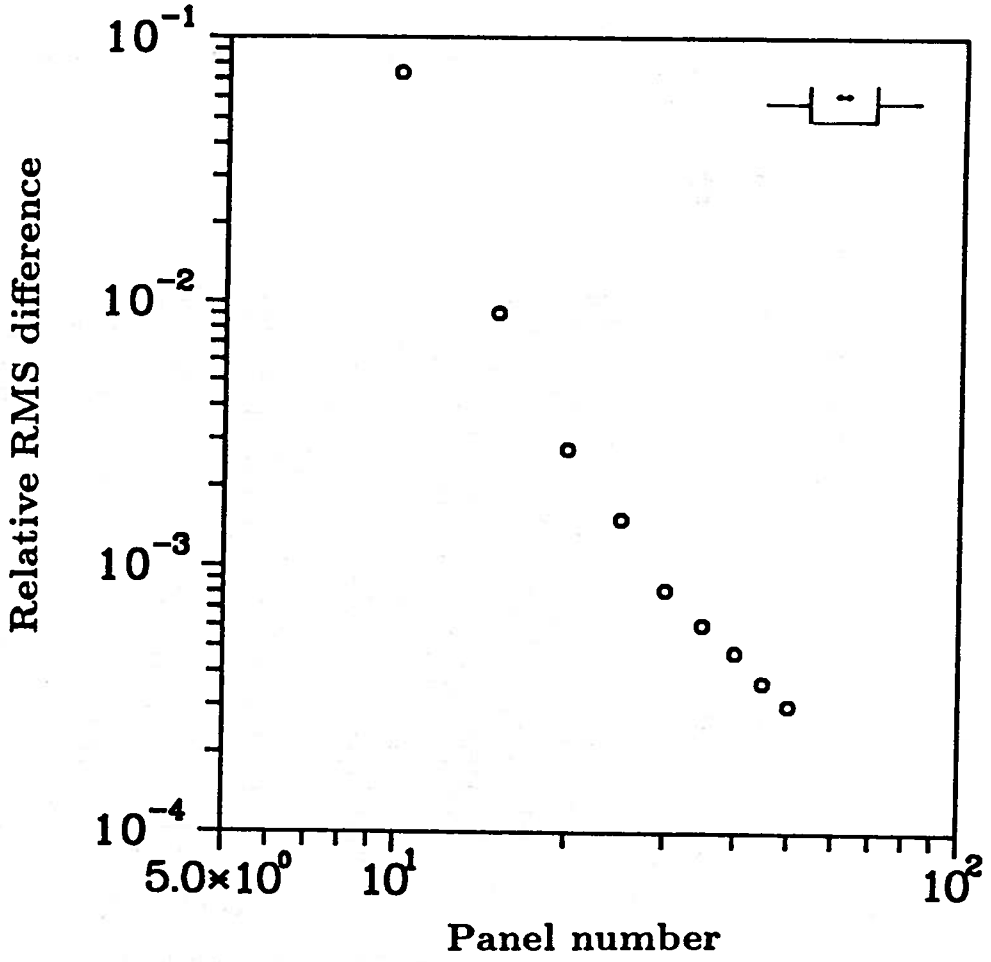

Figure 5.11: Convergencce of RMS error in free surface elevations for a swaying three-dimensional cylinder in infinite water depth, $R = 1.0$, $H = 1.0$, $L_{in} = 1\lambda$, $L_{out} = 40\lambda$, motion amplitude = 0.1

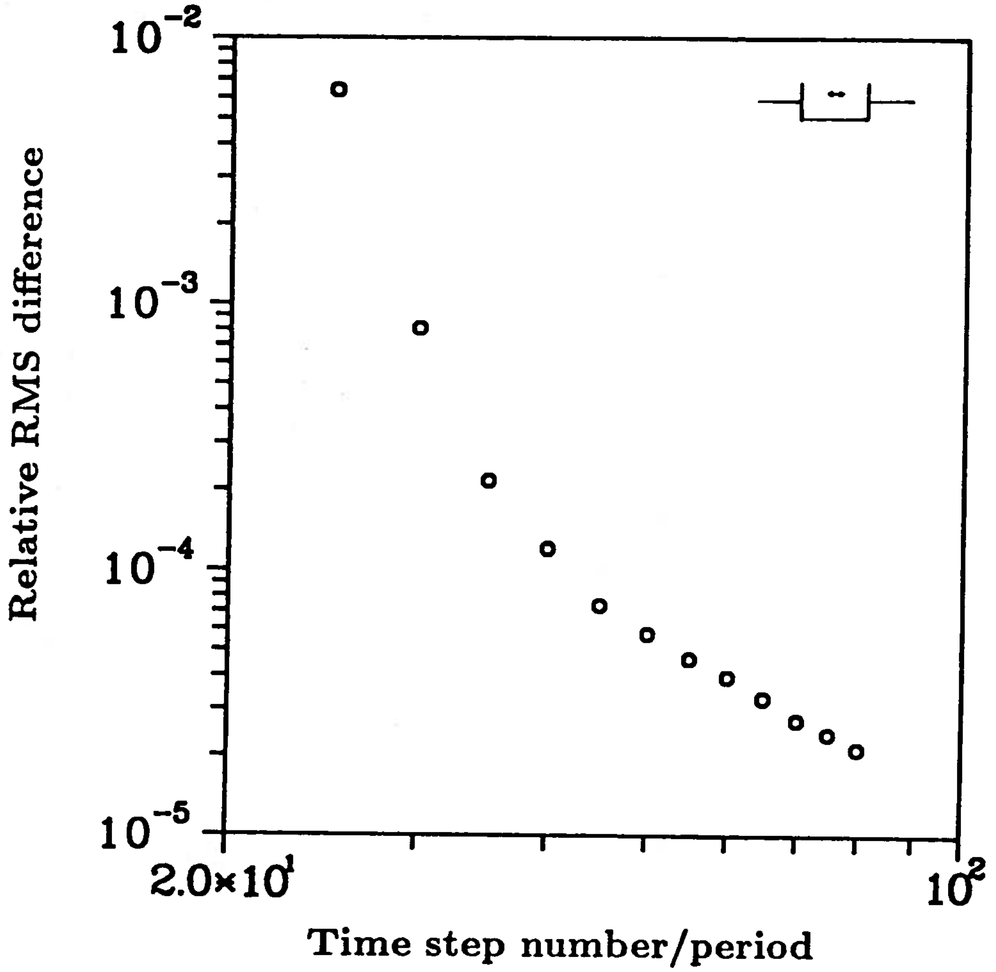

Figure 5.12: Convergencce of RMS error in free surface elevations for a swaying three-dimensional cylinder in infinite water depth, $R = 1.0$, $H = 1.0$, $L_{in} = 1\lambda$, $L_{out} = 40\lambda$, motion amplitude = 0.1, panel size = $\frac{\lambda}{30}$

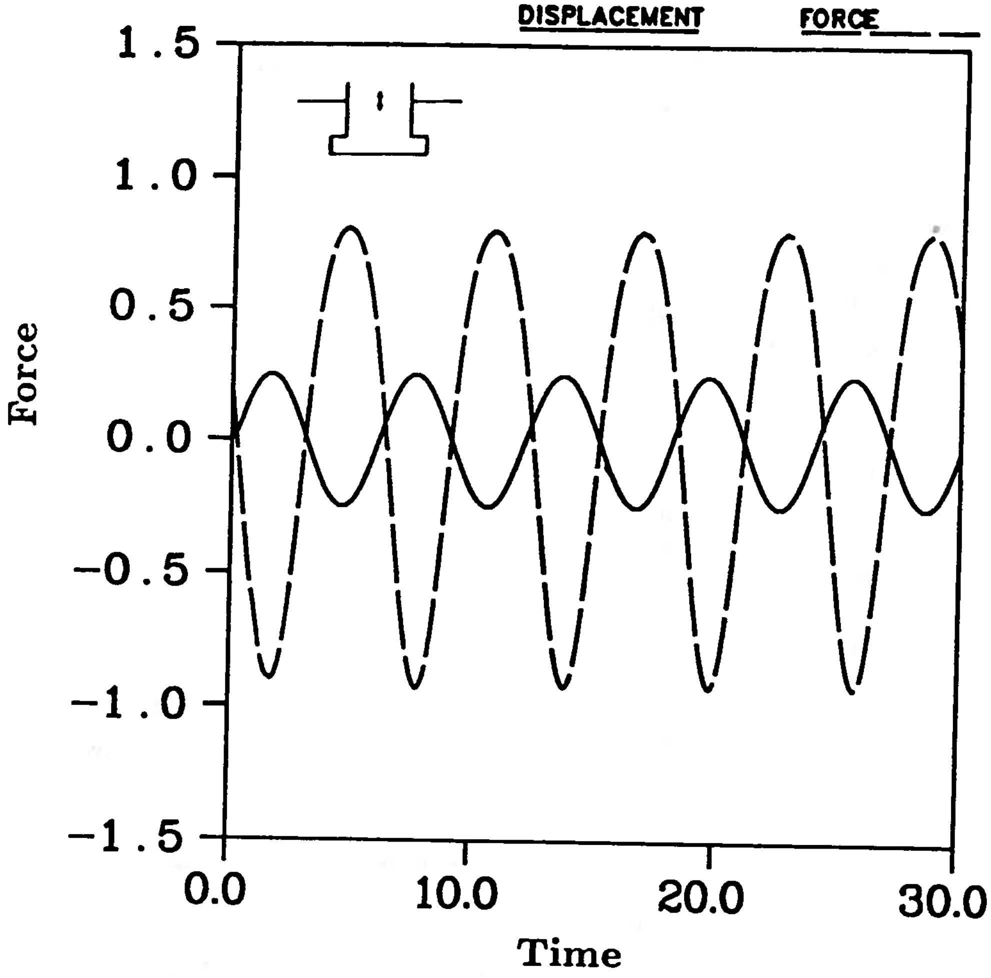

Figure 5.13: Time history of the heaving amplitude and vetical force on a three-dimensional double cylinder in infinite water depth, $R_{upper} = 1.0$, $H_{upper} = 1.0$, $R_{lower} = 1.5$, $H_{lower} = 0.5$, $L_{in} = 4\lambda$, $L_{out} = 40\lambda$, motion amplitude = 0.25, panel size = $\frac{\lambda}{30}$

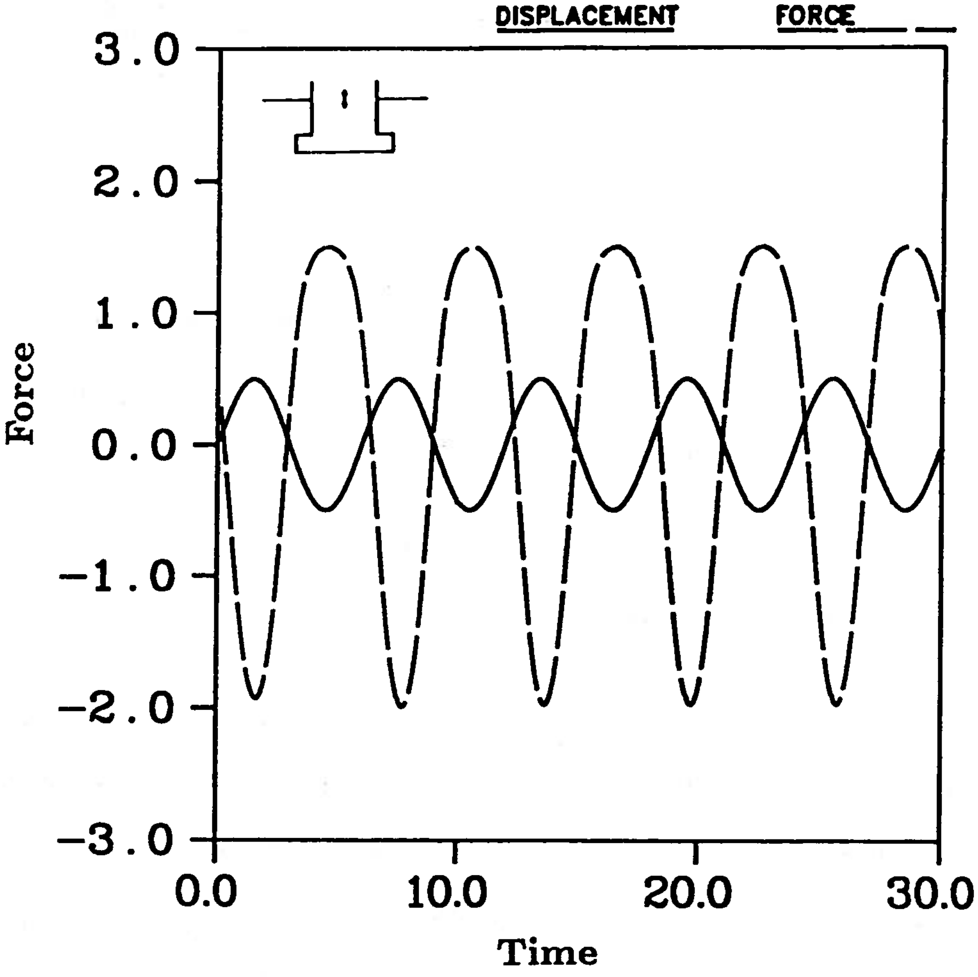

Figure 5.14: Time history of the heaving amplitude and vetical force on a three-dimensional double cylinder in infinite water depth, $R_{upper} = 1.0$, $H_{upper} = 1.0$, $R_{lower} = 1.5$, $H_{lower} = 0.5$, $L_{in} = 4\lambda$, $L_{out} = 40\lambda$, motion amplitude $= 0.50$, panel size $= \frac{\lambda}{30}$

CHAPTER VI

CONCLUSIONS AND SUGGESTIONS FOR FURTHER RESEARCH

The convergence and stability of the indirect version of the desingularized Eulerian-Lagrangian time-domain approach (the DELTA method) have been investigated for wall-sided axisymmetry surface-piercing bodies in two and three dimensions. Both shallow and deep water cases were studied.

6.1 Conclusions

When heaving motions of three-dimensional axisymmetric bodies are studied, the multiple symmetry plane method is preferable to the quarter plane method. The results of the two methods show good agreement. However, more computational time is necessary for the quarter plane method while the multiple symmetry plane method requires much less computation time. The lower limit of the symmetry plane number is 60 so that the results can be performed correctly.

The indirect version of the DELTA method is robust in handling the singularity at the body-free surface intersection line. No extra programming or computational effort is necessary to manage the singularity. In addition, the method demonstrates no difficulty in treating irregular meshes because the method does not require any line or surface integral.

When the Lagrangian description is applied to update the solutions, a redistribution scheme is necessary for swaying motions to avoid the piling up of the field points near the intersection line (points). For heaving motions, the redistribution is also used to reduce the numerical instabilities.

The DELTA method is robust in simulating the motions of floating bodies with complicated shapes. The fully nonlinear hydrodynamic force of a vertical cylinder with a bigger bottom is computed. The vertical force shows a strong nonlinearity when the motion amplitude is large. A mean shift on the computed hydrodynamic force also appears and the time history is no longer sinusoidal. This suggests that the effects from nonlinear hydrodynamic forces are important. Therefore, the method is promising for further application to floating structures with arbitrary shape. A direct and practical application will be analyzing the motions of and hydrodynamic forces acting on a floating offshore structure.

A third-order convergence for a two-dimensional floating body is obtained for both heaving and swaying motions. However, the rate is slightly higher in heaving cases than in swaying cases. For a three-dimensional floating vertical cylinder, the convergence rates for both motions are slightly over second-order. Similar to that in two dimensions, the rate is lower for sway motions. It is belived that the difference in the convergence rate is due to the singularity at the body-free surface intersection point. The statement is checked by comparing the convergence rate of the heaving and swaying motions of a submerged cylinder in two dimensions. No difference is found between the two convergence rates, therefore, the comment is confirmed. In general, the convergence rate is higher in two dimensions than in three dimensions. This may be because the numerical errors caused by the computations and interpolation are larger in three-dimensions.

For the DELTA method, the critical Free Surface Stability numbers (the critical FSS number) at which the solution becomes unstable are 8.67 and 11.20 for the initial boundary value problems in two dimensions and three dimensions, respectively. No special treatment of the matrix of influence coefficients is necessary to stabilize the numerical scheme. Both numbers are located in the unstable region of the FSS number by Dommermuth & Yue (1986). The FSS numbers of the present method are also greater than those obtained by Park & Troesch (1992) when no Green's function constant is used in their calculations. This leads to the conclusion that the stability of the indirect version of the DELTA method is better than that of the conventional boundary integral equation method.

6.2 Suggestions for Further Work

The present method of desingularization is an $O(N^2)$ algorithm. The GMRES scheme is also an $O(N^2)$ algorithm even with the influence matrix preconditioned. The fast Multipole Expansion Method has been developed and studied by Rokhlin (1985), Greengard & Rokhlin (1988), Greengard (1990) and Krosmeyer (1990). A N-body potential problem is investigated. The influence among the N bodies is evaluated by using multiple expansions so that the operation count is reduced from $O(N^2)$ to $O(NlogN)$. In an actual implementation of this method, it is essential to apply the multipole expansions only to well separated regions (Tryggvason, 1991). The adaptive method can also be used to divide the regions into sub-regions as necessary in order to improve the accuracy of the solutions. For very large scale computations, the time for the calculations is expected to be substantially reduced without losing the solution accuracy by combining desingularization, preconditioning and multipole expansions with adaptive capability.

The application of parallel processing to solve the influence matrix iteratively may allow the use of the multipole expansions and adaptive methods to become more practical. The fundamental algorithm of the two methods require many *IF* statements to group the collocation points. When *IF* statements are used in the inner most *DO* loop of the program, the speed of the vectorized calculation is substantially reduced but the speed of parallel computations is not affected. Therefore, parallel calculations show great potential for the same order of magnitude in speeding up computations as was obtained by vector processing over scalar calculations.

The application of a large scale outer region is only a temporary fixed up to postpone the free surface mean shift and absorbing the radiating waves. Therefore, an appropriate treatment at the truncation boundary is necessary to run long time simulations.

A moving window technique is desired so that a small computational domain can be utilized to handle the zero forward speed problem of a floating body experiencing very large swaying motions. The technique has been successfully developed and used by Cao, Schultz & Beck (1990, 1991a, 1991b, 1992) for submerged bodies and surface disturbances with forward speed. When the moving window technique is applied to a large amplitude swaying motion problem, the special treatments used on the upstream and downstream boundaries in the forward speed case are not applicable since there exists neither the upstream nor the downstream. The body keeps on moving back and forth and the upstream now becomes the downstream later. Therefore, a new algorithm to handle the open boundaries of a moving window is desired so that the technique can be used.

Wave breaking problems should be studied. The method developed so far can only handle the problems of floating bodies moving with low speed (Cao, Lee & Beck, 1992). As the speed of a floating body increases, waves generated by the motion become larger. In a fully nonlinear calculation, the waves generated by body motions may overturn and wave breaking happens near the body-free surface intersection line. In order to continue the computations after wave breaking appears, a means of distributing sources in the extreme regions should be modified and the re-entry of the fluid particles onto the free surface must also be considered.

Jets occur when the speed of a body is too big or the impact of an incident wave is too strong. Vorus (1992) investigated the formation of a two-dimensional jet flow by setting up a planing hull impact problem and assuming no gravity effect in jet calculations. The present method should be adjusted in order to manage the jet problems in which the gravity effect is included.

The combined effects of the incident and diffraction waves is very important for practical seakeeping problems. However, fully nonlinear exciting force problems have not yet been solved. Part of the difficulty is defining a fully nonlinear wave field. If the wave field can be completely defined, the basic difference between the radiation and exciting force problems is only a modification of the body boundary condition. A nonlinear interaction between the radiation forces and the exciting forces is expected in the fully nonlinear computations. A natural consequence of the fully nonlinear calculations is the second and higher order forces and moments. Therefore, no extra numerical effort need to be made. The results of the nonlinear computations can be utilized as a guide line to design safer offshore structures.

BIBLIOGRAPHY

BIBLIOGRAPHY

[1] Baker, G.R., D.I. Meiron and S.A. Orszag (1982), Generalized Vortex Methods for Free Surface Flow Problems, *Journal of Fluid Mechnamics*, Vol. 123, pp. 477-501.

[2] Beck, R.F. and S.J. Liapis (1987), Transition Motions of Floating Bodies at Zero Forward Speed," *Journal of Ship Research*, Vol. 31, No. 3, pp. 164-176.

[3] Beck, R.F. and A.R. Magee (1990), Time-domain Analysis for Predicting Ship Motions , *Proc. of the IUTAM symposium on Dynamics of Marine Vehicles and Structures in Waves*, Uxbridge, U.K.: Brunel University.

[4] Bertram, V. (1990), Ship Motion by Rankin Source Method," *Ship Technology Research*, Vol. 37, No. 4, pp.143-152.

[5] Cao, Y., W.W. Schultz and R.F. Beck (1990), Three-dimensional, unsteady computations of nonlinear waves caused by underwater disturbance , *Proceedings 18th Symposium on Naval Hydrodynamics*, Ann Arbor, MI, USA, pp. 417-427.

[6] Cao, Y., W.W. Schultz and R.F. Beck (1991a), Three-Dimensional Desingularized Boundary Integral Methods for Potential Problems , *International Journal of Num. Meth. Fluids*, Vol. 12, pp. 785-803.

[7] Cao, Y., W.W. Schultz and R.F. Beck (1991b), Two-dimensional Solitary Waves Generated By a Moving Disturbance, *6th International Workshop on Water Waves and Floating Bodies*, Woodshole, MA, USA.

[8] Cao, Y. 1991. Computations of Nonlinear Gravity Waves by a Desingularized Boundary Integral Method , *Ph.D. Diss.*, Dept. of Naval Archtechure and Marine Engineering, The University of Michigan, Ann Arbor, USA.

[9] Chan, R.K.-C. (1975), Two Dimensional Time-Dependent Calculations of Large-Amplitude Surface Gravity Waves due to a Surface Disturbance, *Proceedings 1st International Conference on Numerical Ship Hydrodynamics*, Gaithersburg, Maryland.

[10] Chang, M.-S. (1977), Computation of Three-Dimension Ship Motions with Forward Speed," *Preceedings 2nd International Conference on Numerical Ship Hydrodynamics*, The University of California, Berkeley, CA, pp. 124-135.

[11] Commins, W.E. (1962), "The Impulse Response Function and Ship Motions," *Schiffstechnik*, Vol. 9 pp. 101-109.

[12] Doctors, L.J. and R.F. Beck (1987), Convergence Properties of the Neumann-Kelvin Problem for a Submerged Body, *Journal of Ship Research*, **31**, pp. 227-234.

[13] Dommermuth, D.G. and D.K.-P. Yue (1988), Study of Nonlinear Axisymmetric Body-Wave Interactions," *Proceedings 16th Symposium of Naval Hydrodynamics*, Berkeley.

[14] Dommermuth, D.G. and D.K.-P. Yue (1987), Numerical Simulations of Nonlinear Axisymmetric Flows with a Free Surface, *Journal of Fluid Mechnamics*, Vol. 178, pp. 195-219.

[15] Eatock Taylor, R. and E.R. Jeffreys (1986), Variability of Hydrodynamoc Load Prediction for a Tension Leg Platform," *Ocean Engineering*, Vol. 13, No. 5, pp. 449-490.

[16] Faitisen, O.M. (1977), Numerical Solution of Transient Nonlinear Gree-Surface Motion Outside or Inside Moving Bodies," *Preceedings 2nd Conf. on Num. Ship Hydro.*, U.C. Berkeley, pp. 347-357, University Extension Publications.

[17] Ferrant, P. (1989), Radiation d'Ondes de Gravite par les Mouvements de Grande Amplitude d'Un Corps Immerge," *P.h.D. Diss.*, Universite de Nantes.

[18] Ferrant, P. (1990), A Coupled Time and Frequency Approach for Nonlinear Wave Radiation," *Proceedings 18th Symposium on Naval Hydrodynamics*, Ann Arbor, MI, USA, pp. 67-84.

[19] Finklestein, A. (1957), The Initial Value Problem for Transient water Waves," *Communication on Pure and Applied Mathematics*, No. 10, pp. 511-522.

[20] Greenhow, M. and W.M. Lin (1983), Nonlinear Free Surface Effects : Experiments and Theory, Dept. Ocean Engineering, MIT, Rep. No. 83-19.

[21] Greenhow, M., T. Vinje, P. Brevig and J. Taylor (1982), A Theoretical and Experimental Study of the Capsize of Salter's Duck in Extreme Waves, *Journal of Fluid Mechanics*, Vol. 118, pp.221-239.

[22] Grosenbaugh, M.A. and R.W. Yeung (1988), Nonlinear Bow Flows - An Experimental and Theoretical Investigation," *Proceedings 17th Symposium on Naval Hydrodynamics*, The Hague, Netherland, pp. 195-214.

[23] Guevel and Gougis (1982), Ship Motions with Forward Speed in Finite Depth," *International Shipbuilding Progress*, No. 29, pp. 103-117.

[24] Hess, J.L. and A.M.O. Smith (1964), Calculation of Nonlinear Potential Flow About Arbitrary Three-Dimensional Bodies," *Journal of Ship Research*, Vol. 8, No. 2 pp. 22-44.

[25] Heise, U., 1978. Numerical Properties of Integral Equations in Which the Given Boundary Values and the Solutions Are Defined on Different Curves, *Comput. Struct.*, Vol. 8, 199-205.

[26] Inglis, R.B. and W.G. Price (1981), A Three-Dimensional Ship Motion Theory - Comparison Between Theoretical Prediction and Experimental Data of the Hydrodynamic Coefficients with Forward Speed," *Transactions of the Royal Institution of Naval Architects*, Vol. 124, pp. 141-157.

[27] Isaacson, M (1982), Nonlinear-Wave Effects on Fixed and Floating Bodies, *Journal of Fluid Mechanics*, Vol. 120, pp.267-281.

[28] Iwashita, H. and M. Ohkusu (1992), The Green Function Methods for Numerical Solution of the Steady Wave Resistance Problem," *Proceeding 16th Symposium on Naval Hydrodynamics*, the University of California, Berkeley, pp. 1-21.

[29] Jensen, G., Z.X. Mi and H. Söding (1986), Rankine Source Methods for Numerical Solutions of the Steady Wave Resistance Problem, *Proceedings 16th Symposium on Naval Hydrodynamics*, the University of California, Berkeley.

[30] Kang, C.G. (1988), Bow Flare Slamming and Nonlinear Free Surface Body Interaction in the Time Domain , PhD thesis, Dept. of Naval Architecture and Marine Engineering, The University of Michigan, Ann Arbor,USA.

[31] King, B.K. 1987. Time-domain Analysis of Wave Exciting Forces on Ships and Bodies , Ph.D. Diss., The University of Michigan.

[32] King, B., R.F. Beck and A. Magee (1988), Seakeeping Calculations with Forward Speed Using Time-Domain Analysis, *Proceedings 17th Symposium of Naval Hydrodynamics*, the Hague.

[33] Krosmeyer, F.T. (1988), The First and Second Order Transient Free-Surface Wave Radiation Problems," *P.h.D. Diss.*, Dept. of Ocean Engineering, MIT.

[34] Krosmeyer, F.T., C.-H. Lee, J.N. Mewman and P.D. Sclavonous (1988), The Analysis of Wave Effects on Tension-Leg Plateforms," *Proceedings of the Conf. on Offshore Mechanics and Arctic Engineering*, ASME, 2, Houston, pp 1-20.

[35] Korsmeyer, F.T. (1990), An Order *N* Algorithm for the Solution of the Boundary Integral Equations of Potential Flow, *5th International Workshop on Water Waves and Floating Bodies*, Manchester, England, March 1990.

[36] Kupradze, V. (1967), On the Approximate Solution of Problems in Mathematical Physics, *Russ. Math. Surveys*, Vol. 22, pp. 59-107.

[37] Lamb, H. (1929), *Hydrodynamics*, U.K.: Cambridge University Press.

[38] Liapis, S.J. and Beck, R.F. 1985. Seakeeping Computations using time domain analysis , *Proc. of 4th International Conference on Numerical Hydrodynamics*, Washington, D.C.,: National Academy of Sciences.

[39] Lin, W.M. (1984), Nonlinear Motion of the Free Surface near A Moving Body," *P.h.D. Diss.*, Dept. Ocean Engineering, MIT.

[40] Lin, W.M. and D.K.-P. Yue (1990), Numerical Solutions for Large Motions in the Time Domain," *Proceedings 18th Symposium on Naval Hydrodynamics*, Ann Arbor, MI, pp. 41-66.

[41] Lin, W.M., J.N. Newman and D.K.-P. Yue (1984), Nonlinear Force Motion of Floating Bodies," *Proceedings 15th Symposium on Naval Hydrodynamics*, Hamburg, pp.33-49, Washington, National Academy Press.

[42] Lindman, E.L. (1975), Free-Space Boundary Condition for the Time Dependent Wave Equation, *Journal of Computational Physics*, Vol. 18, No. 1.

[43] Longuet-Higgins M.S. and C.D. Cokelet (1976), The Deformation of Steep Surface Waves on Water: I. A Numerical Method of Computation, *Proceedings of Royal Society London*, **A350**, pp. 1-26.

[44] Longuet-Higgins M.S. (1986), Eulerian and Lagrangian Aspects of Surface Waves, *Journal of Fluid Mechanics*, Vol. 173, pp. 683-707.

[45] Magee, A. and R.F. Beck (1988), Nonlinear Motion in the Time Domain, *Proceedings 3rd International Workshop on Water Wavea and Floating Bodies*, Cambridge, MA : MIT Press.

[46] McIver P. and D.H. Peregrine (1981), Comparison of Numerical and Analytical Results for Waves that are Starting to Break, *International Symposium of Hydrodynamics and Ocean Engineering*

[47] Martin, P.A. (1981), On the Null-Field Equations for Water-Wave Radiation Problems, *Journal Fluid Mechnamics*, Vol. 113, pp. 315-332.

[48] Medina, D.E. and J.A. Liggett (1991), A Consistant Boundary Element Method for Free Surface Hydrodrodynamic Calculations, *International Journal of Numerical Method in Fluids.*

[49] Miloh, T. (1980), Irregularities in Solutions of the Nonlinear Wave Diffraction Problem by Vertical Cylinder, Proceedings ASCE J. Waterway, Port, Coastal and Ocean Div., Vol. 106, pp.279-284.

[50] Nakos, D.E. and P. Sclavonous (1990a), Ship Motion by a Three-Dimensional Rankine Panel Method, *Proceedings 18th Symposium on Naval Hydrodynamics*, Ann Arbor, MI, pp.21-41.

[51] Nakos, D.E. and P. Sclavonous (1990b), On Steady and Unsteady Ship Wave Patterns, *Journal of Fluid Mechnamics*, Vol.215, pp. 263-288.

[52] Newman, J.N. (1977), Marine Hydrodynamics, *MIT Press.*

[53] Newman, J.N. (1985), Transient Axisymmetric Motion of a Floating Cylinder, *Journal of Fluid Mechanics*, Vol. 157, pp. 17-33.

[54] Newman, J.N. (1986), Distribution of Sources and Normal Dipoles Over a Quadrilateral Panel, *Journal of Engineering Mathematics*, 20, pp.113-126.

[55] Newman, J.N. and C.-H. Lee (1992), Sensitivity of Wave Wave Loads to The Discretization of Bodies, *Proceedings of the Intl. Conf. on the Behavior of Offshore Structures Conference (BOSS,1992)*, London, July, 1992.

[56] Newman, J.N. and P. Sclavounos (1988), The Computation of Wave Loads on Large Offshore Structures, *Proceedings of the Intl. Conf. on the Behavior of Offshore Structures Conference (BOSS,1988)*, Trondheim, Norway, pp.605-622.

[57] Ogilive, T.F. (1964), Recent Progress Toward the Understanding and Prediction of Ship Motions, *Proceedings 5th Symposium on Naval Hydrodynamics*, Washington D.C., pp. 3-128.

[58] Olson, L.G. 1989. GMRES Iterative Solution of Matrix Systems Derived from Boundary Element Techniques , *PSH report*, Dept. of Mechanical Engineering and Applied Mechanics, The University of Michigan, Ann Arbor, USA.

[59] Park, J.H. and A. Troesch (1992), "Numerical Modeling of Short-Time Scale Nonlinear Water Waves Generated by Large Vertical Motions of Non-Wallsided Bodies," *Proceedings 19th Symposium on Naval Hydrodynamics*, Soul, Korea.

[60] Peregrine, D.H. (1972), Flow due to a vertical Plate Moving in a Channel. *Unpublished Note.*

[61] Peregrine, D.H. (1983), Breaking Waves on Beaches, *Annual Review of Fluid Mechanics*, Vol. 15, pp. 149-178.

[62] Raven, H.C. (1992), A practical Nonlinear Method for Calculating Ship Wavemaking and Wave Resistance," *Proceedings 19th Symposium on Naval Hydrodynamics*, Soul, Korea.

[63] Roberts, A.J. (1983) A Stable and Accurate Numerical Method to Calculate the Motion of a Sharp Interface between Fluids, *Journal of Applied Mathematics*, Vol. 31, pp. 13-35.

[64] Saad, Y. and M.H. Schultz (1986), GMRES: A Generalized Minimal Residual Algorithm for Solving Nonsymmetric Linear Systems, *SIAM J. Sci. Stat. Comp.*, Vol. 7, pp. 856-869.

[65] Schultz, W.W., Y. Cao and R.F. Beck (1990), Three-Dimensional Nonlinear Wave Computation by Desingularized Boundary Integral Method, *5th International Workshop on Water Waves and Floating Bodies*, Manchester, England.

[66] Stoker, J.J. 1957. *Water Waves.* New York: Interscience Publishers.

[67] Tryggvason, A. (1991), *MEAM 526 Lecture Note*

[68] Vinje, T. and P. Brevig (1981), Nonlinear Ship Motions, *Proceedings 3rd Int. Conf. on Numerical Ship Hydrodynamics*, Paris.

[69] von Kármám, T., 1930. Calculation of Pressure Distribution on Airship Hulls, *NACA Technical Memorandum* No. 574.

[70] Vorus, W.S. (1992), An Extended Slender Body Model for Planing Hull Hydrodynamic, *SNAME Section Meeting at Cleveland, Ohio.*

[71] Vugts, J.H. (1968), The Hydrodynamic Coefficients for Swaying, Heaving and Rolling Cylinder in a Free Surface, *International Shipbuilding Progress*, Vol. 15, pp. 251-276.

[72] Webster, W.C. (1975), The Flow About Arbitrary, Three-Dimensional Smooth Bodies, *Journal of Ship Research*, Vol. 19, pp. 206-218.

[73] Wehausen, J. V. (1967), Initial Value Problem for the Motion in an Undulating sea of a Body with Fixed Equilibrium Position," *Journal of Engineering Mathematics*, Vol. 1, pp. 1-19.

[74] Wehausen, J. V. (1971), The Motion of Floating Bodies, *Annual Review of Fluid Mechanics*, Vol. 3, pp. 237-268.

[75] Wehausen, J.V. and E.V. Laitone (1960), Surface Waves , *Encyclopedia of Physics*, Springer-Verlag, Berlin, Vol. IX, pp. 446-778.

[76] Wu, G.X. and R. Eatock Taylor (1987), A Green's Function Form for Ship Motions at Forward Speed, *International Shipbuilding Progress*, Vol. 34, No. 398, pp. 189-196.

[77] Yeung, R.W. (1973), A Singularity Distribution Method for Free-Surface Problem with an Oscillating body, College of Engineering, the University of California, Berkeley, Rep. N.A. 73-6.

[78] Yeung, R.W. (1982), Numerical Methods in Frre-Surface Flows, *Annual Review of Fluid Mechanics*, Vol. 14, pp. 395-442.

[79] Yih, C.S. (1977), Fluid Mechanics, *Mcgraw-Hill.*